

Characterization of the slow DNA double-strand break repair component in G1 phase

Vom Fachbereich Biologie der Technischen Universität Darmstadt

zur

Erlangung des akademischen Grades

eines Doctor rerum naturalium

genehmigte Dissertation von

M.Sc. Monika Steinlage

aus Heidelberg

1. Referent: Prof. Dr. Markus Löbrich

2. Referent: Prof. Dr. Alexander Löwer

Tag der Einreichung: 13.01.2017

Tag der mündlichen Prüfung: 17.03.2017

Darmstadt 2017

D17



Für Sebi





Ehrenwörtliche Erklärung

Ich erkläre hiermit ehrenwörtlich, dass ich die vorliegende Arbeit entsprechend den Regeln guter wissenschaftlicher Praxis selbstständig und ohne unzulässige Hilfe Dritter angefertigt habe.

Sämtliche aus fremden Quellen direkt oder indirekt übernommenen Gedanken sowie sämtliche von Anderen direkt oder indirekt übernommenen Daten, Techniken und Materialien sind als solche kenntlich gemacht. Die Arbeit wurde bisher bei keiner anderen Hochschule zu Prüfungszwecken eingereicht.

Darmstadt, den 13.01.2017

Monika Steinlage

Table of Contents

EHRENWÖRTLICHE ERKLÄRUNG	II
TABLE OF CONTENTS	I
FIGURES	III
TABLES	V
ABBREVIATIONS	VI
PREFACE	IX
1 SUMMARY	X
2 INTRODUCTION	1
2.1 IONIZING RADIATION	1
2.1.1 COMPLEX DNA DAMAGE AND ITS DEPENDENCE ON LINEAR ENERGY TRANSFER	2
2.1.2 ANNUAL RADIATION EXPOSURE	3
2.2 DNA DAMAGE RESPONSE	4
2.2.1 REPAIR OF DOUBLE-STRAND BREAKS	4
2.2.2 CLASSICAL NON-HOMOLOGOUS END-JOINING	4
2.2.3 ALTERNATIVE NON-HOMOLOGOUS END-JOINING	6
2.2.4 HOMOLOGOUS RECOMBINATION	7
2.2.5 BIPHASIC DOUBLE-STRAND BREAK REPAIR KINETICS	9
2.3 AIM OF THE STUDY	10
3 MATERIALS AND METHODS	12
3.1 MATERIALS	12
3.1.1 LABORATORY CONSUMABLES	12
3.1.2 INSTRUMENTS AND DEVICES	12
3.1.3 SOFTWARE	13
3.1.4 CHEMICALS	13
3.1.5 siRNA	14
3.1.6 DNA VECTORS	15
3.1.7 TRANSFECTION REAGENTS AND KITS	16
3.1.8 INHIBITORS	17
3.1.9 PROTEIN STANDARD	17
3.1.10 ANTIBODIES	17
3.1.11 SOLUTIONS, BUFFERS AND MEDIA	18
3.1.12 CELL LINES AND BACTERIA	20
3.2 METHODS	22
3.2.1 PREPARATION OF 24-WELL PLATES WITH MYLAR BOTTOM	22
3.2.2 CELL CULTURE	23
3.2.3 TRANSFECTIONS AND INHIBITOR TREATMENTS	24
3.2.4 DNA DAMAGE INDUCTION	25
3.2.5 IMMUNOFLUORESCENCE STAINING	26
3.2.5.1 BrdU foci staining	27
3.2.5.2 Ku80 foci staining	27
3.2.5.3 Analysis	27
3.2.6 AMPLIFICATION OF DNA VECTORS	29
3.2.7 SDS-PAGE AND WESTERN BLOT	29

4	RESULTS	31
4.1	ARTEMIS AND CTIP	31
4.2	POLO-LIKE KINASE 3	40
4.3	NUCLEASES	48
4.4	53BP1 AND BRCA1	54
4.5	RESECTION IN G1 AFTER HIGH X-RAY DOSES	60
4.6	C-NHEJ OR ALT-NHEJ?	62
5	DISCUSSION	65
5.1	CTIP AND PLK3	66
5.2	ARTEMIS	68
5.3	DISTINCT NUCLEASE REQUIREMENTS FOR RESECTION IN G1	69
5.4	53BP1 AND THE BRCA1-CTIP INTERACTION IN G1	71
5.5	ERROR-PRONE REPAIR IS COMPLETED BY C-NHEJ IN G1	73
5.6	OUTLOOK	75
5.6.1	SIGNIFICANCE OF RESECTION-DEPENDENT C-NHEJ	75
5.6.2	FACTORS LIMITING END RESECTION IN G1	77
6	REFERENCES	80
7	APPENDIX	85
7.1	CURRICULUM VITAE	85
7.2	PUBLICATIONS	86
7.3	POSTER PRESENTATIONS	86
7.4	AUTHOR CONTRIBUTIONS	87
7.5	DANKSAGUNG	89

Figures

Figure 2.1 DNA damage distribution patterns after exposure to low LET vs. high LET radiation.....	3
Figure 2.2 Model for DSB repair by c-NHEJ.	6
Figure 2.3 Model for DSB repair by alt-NHEJ.....	7
Figure 2.4 (A) Model for DSB repair by HR. (B) Model for resection in G2.....	9
Figure 3.5 Preparation of 24-well plates with Mylar foil bottom.....	22
Figure 3.7. Identification of cell cycle phases using a semi-automated scanning system.	28
Figure 4.1 CtIP depletion rescues the Artemis repair defect in G1 after X-IR.....	32
Figure 4.2 Artemis and CtIP are required for repair of complex DSBs.....	34
Figure 4.3 Resection and repair of complex DSBs in G1 requires Artemis and CtIP.	36
Figure 4.4 Resection in G1 requires the Artemis endonuclease function.....	37
Figure 4.5 CtIP phosphorylation at Ser327 and Thr847 is required for G1 resection.....	38
Figure 4.6 Resection in G1 is not dependent on CDK2.....	39
Figure 4.7 Repair of complex DSBs is dependent on Plk1/3.....	40
Figure 4.8 Resection in G1 is dependent on Plk1/3.....	41
Figure 4.9 Plk3 promotes resection in G1.	42
Figure 4.10 Plk3 and ATM promote resection in G1.....	43
Figure 4.11 Plk3 phosphorylates CtIP at Ser327 and Thr847 in G1.	44
Figure 4.12 Resection in G1 requires the Plk3 PBD.....	46
Figure 4.13 Plk3 depletion rescues the Artemis repair defect in G1 after X-IR.	47
Figure 4.14 Formation of pATM foci after Mre11 inhibitor treatment.	49
Figure 4.15 Control experiments with Mre11 endonuclease and exonuclease inhibitors. ..	50
Figure 4.16 Resection in G1 requires specific nuclease activities.....	51
Figure 4.17 Depletion of Exo1, EXD2, or Mre11i exo treatment rescue the Artemis repair defect in G1 after X-IR.....	53
Figure 4.18 Depletion of 53BP1 causes hyper-resection in G1.	55

Figure 4.19 Brca1 accumulation at DSBs after X-IR and α -IR.....	57
Figure 4.20 Brca1 promotes resection and is required for displacement of 53BP1 in G1.	58
Figure 4.21 The Brca1 BRCT domain is required for resection in G1.....	58
Figure 4.22 Brca1 depletion rescues the Artemis repair defect in G1 after X-IR.	59
Figure 4.23 pRPA foci form in G1 after high doses of X-IR.	61
Figure 4.24 PARPi treatment does not affect DSB repair in G1.	62
Figure 4.25 Ku80 foci co-localize with pRPA foci in G1.	63
Figure 5.1 Plk3 binds to CtIP via its PBD.....	67
Figure 5.2 Speculative model for resection in G1.	70

Tables

Table 3.1 siRNA target sequences	14
Table 3.2 Inhibitors	17
Table 3.3 Primary Antibodies	17
Table 3.4 Secondary Antibodies	18
Table 3.6 siRNA transfection solutions	24
Table 3.7 jetPEI transfection solutions	25
Table 7.1 Author contributions "Plk3 regulates CtIP in G1"	87
Table 7.2 Author contributions "Resection occurs during NHEJ in G1"	88

Abbreviations

53BP1	p53 binding protein 1
A	Alanine
aa	Amino acid
alt-NHEJ	Alternative non-homologous end-joining
APS	Ammonium persulfate
ATM	Ataxia telangiectasia mutated
ATR	ATM-and Rad3-related
ATRIP	ATR interacting protein
BLM	Bloom syndrome mutated protein
bp	Base pair
Brca1/2	Breast cancer type 1/2 susceptibility protein
BRCT	Brca1 C-terminal
BrdU	5-bromo-2'-deoxyuridine
BSA	Bovine serum albumin
c-NHEJ	Classical non-homologous end-joining
CDK	Cyclin-dependent kinase
CDK	Cycline-dependent protein kinases
CDS	Clustered damage sites
Chk1/2	Checkpoint kinase 1/2
co-IP	Co-immunoprecipitation
CtIP	C-terminal binding protein-interacting protein
D-loop	Displacement loop
DAPI	4',6-diamidino-2-phenylindole
DDR	DNA damage response
DMEM	Dulbecco's Modified Eagle Medium
DMSO	Dimethyl sulfoxide
DNA	Deoxyribonucleic acid
DNA-PK	DNA-dependent protein kinase
DNA-PKcs	DNA-dependent protein kinase catalytic subunit
DSB	Double-strand break
dsDNA	Double stranded DNA
EDTA	Ethylenediaminetetraacetic acid
EdU	5-ethynyl-2'-deoxyuridine

Exo1	Exonuclease 1
FCS	Fetal calf serum
Gy	Gray
h	Hour
H4K20me2	Histone 4 dimethylated on lysine 20
HR	Homologous recombination
HRP	Horseradish peroxidase
hTert	Human Telomerase reverse transcriptase
IF	Immunofluorescence
IR	Ionizing radiation
K	Lysine
kDa	Kilo Dalton
keV	Kiloelectron volt
kV	Kilo volt
LET	Linear energy transfer
Lig1	Ligase I
Lig3	Ligase III
Lig4	Ligase IV
mA	Milli Ampere
mBq	Megabecquerel
MEF	Mouse embryonic fibroblasts
MEM	Minimum Essential Medium Eagle
MeV	Megaelectron volt
MilliQ	Purified water
min	Minutes
Mre11	Meiotic recombination 11
MRN	Mre11-Rad50-Nbs1
mSv	Millisievert
Nbs1	Nijmegen breakage syndrome 1
NEA	Non-essential amino acids
NHEJ	Non-homologous end-joining
nt	Nucleotide
OH	Hydroxyl
P	Phosphate
PAGE	Polyacrylamide gel electrophoresis

PAR	Poly(ADP-ribose)
PARP1	Poly(ADP-ribose) polymerase-1
PAXX	Paralog of XRCC4 and XLF
PBD	Polo-box domain
PBS	Phosphate buffered saline
PFA	Paraformaldehyde
Plk3	Polo-like kinase 3
PNKP	Polynucleotide kinase 3'phosphatase
PTIP	Pax transactivation domain-interacting protein
PVDF	Polyvinylidene difluoride
Rad51	Radiation repair protein 51
RBE	Relative biological effectiveness
Rif1	RAP1 interacting factor 1
RING	Really interesting new gene
RNA	Ribonucleic acid
RNase	Ribonuclease
RNF168	Ring finger protein 168
RNF8	Ring finger protein 8
RPA	Replication protein A
RT	Room temperature
S	Serine
SDS	Sodium dodecyl sulfate
sec	Second
siRNA	Small interfering RNA
SMART	Single-molecule analysis of resection tracks
SSB	Single-strand break
ssDNA	Single stranded DNA
T	Threonine
TBS	Tris buffered saline
V	Volt
V(D)J	Variable (diversity) joining
WB	Western blot
wt	Wild type
XLF	XRCC4-like factor
XRCC1/4	X-ray cross complementing protein 1/4

Preface

The purpose of this preface is to clarify the structure and concept of this thesis. A thesis in the biological sciences is typically divided into 4 sections: introduction, materials and methods, results and discussion. This thesis generally adheres to this structure; however, some adaptations have been implemented.

The results presented in the results section are structured in a way that each new aspect strongly builds on the last results and their conclusions. Therefore, to make it easier for the reader to follow the logical structure of the results section, it was necessary to include some discussion elements. The majority of results presented here were published as part of two peer-reviewed scientific papers. Therefore, the discussion section summarizes my results and discusses them in the context of other data that were included in the publications. The model that arose from the collaborative work for the publications is also presented and discussed in this section.

1 Summary

DNA double-strand breaks (DSBs) represent the most deleterious type of DNA damage as they pose a serious threat to genome integrity. Two major pathways are available for the repair of DSBs: canonical non-homologous end joining (c-NHEJ) and homologous recombination (HR). During c-NHEJ, the DSB ends are re-ligated after minimal end processing steps. The HR pathway is more complex and is initiated by CtIP-dependent DSB end resection to form 3' ssDNA overhangs for subsequent homology search in the sister chromatid. In wild type human G1-phase cells only c-NHEJ is available for DSB repair, as in this cell cycle phase the homologous sister chromatid required for HR is missing. DSB repair in G1, as well as in G2, shows biphasic kinetics consisting of a fast component that repairs the majority of breaks within the first few hours after damage induction, followed by a slow component that repairs the remaining breaks. The fast component in both G1 and G2 phase is well characterized and represents c-NHEJ, while the slow component in G2 represents repair by HR. Previous work has suggested that the slow repair component in G1 represents a sub-pathway of NHEJ that requires the activities of Artemis and ATM. However, the mechanism underlying the slow repair component in G1 is not fully understood and its characterization was the focus of this work.

To specifically study slow repair in G1, high LET α -particle radiation was used to induce complex DNA damages that are repaired with slow kinetics. RPA rapidly binds ssDNA in the cell to protect it from nucleolytic degradation and is phosphorylated in response to DNA damage. Exploiting the qualities of α -particle radiation, an assay was developed to monitor pRPA-foci formation in G1 and used as a tool to measure DSB end resection in this cell-cycle phase. Another approach to study the slow repair component was the quantification of γ H2AX foci, a histone modification in response to DSBs, at late time points post IR.

Collectively, it was shown that slowly repairing DSBs in G1 undergo resection and subsequent repair by c-NHEJ. This pathway is regulated by Plk3, which after DNA damage phosphorylates CtIP on amino acids Ser327 and Thr847 in G1. Using the pRPA assay, it was demonstrated that Plk3 phosphorylates CtIP on these amino acid residues to promote resection. CtIP phosphorylation on Ser327 also mediates its interaction with Brca1 in G1, which antagonizes 53BP1 to allow resection. The results indicate that the interaction of CtIP and Brca1 is required to promote resection in G1, while depletion of 53BP1 causes hyper-resection of DSBs

in G1. The primary function of Brca1 in G1 appears to be the displacement of 53BP1, similar to the mechanism in G2.

Furthermore, a number of nucleases required for G1 resection were identified. Similar to the process in G2, G1 resection requires the exonuclease activities of Exo1, EXD2 and Mre11. Contrary to G2, the endonuclease activity of Mre11 is dispensable in G1, as are the activities of BLM/DNA2. Thus, it is proposed that resection in G1 might be initiated from the break end and therefore differs from the mechanism in G2 where Mre11 endonuclease function initiates bi-directional resection several hundred nucleotides away from the break end. γ H2AX studies indicated that Artemis, an endonuclease which is specifically required for DSB repair during the slow component, functions downstream of the aforementioned factors. Thus, it is proposed that once resection is initiated in G1, resection intermediates have to be resolved by Artemis to complete repair.

Finally, the results indicate that break ends are rejoined via a c-NHEJ process, therefore it was hypothesized that the Ku70/80 heterodimer stays bound to the DSB ends throughout the entire repair time and translocates inwards to expose DNA ends for resection while at the same time limiting the process. Immunofluorescence data support this notion by providing evidence that Ku80 co-localizes with pRPA in G1. Compared to resection in G2, which is always followed up by error-free repair via HR, resection in G1 needs to be much more limited in length. Future work will focus on the elucidation of the mechanisms restricting the extent of resection in G1.

DNA-Doppelstrangbrüche (DSBs) zählen zu den schwerwiegendsten DNA Schäden, da sie die Integrität des Genoms gefährden. Für die Reparatur von DSBs stehen zwei Hauptreparaturwege zur Verfügung: die klassische nicht-homologe Endverknüpfung (c-NHEJ) und die homologe Rekombination (HR). Beim c-NHEJ werden die DSB-Enden nach minimalen Prozessierungsschritten wieder zusammengesetzt. Die HR ist ein komplexerer Prozess, der mit dem CtIP-abhängigen nukleolytischen Verdau des 5'-Endes beginnt, um einen 3'-einzelsträngigen Überhang für die Homologiesuche im Schwesterchromatid zu erzeugen. In humanen Wildtyp-Zellen, die sich in der G1-Phase befinden, können DSBs nur durch das c-NHEJ repariert werden, da in dieser Zellzyklusphase das homologe Schwesterchromatid, welches für die HR gebraucht wird, nicht zur Verfügung steht.

Die DSB-Reparatur in G1 und G2 weist eine biphasische Reparaturkinetik auf. Diese besteht aus einer schnellen Reparaturkomponente, in der die Mehrheit der Brüche innerhalb der ersten paar Stunden nach Schadensinduktion repariert wird, gefolgt von einer langsamen Reparaturkomponente. Die schnelle Komponente in G1 und in G2 stellt die Reparatur durch das c-NHEJ dar, während Brüche in der langsamen Komponente in G2 mittels HR repariert werden. Frühere Studien konnten zeigen, dass die langsame Komponente einen Unterweg des NHEJ darstellt, der Artemis- und ATM-Funktionen benötigt. Desweiteren konnte gezeigt werden, dass CtIP auch eine Rolle bei der Reparatur in der G1-Phase spielt, der genaue Mechanismus der langsamen Reparatur in G1 war jedoch unklar. Daher lag der Fokus dieser Arbeit darauf, die langsame Reparaturkomponente in G1 zu charakterisieren.

Um die langsame Reparaturkomponente gezielt zu untersuchen, wurde in dieser Arbeit α -Teilchen-Strahlung genutzt, um komplexe DNA-Schäden zu erzeugen, die mit langsamer Kinetik repariert werden. RPA bindet schnell an entstehende einzelsträngige DNA in der Zelle, um diese vor nukleolytischem Verdau zu schützen und wird nach Bestrahlung phosphoryliert. Die Eigenschaften von α -Teilchen-Strahlung wurden genutzt, um einen Ansatz zu entwickeln, mithilfe dessen es möglich war pRPA-Foci in G1 zu messen. Diese Methode wurde genutzt, um die Resektion von DSB-Enden in der G1-Phase zu untersuchen. Eine weitere Methode, mit welcher die langsame Reparaturkomponente in G1 untersucht wurde, war die Quantifizierung von γ H2AX-Foci zu späten Zeitpunkten nach Bestrahlung. γ H2AX ist eine Histonmodifikation, die um einen DSB herum auftritt.

In dieser Arbeit konnte gezeigt werden, dass langsam reparierende DSBs in G1 resektiert werden und anschließend mittels c-NHEJ repariert werden. Dieser Reparaturweg wird von Plk3 reguliert, welche nach DNA-Schadensinduktion in G1 CtIP an den Aminosäuren Ser327 und Thr947 phosphoryliert. Mithilfe von pRPA-Focimessungen konnte gezeigt werden, dass CtIP an diesen Aminosäuren von Plk3 phosphoryliert werden muss, um Resektion zu gewährleisten. Desweiteren ermöglicht die Phosphorylierung von CtIP an Ser327 auch eine Interaktion mit Brca1 in G1. Brca1 wird gebraucht, um 53BP1 in G1 zu antagonisieren. Die Interaktion zwischen CtIP und Brca1 wird für die Resektion in G1 benötigt, während eine Depletion von 53BP1 zu erhöhter Resektion führt. Die Funktion von Brca1 in G1 scheint die Verdrängung von 53BP1 vom Bruchende zu sein, ähnlich wie es für G2 beschrieben wurde.

Desweiteren wurden eine Reihe Nukleasen identifiziert, die an der Resektion in G1 beteiligt sind. Ähnlich wie in G2 werden die Exonuklease-Funktionen von Exo1, EXD2 und Mre11 für die Resektion in G1 benötigt. Im Gegensatz zu G2 sind BLM/DNA2 und die Endonuklease-

Funktion von Mre11 dagegen nicht an der Resektion in G1 beteiligt. Daher ist es denkbar, dass die Resektion in G1 vom Bruchende initiiert wird. Der Mechanismus ist somit anders als in G2, wo die Endonuklease-Funktion von Mre11 die bi-direktionale Resektion mehrere hundert Nukleotide entfernt vom Bruchende initiiert. γ H2AX-Studien haben gezeigt, dass Artemis downstream der bisher erläuterten Faktoren wirkt. Daher wird ein Modell vorgeschlagen, in dem die durch Resektion entstandenen Intermediate von Artemis aufgelöst werden müssen um die Reparatur abzuschließen.

Abschließend konnte gezeigt werden, dass die Bruchenden durch c-NHEJ zusammengefügt werden. Daher wurde postuliert, dass der Ku70/80-Heterodimer während der gesamten Reparaturzeit am Bruchende sitzt und sich langsam vom Bruchende wegbewegt, um die DNA-Enden für die Resektion freizugeben und gleichzeitig die Resektionslänge zu begrenzen. Diese Hypothese wurde durch Immunfluoreszenzbilder von kolocalisierenden Ku80- und pRPA-Foci in G1 unterstützt. Im Vergleich mit Resektion in G2, auf die immer die fehlerfreie HR folgt, muss die Resektionslänge in G1 limitiert sein. Weitere Studien werden sich damit befassen, wie die Resektion in G1 begrenzt wird.

2 Introduction

Living organisms are continuously exposed to a variety of different factors that can damage the deoxyribonucleic acid (DNA) and its inherent genetic blueprint. Thus, the preservation of the information stored in the DNA is of fundamental importance for the integrity of the genome.

One of the most deleterious DNA damages is the DNA double-strand break (DSB). This type of damage represents a particularly critical threat to the structural and genetic integrity of the genome because the sugar-phosphate backbone of the DNA molecule is completely severed on both strands. Unrepaired or incorrectly repaired DSBs can have serious consequences for the organism as they can lead to an accumulation of mutations and genomic rearrangements which can ultimately result in cell death, carcinogenesis, or the propagation of mutations to subsequent generations (Hiom 2010).

DSBs arise in cells as a byproduct of regular physiological processes such as meiosis, DNA replication, and V(D)J recombination. Moreover, a number of exogenous factors can lead to the formation of DSBs, including ionizing radiation (IR) and certain chemotherapeutic drugs (Hiom 2010; Goodarzi & Jeggo 2013; Mehta & Haber 2014).

2.1 Ionizing radiation

Ionizing radiation (IR) comprises all types of radiation that harbor enough energy to cause the ionization of an atom, i.e. the removal of an electron from its outer electron shell. The vast spectrum of IR encompasses electromagnetic radiation (e.g. X-rays, gamma rays), and particle radiation (e.g. alpha and beta particles). Alpha particles, a type of particle radiation, consist of two protons and two neutrons, making them structurally identical to a helium nucleus. They harbor a double positive charge and therefore have a high potential to cause ionizations when interacting with matter. The penetration depth of alpha particles is very low, only about 40 μm in tissue (Stap et al. 2008), therefore this type of radiation can be shielded by a single piece of paper. Alpha particles consequently only pose a threat to human health when the particles are inhaled or ingested, as the skin normally provides a sufficient barrier.

When IR interacts with cells or biological tissues it can cause direct ionizations through the direct interaction of IR with molecules in the cell. Furthermore, IR can cause ionizations indirectly when hydroxyl radicals, which are generated during the radiolysis of water, attack

the DNA. Due to the high amount of intracellular water, indirect ionizations usually account for the majority of DNA damages in living cells. A variety of different lesions including sugar and base damages can be generated. Some types of sugar damages can result in the disruption of the DNA backbone, leading to single-stranded DNA breaks (SSBs). DSBs then occur when two SSBs coincidentally arise in close proximity on opposite DNA strands. Even though sugar and base damages outnumber DSBs by approximately 20:1 (Schipler & Iliakis 2013), DSBs are among the most hazardous DNA lesions due to the high risk that genetic information is lost.

2.1.1 Complex DNA damage and its dependence on linear energy transfer

The biological effect of X-rays or charged particles can be very different due to the different energy deposition patterns of these radiation types. Linear energy transfer (LET) is defined as the energy loss per unit path length of a charged particle, i.e. the amount of energy that is released within a certain distance. The LET varies over the particle trajectory: as the velocity of a particle decreases near the end of its range, the LET increases. Therefore, more energy is deposited, causing more damages in the surrounding tissue. Charged particles (such as α -particles) that have a high LET are therefore densely ionizing, while photon radiation (such as X-rays) has a low LET and is sparsely ionizing (Asaithamby & Chen 2011) (figure 2.1).

The simplest DSB type retains the 5'-phosphate (5'-P) and 3'-hydroxyl (3'-OH) groups required for simple re-ligation at the DSB ends. However, such uncomplicated DSB termini are rarely found after IR. DSBs induced by IR generally do not have easily ligatable "clean" ends. X-ray IR (X-IR)-induced DSBs often suffer collateral damage to DSB ends, resulting in 5'-OH or 3'-phosphoglycolate groups that make end processing before ligation necessary (Schipler & Iliakis 2013). High LET radiation adds another level of damage complexity that derives from a clustering of DSBs and other DNA damages within a few helical turns of the DNA. So-called clustered damage sites (CDS) result from high LET α -particle IR (α -IR), for instance, because this type of IR causes more ionizations along the particle track than low-LET X-rays (Schipler & Iliakis 2013, figure 2.1). In this thesis, α -IR-induced DSBs will be referred to as "complex DSBs" compared to "simple" X-IR-induced DSBs, based on the occurrence of CDS after α -IR.

Hence, DNA damage caused by high LET radiation is more clustered and complex than damage caused by low LET radiation. As the LET of the radiation increases, the damage complexity, i.e. the density of different types of DNA lesions, also increases, making the repair

of the lesions progressively more difficult (Okayasu 2012; Asaithamby et al. 2011). Heightened break complexity is also linked to an increasing occurrence of chromosome aberrations. Hence, high LET radiation is highly mutagenic and contributes significantly to genomic instability (Hada & Georgakilas 2008; Asaithamby et al. 2011).

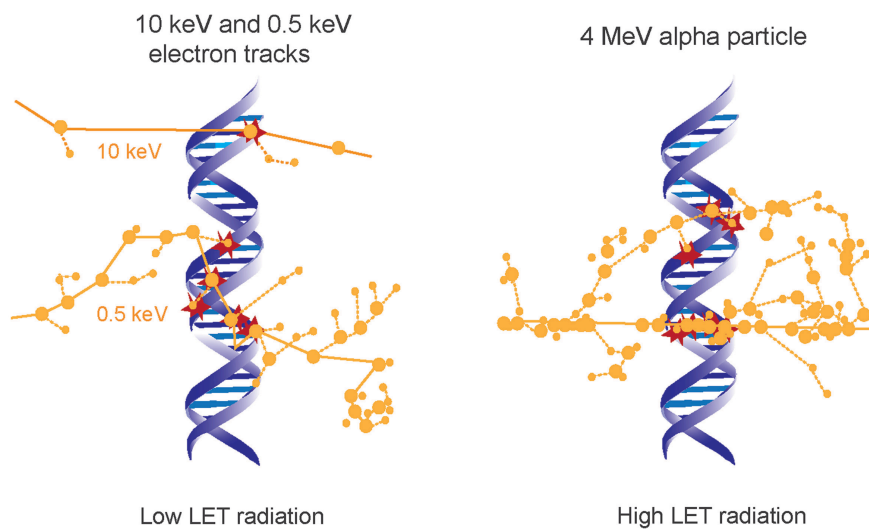


Figure 2.1 DNA damage distribution patterns after exposure to low LET vs. high LET radiation. Induction of clustered DNA damage after alpha-particle irradiation is visible along the particle tracks. Large dots indicate ionizations, smaller dots indicate excitations along the radiation track (Schipler & Iliakis 2013).

2.1.2 Annual radiation exposure

The human body is continuously exposed to different types of IR. It is estimated that the average radiation exposure for people living in Germany amounts to approximately 4 millisievert (mSv) per annum. This amount is composed of natural background radiation (2.1 mSv) and artificial man-made radiation (1.9 mSv). Inhalation of radon, a naturally occurring radioactive noble gas which emits alpha particles during its decay, makes up more than half (1.1 mSv) of the background radiation (Strahlenschutzkommission 2013). While it is difficult to estimate an individual person's annual radiation exposure, due to confounding factors such as living location and employment, it is evident that alpha particle radiation represents a substantial part of the background radiation for everyone.

Moreover, radiation not only triggers carcinogenesis but is also used to treat cancer. The use of heavy-ion radiotherapy has been gaining importance worldwide (Sage & Harrison 2011). Thus, understanding the mechanism underlying the repair of complex DNA damages is crucial

not only due to background radiation exposure, but also for long-term risk assessment after high LET cancer therapy (Newhauser & Durante 2011).

2.2 DNA damage response

It is estimated that each cell in the body incurs an average of ten DSBs per day (Lieber 2010). Thus, to maintain genomic integrity, cells rapidly detect DNA damages and initiate the appropriate response mechanisms. The removal of damages from the genome by the activation of repair pathways stands at the center of the DNA damage response (DDR). To prevent progression into the next cell cycle phase with unrepaired damages, cell-cycle checkpoints are activated to allow prolonged time for repair. Programmed cell death (apoptosis) is initiated when the damages are irreparable. This process removes severely damaged cells from tissues to prevent mutagenesis (Sancar et al. 2004).

In response to DSBs, the histone variant H2AX is rapidly phosphorylated on serine 139, forming γ H2AX (Rogakou et al. 1998). The phosphorylation of H2AX is mediated by the kinases Ataxia telangiectasia mutated (ATM), ATM-and Rad3-related (ATR) and DNA-dependent protein kinase (DNA-PK) and it extends several megabase chromatin domains around the DSB (Rogakou et al. 1999). This histone modification can be easily visualized and quantified by immunofluorescence (IF) staining and it provides a sensitive tool to monitor DSB induction and repair on a single cell level (Löbrich et al. 2010).

2.2.1 Repair of double-strand breaks

The two major repair pathways available for the repair of DSBs are classical non-homologous end joining (c-NHEJ) and homologous recombination (HR). Alternative NHEJ (alt-NHEJ) is a backup pathway that is activated when c-NHEJ is not functional.

2.2.2 Classical non-homologous end-joining

During c-NHEJ, break ends are re-ligated without the requirement for a homologous template. This repair pathway is fast, efficient, and active throughout the entire cell cycle. The majority of DSBs (approximately 80%) in G1 and G2 are repaired by c-NHEJ (Beucher et al. 2009). Limited DSB end processing may be required before ligation, depending on the structure of

the break end, potentially resulting in the loss of some nucleotides (nt). Thus, NHEJ harbors the potential for erroneous repair (Davis & Chen 2013).

C-NHEJ is initiated by the rapid binding of the Ku heterodimer to DSB ends. This highly abundant nuclear protein, which consists of two subunits, Ku70 and Ku80, protects the DNA ends from nucleolytic degradation and forms a scaffold for the subsequent recruitment of other NHEJ proteins (Grundy et al. 2014; Goodarzi & Jeggo 2013). Ku recruits DNA protein kinase catalytic subunit (DNA-PKcs), forming the DNA-PK holoenzyme, which functions to tether the broken DNA ends together (figure 2.2). Subsequently, the ends of the DSB may undergo limited end processing if simple re-ligation is not possible. For instance, break ends that contain a 3'-P or a 5'-OH group preclude direct ligation and thus require end processing steps to produce compatible break ends (Schipler & Iliakis 2013).

A number of different factors are involved in the end processing steps of NHEJ, including polynucleotide kinase 3' phosphatase (PNKP) and Artemis. PNKP harbors kinase and phosphatase activity to generate 5'-P ends or remove 3'-P ends, respectively (Davis & Chen 2013; Goodarzi & Jeggo 2013).

Artemis, a member of the metallo- β -lactamase superfamily of nucleases, has endonuclease activity at DNA hairpins as well as at 5' or 3' single-stranded DNA (ssDNA) overhangs. The endonuclease activity of Artemis is dependent on its interaction with autophosphorylated DNA-PKcs. Artemis binds directly to DNA-PKcs and gains endonuclease activity when DNA-PKcs is autophosphorylated, presumably because DNA-PKcs autophosphorylation causes a conformational change in the DNA-PK holoenzyme, exposing the ideal substrate structure (ssDNA-dsDNA junction) for Artemis to cut. After autophosphorylation, DNA-PKcs loses its kinase activity and dissociates from the break ends (Chan et al. 2002; Goodarzi et al. 2006). A recent study has provided evidence that Artemis also possesses intrinsic 5'-exonuclease activity *in vitro*, which is independent of DNA-PKcs (Li et al. 2014). Artemis was originally described for its role during V(D)J recombination in developing lymphocytes where physiological DSBs are formed. In this process, the DNA-PKcs-Artemis complex is required for the opening of RAG-complex-generated DNA hairpin intermediates (Moshous et al. 2001; Ma et al. 2002). As V(D)J recombination is part of the adaptive immune response, patients with mutations in the Artemis gene do not have any T- or B-lymphocytes and suffer from *severe combined immunodeficiency* (SCID) (Moshous et al. 2001; Chang & Lieber 2016). Aside from its function during V(D)J recombination, Artemis is also required for the repair of a subset of IR-induced DSBs (Riballo et al. 2004).

During the final step of c-NHEJ, the DSB ends are ligated. This step is carried out by ligase IV (Lig4), which is stabilized by X-ray cross complementing protein 4 (XRCC4) and stimulated by XRCC4-like factor (XLF) (figure 2.2). Paralog of XRCC4 and XLF (PAXX) is a newly identified member of the XRCC4-superfamily that interacts directly with Ku and promotes Ku-dependent ligation (Ochi et al. 2015). After ligation, Ku becomes trapped on DNA strands due to its ring-like structure, so it is eventually polyubiquitinated to signal its degradation by the proteasome (Davis & Chen 2013).

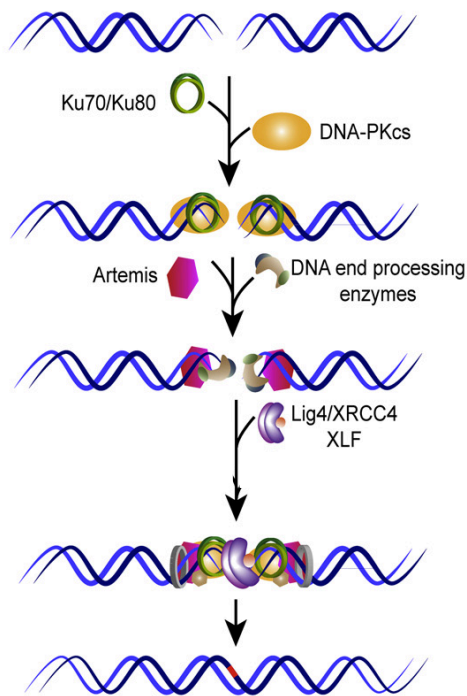


Figure 2.2 Model for DSB repair by c-NHEJ. The DSB ends are immediately bound by Ku70/80, which recruits DNA-PKcs, forming DNA-PK. After limited end processing by Artemis and other end processing enzymes, the DNA ends are ligated by Lig4, XRCC4, and XLF (modified from Iliakis et al. 2015).

2.2.3 Alternative non-homologous end-joining

Alt-NHEJ serves as a backup pathway that only becomes active when cells are lacking the core c-NHEJ protein Ku (Mansour et al. 2013). Consequently, in wild type (wt) cells, this pathway does not contribute to DSB repair

Alt-NHEJ requires the activity of poly(ADP-ribose) polymerase-1 (PARP1) (Wang et al. 2006). PARP enzymes are highly abundant nuclease proteins that catalyze the post-transcriptional modification poly(ADP-ribosyl)ation (PARylation), i.e. the covalent attachment of PAR

polymers to target proteins. PARP1 is one of three PARPs implicated in the DDR and has high affinity for SSBs and DSBs. PARP1 also has a well described role during SSB repair and plays a role at replication-dependent DSBs (Pines et al. 2013).

Alt-NHEJ repair is slow and involves DSB end resection at the break site, which is dependent on C-terminal binding protein- interacting protein (CtIP) and meiotic recombination 11 (Mre11). This can result in large deletions of up to 100 base pairs (bp), therefore alt-NHEJ is highly mutagenic (Mansour et al. 2010). The ligation step requires ligase I or III (Lig1, Lig3) and X-ray cross complementing protein 1 (XRCC1) (figure 2.3).

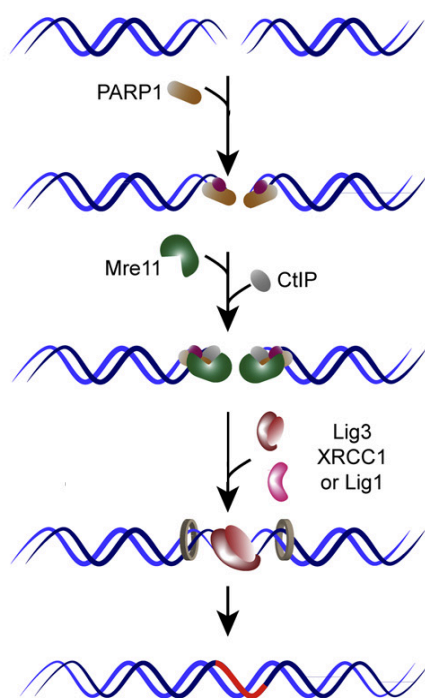


Figure 2.3 Model for DSB repair by alt-NHEJ. PARP1 is rapidly recruited to the DSB ends. After limited CtIP- and Mre11-dependent end resection, DNA ends are ligated by Lig1, Lig3, and XRCC1 (modified from Iliakis et al. 2015).

2.2.4 Homologous Recombination

The second major pathway for DSB repair is homologous recombination (HR). As opposed to NHEJ, which functions throughout the entire cell cycle, HR is only active during late S- and G2 phase because it requires a homologous template, usually the sister chromatid, for repair synthesis. HR is a slower process compared to c-NHEJ, but since it uses a template for strand synthesis, it is regarded as an error-free repair mechanism (Thompson 2012).

The first step of HR is the 5' to 3' nucleolytic degradation of the DSB end, also known as DSB end resection, yielding a 3' ssDNA tail. End resection is initiated by the dsDNA endonuclease activity of Mre11, which is promoted by CtIP (Cannavo & Cejka 2014). The initial endonucleolytic incision (made by Mre11 endonuclease) is located up to 300 nt away from the DSB (Garcia et al. 2011) and followed by bidirectional resection (figure 2.4B). Mre11 exonuclease, which has 3'-5' polarity, resects towards the DSB end. Recently, EXD2 was identified as a novel nuclease that promotes end resection and HR in G2. EXD2 interacts with CtIP and has 3'-5' polarity. Thus, EXD2 was postulated to promote the generation of ssDNA downstream of Mre11 endonuclease where it collaborates with Mre11 exonuclease (Broderick et al. 2016). Exonuclease 1 (Exo1) or BLM/DNA2 have 5' to 3' polarity and resect away from the break end (Mimitou & Symington 2009; Gravel et al. 2008). The single-stranded DNA-binding protein replication protein A (RPA) rapidly coats the 3' ssDNA strand that emerges to protect it from degradation (figure 2.4A). RPA is a heterotrimeric protein composed of three subunits, of which the 32-kDa subunit becomes hyper-phosphorylated in response to DNA damage (Binz et al. 2004). Breast cancer type 2 susceptibility protein (Brca2) then replaces RPA with radiation repair protein 51 (Rad51), forming the Rad51 nucleoprotein filament needed for homology search in the sister chromatid. Once the Rad51 nucleoprotein filament invades the double-stranded donor molecule, a D-loop is formed (Mazón et al. 2010; Goodarzi & Jeggo 2013). During the subsequent repair synthesis the DNA strand is elongated by DNA polymerases, using the homologous sequence as a template (figure 2.4A). Finally, the resulting Holliday junction is dissolved creating crossover or non-crossover products depending on the location where they are cut (Ciccica & Elledge 2010).

The tumor suppressor breast cancer type 1 susceptibility protein (Brca1) plays a pivotal role in maintaining genome stability: germline mutations in the BRCA1 gene have been linked to early-onset familial breast and ovarian cancers (Christou & Kyriacou 2013). The role of Brca1 in HR is well established. Brca1 forms at least four distinct protein complexes and as part of these macromolecular complexes, Brca1 is recruited to DSBs and the surrounding chromatin at different stages of HR (Savage & Harkin 2015). In S/G2, CtIP is constitutively phosphorylated on residues Ser327 and Thr847 in a CDK-dependent manner and Brca1 interacts with CtIP at pSer327 via its C-terminal BRCT domain (Yu & Chen 2004; Huertas & Jackson 2009). The Brca1-C complex, composed of Brca1, CtIP and the Mre11-Rad50-Nbs1 (MRN) complex is rapidly recruited to DSBs and promotes end resection in S/G2 (Clark et al. 2012; Christou & Kyriacou 2013; Escribano-Díaz et al. 2013). As part of the Brca1-A complex

(Brca1, Rap80 and Abraxas), Brca1 is also recruited to DSBs at later times after damage induction to block aberrant resection (Savage & Harkin 2015).

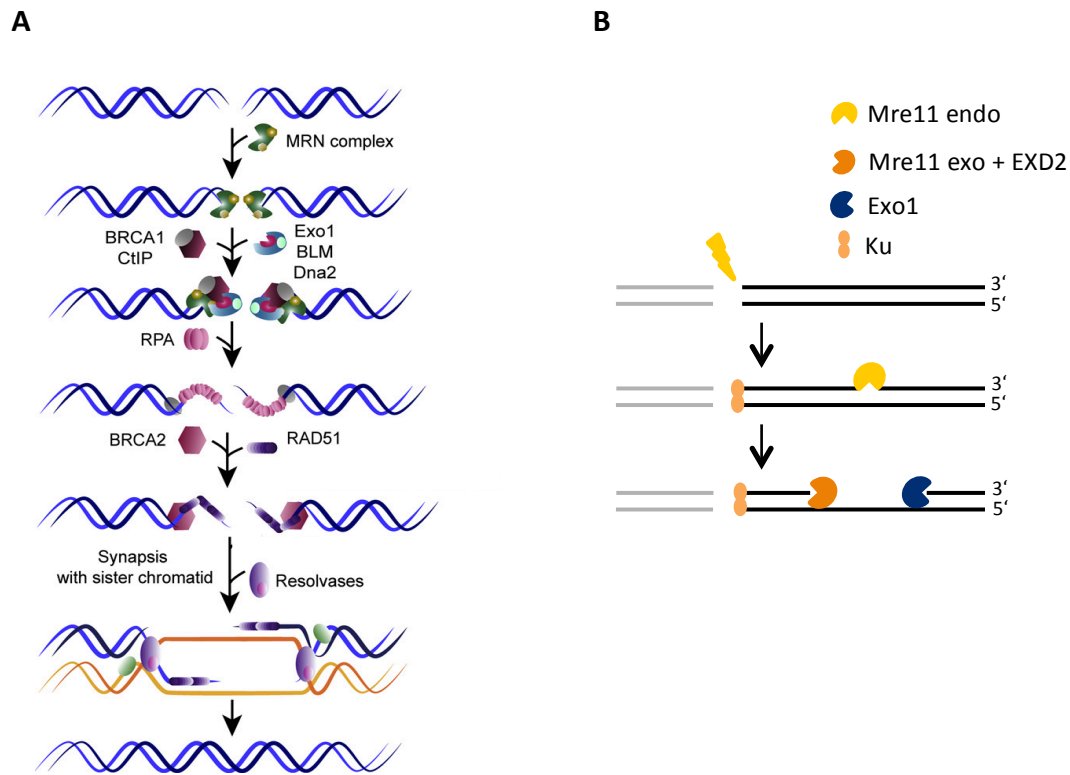


Figure 2.4 (A) Model for DSB repair by HR. DNA end resection generates a 3' ssDNA overhang, which is coated by RPA. Rad51 replaces RPA, forming the Rad51 nucleoprotein filament. Homology search in the sister chromatid is followed by DNA synthesis using the homologous template (modified from Iliakis et al. 2015). **(B) Model for resection in G2.** Resection is initiated by the endonuclease activity of Mre11. Resection then ensues bi-directionally: Mre11 exonuclease together with EXD2 resects towards the break end (3' to 5' direction) and Exo1 carries out long-range resection away from the break end (5' to 3' direction) (Biehs et al. 2017).

2.2.5 Biphasic double-strand break repair kinetics

DSB repair in G1 and G2 displays biphasic kinetics. During the first two hours after damage induction the majority of DSBs (approximately 80%) in both cell cycle phases are repaired via c-NHEJ (Beucher et al. 2009). The remaining 20% of DSBs are repaired with slow kinetics in the following hours. In G2, slow repair is channeled into the HR pathway and requires ATM and the endonuclease activity of Artemis (Beucher et al. 2009). In G1, the slow repair component also requires Artemis and ATM signaling but the breaks are rejoined using a sub-pathway of NHEJ (Riballo et al. 2004).

One of the reasons why lesions are repaired with slow kinetics is DSB localization in the heterochromatin. Heterochromatic breaks require ATM signaling to phosphorylate Kap-1 for chromatin relaxation and subsequent access for repair proteins (Goodarzi et al. 2008). Another factor influencing repair speed is break end complexity. Complex DSBs are particularly difficult to repair because DNA lesions are clustered in close proximity, thus complex DSBs are repaired with slower kinetics than DSBs induced by low LET radiation (Riballo et al. 2004; Okayasu 2012; Shibata et al. 2011).

2.3 Aim of the study

In S and G2 phase, HR plays a major role in the repair of complex damages. Due to highly complex lesions at the DSB end, it was hypothesized that extensive end resection followed by HR would be the most feasible way for cells to deal with the damage (Zafar et al. 2010). Indeed, DSB complexity has been linked to a higher propensity to undergo resection in G2 (Yajima et al. 2013; Shibata et al. 2011).

But what happens to complex lesions in G1 where HR is not available for repair? Zafar et al. hypothesized that complex breaks in G1 stay unrepaired and are eventually processed in S phase when HR becomes available (Zafar et al. 2010). Other studies, however, observed that complex DSBs in G1 are completely repaired to background level only with much slower kinetics (Riballo et al. 2004). Moreover, Riballo et al. showed that the endonuclease activity of Artemis is indispensable for the repair of complex breaks, suggesting an increased requirement for end processing before ligation. Furthermore, increasing evidence suggested that CtIP also plays a role during repair in G1. CtIP-dependent repair occurs in G1 wt chicken cells (Yun & Hiom 2009) and CtIP plays a role during the repair of etoposide-induced DSBs in G1 (Quennet et al. 2011). Due to the higher propensity for complex lesions to undergo resection in G2 and the increasing evidence that CtIP also plays a role in G1, it was speculated that the slow repair component in G1 involves limited end resection. Studying DSB repair in G1 phase is of particular importance because the majority of cells in the human body are post-mitotic. Therefore, error-free HR is not available in most somatic cells and complex damages incurred by radon inhalation, for instance, have to be repaired by NHEJ. Therefore, the aim of this study was to characterize the slow repair component in G1.

To specifically study the slow repair component, the high LET qualities of alpha particles were exploited. This type of radiation induces highly complex lesions, which are not easily religated during the fast repair component. Thus, the repair of alpha-particle-induced DSBs ensues with slow kinetics providing the ideal conditions to study this repair component in G1.

3 Materials and Methods

3.1 Materials

3.1.1 Laboratory consumables

Blotting paper, 703	VWR
Cell culture dishes (35x10 mm, 60x15 mm)	nunc™ VWR
Cell culture flasks (25 cm ² , 75 cm ²)	TPP
Cover slips	Roth
Centrifuge tubes (15 ml, 50 ml)	Greiner
Imaging Plate 24 FC (24-well plates)	MoBiTec
Immersion oil	Zeiss
KimWipes	NeoLab
Micro tubes (Eppis)	Roth
Microscope slides, superfrost	Roth
Mylar® polyester film (2 μm)	DuPont Teijin Films
Parafilm	Bemis
Pasteur pipets, glas	Roth
Pasteur pipets, plastic	Roth
Pipet tips	Sarstedt
Pipet tips, filtered	Roth
PVDF membrane	Thermo Scientific
UHU Plus Endfest (epoxy 2-component glue)	UHU

3.1.2 Instruments and devices

²⁴¹ Americium α-source		Amersham-Buchler
Camera system (microscope)	AxioCam MRm	Zeiss
Centrifuge	5415 R/5804 R	Eppendorf
Centrifuge	Biofuge pico	Heraeus
Cell counting chamber	Neubauer improved	Marienfeld Superior
Chemiluminescence detection	ChemiSmart 5000	Vilber Lourmat
Chemiluminescence detection	Fusion FX	Vilber Lourmat
Microscope	Axiovert 200M	Zeiss
Microscope	Imager.Z2	Zeiss



Microscope (cell culture)	Eclipse TS100	Nikon
Nanophotometer	P-Class	Implen
pH Meter	pMX2000	WTW
Power supply	PowerPac™HC	BIO-RAD
Scale	TE 1502S/TE 153S-DS	Sartorius
Thermomix	Comfort	Eppendorf
Ultrasound bath	1083	GFL
Vortex	Vortex genie2	Scientific Industries
Water bath	1083	GFL
Western blotting system	Mini Trans-Blot® Cell	BIO-RAD
X-Ray tube	MCN 165/796704	Philips

3.1.3 Software

AxioVision V4.6.3.0	Zeiss Imaging Solutions
ChemiCapt	Vilber Lourmat
FusionCapt Advance FX7	Vilber Lourmat
ImageJ	Open Source
Metafer	MetaSystems

3.1.4 Chemicals

Agar	Roth
APS	Roth
Bromophenol blue	Roth
BSA	AppliChem
BrdU (1 mM)	BD Bioscience
DAPI	Sigma-Aldrich
DMSO	Sigma-Aldrich
EDTA	Roth
EdU (10 mM)	Invitrogen
Ethanol, denatured	Roth
Formaldehyde	Roth
Glycerin	Roth
Glycine	Roth
HCl	Roth



Isopropanol	Roth
KCl	Roth
KH ₂ PO ₄	Roth
Methanol	Roth
MgCl ₂	Roth
Mounting medium	Vectashield® Axxora Alexis
Nonfat-dried milk	Reformhaus
Na ₂ HPO ₄	Roth
NaCl	Roth
NaOH	Roth
PFA	Roth
PhosStop 10x	Roche
PIPES	Roth
Proteaseinhibitor 25x Complete	Roche
RNase A	Sigma-Aldrich
SDS	Roth
Sodium deoxycholate	Roth
Sucrose	Roth
TEMED	Roth
Tris	Roth
TritonX-100	Roth
Trypsin	Roth
Tween®20	Roth
β-Mercaptoethanol	Sigma-Aldrich

3.1.5 siRNA

Table 3.1 siRNA target sequences

siRNA	Sequence	Concentration	Vendor
Negative control	5' AATTCTCCGAACGTGTCACG 3'	25 nM	Qiagen
Artemis (human)	5' AACTGAAGAGAGCTAGAACAG 3'	25 nM	Qiagen
Artemis (mouse)	5' AAGGATCACATGAAAGGATTA 3'	25 nM	Qiagen
Brca1_14	5' CAGGAAATGGCTGAACTAGAA 3'	25 nM	Qiagen
Brca1 (construct)	5' AATCACAGTGTCTTTATGTA 3'	25 nM	Qiagen
BLM	5' AAGCTAGGAGTCTGCGTGCGA 3'	50 nM	Qiagen
CtIP	5' TCCACAACATAATCCTAATTT 3'	50 nM	Qiagen

CtIP (2)	5' AAGCTAAAACAGGAACGAATC 3'	50 nM	Qiagen
DNA2	5' AAATAGCCAGTAGTATTTCGAT 3'	25 nM	Qiagen
EXD2	Smartpool	25 nM	Dharmacon
Exo1	5' CAAGCCTATTCTCGTATTTTT 3'	50 nM	Qiagen
Plk1_2	SI00071624	25 nM	Qiagen
Plk1_6	SI02223837	25 nM	Qiagen
Plk3	5' CTGCATCAAGCAGGTTCACTA 3'	25 nM	Qiagen
Plk3_1	SI00059388	25 nM	Qiagen
Plk3_11	SI05056450	25 nM	Qiagen
53BP1	5' GAGAGCAGATGATCCTTTA 3'	25 nM	Dharmacon
53BP1 (construct)	5' AGAACGAGGAGACGGUAAUAGUGGG 3'	25 mM	Qiagen

3.1.6 DNA vectors

GFP	Vector for GFP expression in mammalian cells; pEGFP-C1, purchased from Clontech
GFP_CtIP wt	siRNA resistant vector for expression of GFP-tagged wt CtIP; pEGFP_CtIP wt_C1, (Barton et al. 2014)
GFP_CtIP S327A	siRNA resistant vector for expression of GFP-tagged CtIP with Ser327 mutated to Ala327 (phosphomutant); pEGFP_CtIP S327A_C1, (Barton et al. 2014)
GFP_CtIP S327E	siRNA resistant vector for expression of GFP-tagged CtIP with Ser327 mutated to Glu327 (phosphomimic); pEGFP_CtIP S327E_C1, (Barton et al. 2014)
GFP_CtIP847A	siRNA resistant vector for expression of GFP-tagged CtIP with Thr847 mutated to Ala847 (phosphomutant); pEGFP_CtIP847A_C1 (Barton et al. 2014)
GFP_CtIP847E	siRNA resistant vector for expression of GFP-tagged CtIP with Thr847 mutated to Glu847 (phosphomimic); pEGFP_CtIP847E_C1, (Barton et al. 2014)
GFP_CtIP327E/847E	siRNA resistant vector for expression of GFP-tagged CtIP with Ser327 mutated to Glu327 and Thr847 mutated to Glu847 (double-phosphomimic); pEGFP_CtIP327E/847E_C1, (Barton et al. 2014)



cMyc_Artemis wt	siRNA resistant vector for expression of cMyc-tagged wt Artemis; pCIneo-cmyc_Artemis wt (Beucher et al. 2009)
cMyc_Artemis D37N	siRNA resistant vector for expression of cMyc-tagged Artemis with Asp37 mutated to Asn37 (endonuclease deficient); pCIneo-cmyc_Artemis D37N, (Beucher et al. 2009)
FLAG_Plk3 wt	siRNA resistant vector for expression of FLAG-tagged wt Plk3; Gateway LR Clonase Enzyme mix kit purchased from Life Technologies (Barton et al. 2014)
FLAG_Plk3 Δ PBD	siRNA resistant vector for expression of FLAG-tagged Plk3 with a deleted polo-box domain; Gateway LR Clonase Enzyme mix kit purchased from Life Technologies (Barton et al. 2014)
FLAG_Exo1 wt	siRNA resistant vector for expression of FLAG-tagged wt Exo1; Gateway LR Clonase Enzyme mix kit purchased from Life Technologies
FLAG_Brca1 wt	siRNA resistant vector for expression of FLAG-tagged wt Brca1 (Shakya et al. 2011)
HA_53BP1 wt	siRNA resistant vector for expression of HA-tagged wt 53BP1 (Iwabuchi et al. 2003)

3.1.7 Transfection reagents and kits

siRNA transfection

HiPerFect Qiagen

DNA transfection

Effectene Qiagen

JetPEI Polyplus

Kits

EdU-Click Kit baseclick

peqGOLD Xchange Plasmid maxi-EF Kit peqlab

3.1.8 Inhibitors

Table 3.2 Inhibitors

Inhibitor	Concentration	Vendor
ATM (Ku60019)	0.5 μ M	Tocris Bioscience
DNA-PK (Nu7441)	7.5 μ M	Tocris Bioscience
Mre11 endonuclease (PFM01)	50 μ M	(Shibata et al. 2014)
Mre11 exonuclease (PFM39)	300 μ M	(Shibata et al. 2014)
Nocodazole	100 ng/ μ l	Sigma-Aldrich
PARP (PJ34)	15 μ M	Calbiochem
Plk1/3 (GW843682X)	0.5 μ M	Tocris Bioscience
Cdk1/2 (Roscovitine)	25 μ M	Sigma-Aldrich

3.1.9 Protein Standard

PageRuler Plus Prestained Protein Ladder Fermentas

3.1.10 Antibodies

Primary Antibodies

Table 3.3 Primary Antibodies

Antibody	Species	Dilution	Vendor	Application
anti-Artemis	rabbit	1:3000	GeneTex	WB
anti-pATM (S1981)	rabbit	1:2000	Abcam	IF
anti-53BP1	mouse	1:1000	Millipore	IF
anti-53BP1	rabbit	1:1000	Bethyl	IF
anti-Brcal (D9)	mouse	1:100	Santa Cruz	IF
anti-Brcal (C20)	rabbit	1:500	Santa Cruz	WB
anti-BrdU	mouse	1:100	BD Pharmingen	IF
anti-cMyc	mouse	1:500	Santa Cruz	IF
anti-Exo1	rabbit	1:500	Santa Cruz	WB
anti-FLAG_M2	mouse	1:1000	Sigma	IF
anti-GAPDH	rabbit	1:1000	Santa Cruz	WB
anti-GFP	mouse	1:500	Roche	IF
anti-HA	mouse	1:1000	Abcam	IF

anti- γ H2AX	mouse	1:2000	Merck	IF
anti- γ H2AX	rabbit	1:2000	Epitomics	IF
anti-Ku70	mouse	1:1000	Santa Cruz	WB
anti-Ku80	mouse	1:100	Abcam	IF
anti-pRPA (T21)	rabbit	1:10000	Abcam	IF

Secondary Antibodies

Table 3.4 Secondary Antibodies

Antibody	Dilution	Vendor	Application
Goat anti-mouse AlexaFluor 488	1:1000	Molecular Probes	IF
Goat anti-mouse AlexaFluor 594	1:1000	Molecular Probes	IF
Goat anti-rabbit AlexaFluor 488	1:1000	Molecular Probes	IF
Goat anti-rabbit AlexaFluor 594	1:1000	Molecular Probes	IF
Goat anti-mouse IgG-HRP	1:10000	Santa Cruz	WB
Goat anti-rabbit IgG-HRP	1:30000	Santa Cruz	WB

3.1.11 Solutions, buffers and media

Buffers

PBS	137 mM NaCl 2.7 mM KCl 8 mM Na ₂ HPO ₄ 1.5 mM KH ₄ PO ₄	pH 7.4
TBS	20 mM Tris/HCl 137 mM NaCl	pH 7.6

Cell culture

Dulbecco's Modified Eagle's Medium (DMEM)	Sigma-Aldrich	
Minimum Essential Medium Eagle (MEM)	Sigma-Aldrich	
Fetal calf serum (FCS)	Biochrom	
Non-essential amino acids (NEA)	Biochrom	
Trypsin/EDTA	0.5 M EDTA 2.5% (v/v) Trypsin	pH 8 in PBS

Immunofluorescence

Fixation	2.5% Formaldehyde	in PBS
Washing 1	1% FCS	in PBS
Permeabilization	0.2% TritonX-100	in PBS/1% FCS
Blocking	5% BSA	in PBS/1% FCS
Washing 2	0.1% Tween	in PBS/1% FCS
DAPI	0.4 μ g/ml DAPI	in PBS

BrdU Foci

Fixation	2% Formaldehyde	in PBS
Pre-extraction	0.5% TritonX-100	in PBS
Permeabilization	0.5% TritonX-100	in PBS/1% FCS

Ku Foci

CSK buffer	10 mM PIPES	pH 7
	100 mM NaCl	
	300 mM sucrose	
	3 mM MgCl ₂	
	0.7% TritonX-100	
	0.3 mg/ml RNase (Sigma)	

Bacteria

Ampicillin	50 mg/ml	in MilliQ
LB broth	10 g/l Tryptone	
	2% Yeast extract	
	5 g/l NaCl	
LB Agar plates	1.5% Agar	in LB broth

SDS-PAGE

RIPA buffer	50 mM Tris/HCl	pH 8
	150 mM NaCl	
	0.5% Sodium deoxycholate	
	1% TritonX-100	
	0.1% SDS	



Electrophoresis buffer	25 mM Tris/HCl 0.2 M Glycine 0.5% (w/v) SDS	pH 8.8
5x Loading buffer (Laemmli)	60 mM Tris/HCl 2% (w/v) SDS 5% (v/v) β -Mercaptoethanol 10% (v/v) Glycerin 0.01% Bromophenol blue	pH 6.8
Stacking gel buffer	0.5 M Tris/HCl 1% SDS	pH 6.8
Running gel buffer	1.5 M Tris/HCl 1% SDS	pH 8.8

Western Blot

Transfer buffer	20 mM Tris/HCl 150 mM Glycine	pH 8.3
Washing	0.1% Tween20	in TBS
Blocking	5 % nonfat milk 0.1% Tween20	in TBS
Antibody solution	1 % nonfat milk 0.1% Tween20	in TBS
Lumi-Light Western Blot	Roche	
WesternBright™ Quantum/Sirius	advansta	

3.1.12 Cell lines and bacteria

HeLa-S3	human cancer cell line derived from cervical cancer cells isolated from Henrietta Lacks in 1951, cultivated in DMEM supplemented with 10% FCS and 1% NEA and passaged bi-weekly (1:8 to 1:10)
82-6 hTert	hTert-immortalized wt human fibroblast cell line, cultivated in MEM supplemented with 20% FCS and 1% NEA and passaged weekly (1:10), cells were kindly provided by Prof. Dr. P. Jeggo (University of Sussex, UK)

CJ179 hTert	hTert-immortalized Artemis-deficient human fibroblast cell line, cultivated in MEM supplemented with 20% FCS and 1% NEA and passaged weekly (1:10), cells were kindly provided by Prof. Dr. P. Jeggo (University of Sussex, UK)
HSC62 hTert	hTert-immortalized Brca2-deficient human fibroblast cell line, cultivated in MEM supplemented with 20% FCS and 1% NEA and passaged weekly (1:8)
2BN hTert	hTert-immortalized XLF-deficient human fibroblast cell line, cultivated in MEM supplemented with 20% FCS and 1% NEA and passaged weekly (1:8), (Dai et al. 2003)
411BR hTert	hTert-immortalized hypomorphic Lig4-deficient human fibroblast cell line, cultivated in MEM supplemented with 20% FCS and 1% NEA and passaged weekly (1:8), cells were kindly provided by Prof. Dr. P. Jeggo (University of Sussex, UK), (O'Driscoll et al. 2001)
MEF Brca1-wt	mouse embryonic fibroblast cell line homozygously expressing the wild type Brca1 protein, cells were cultivated in DMEM supplemented with 10% FCS and 1% NEA and passaged bi-weekly (1:10), cells were kindly provided by T. Ludwig (Shakya et al. 2011)
MEF Brca1-I26A	mouse embryonic fibroblast cell line homozygously expressing Brca1 containing a point mutation in the RING domain, cells were cultivated in DMEM supplemented with 10% FCS and 1% NEA and passaged bi-weekly (1:8 to 1:10), cells were kindly provided by T. Ludwig (Shakya et al. 2011)
MEF Brca1-S1655F	mouse embryonic fibroblast cell line homozygously expressing Brca1 containing a point mutation in the BRCT phospho-recognition domain, cells were cultivated in DMEM supplemented with 10% FCS and 1% NEA and passaged bi-weekly (1:8 to 1:10), cells were kindly provided by T. Ludwig, (Shakya et al. 2011)

3.2 Methods

3.2.1 Preparation of 24-well plates with Mylar bottom

Due to the extremely low penetration depth of α -particles, cells cannot be grown in normal plastic cell culture dishes or on glass cover slips for α -particle irradiation. Instead, cells have to be cultivated on Mylar foil that is only 2 μm thick. 24-well plates with a Mylar foil bottom are not commercially available; therefore the plates used here were custom-made in our lab. To prepare 24-well plates with Mylar foil bottom, the fluorocarbon film bottom (thickness 25 μm) of commercially available 24-well plates was removed and replaced with Mylar foil. To obtain a smooth bottom suitable for microscopy, epoxy 2-component glue (UHU) was applied to the bottom of each well; the 24-well plate was placed on stretched-out Mylar foil and dried overnight (see figure 3.5). The next day, the plates were cut out using a scalpel. Before seeding cells, the individual wells were disinfected with 70% ethanol for 15 minutes (min) and subsequently rinsed twice with sterile PBS.



Figure 3.5 Preparation of 24-well plates with Mylar foil bottom. The bottom of each well was coated with epoxy 2-component glue and then placed on stretched-out Mylar foil to dry overnight.

3.2.2 Cell culture

All cell lines were cultivated at 37°C with 5% atmospheric CO₂. Only sterile media, buffers and cell culture flasks were used and all cell lines were tested by PCR for mycoplasma contamination.

Thawing of cells

To thaw a fresh aliquot of a cell line, the cryotube containing the frozen cells was removed from the liquid nitrogen tank and placed in a 37°C waterbath for approximately 1 minute. The cell suspension was mixed with 5 ml media and centrifuged for 5 min at 4°C and 1000 rpm. After removal of the supernatant, the cell pellet was resuspended in 5 ml of fresh media and transferred to a 25 cm² cell culture flask. After 24 h, the cell culture medium was changed and, depending on the confluency, cells were transferred to a 75 cm² cell culture flask.

Cell passaging

For cell passaging, old media was removed and cells were carefully washed with PBS. 2 ml Trypsin/EDTA was added and cells were incubated for approximately 5 min at 37°C to ensure complete detachment from the flask surface. The trypsinization reaction was stopped by addition of 6-8 ml of media. After resuspension, cells were passaged at a ratio of 1:8 to 1:10 depending on cell line and confluency. All cell lines, appropriate media and passaging frequencies are listed in section 3.1.12.

Cell seeding

For cell seeding, the cell number was determined using a Neubauer counting chamber. In 24-well plates with Mylar foil bottom, 3.5×10^4 cells were seeded in 1 ml medium per well. For cell seeding on glass coverslips, sterile coverslips were placed in 35 mm cell culture dishes and 2.5×10^5 cells were seeded in 2.2 ml medium. In 60 mm cell culture dishes, 5.0×10^5 cells were seeded in 5.5 ml medium. If applicable, cells were treated with siRNA immediately after seeding and then returned to the incubator and maintained at 37°C with 5% atmospheric CO₂.

3.2.3 Transfections and inhibitor treatments

siRNA Transfection

Cells were transfected with small interfering RNA (siRNA) (see Table 3.1) using HiPerFect transfection reagent immediately after cell seeding, followed by a second transfection 24 h later. For the transfection solution, medium without serum was combined in an Eppi with siRNA and HiPerFect (table 3.6). The mixture was then vortexed for 1 min, and after 10 min incubation at room temperature (RT), the solution was added dropwise to the cells under constant, slow rotation of the dish. Irradiation of cells was always performed 72 h after the first transfection to ensure the most efficient depletion of the target protein. Cells were incubated at 37°C with 5% atmospheric CO₂ after siRNA transfection until irradiation and fixation.

Table 3.6 siRNA transfection solutions

Cell culture dish	Medium without serum	HiPerFect	siRNA
24 well (1 ml medium)	44.4 μ l	4.44 μ l	0.53 – 2.5 μ l
35 mm (2.2 ml medium)	100 μ l	12 μ l	1.2 – 3 μ l
60 mm (5.5 ml medium)	240 μ l	28.8 μ l	2.88 – 7.2 μ l

DNA vector transfection

Cells were transfected with DNA vectors (see section 3.1.6) using either Effectene or jetPEI transfection reagents. For Effectene transfections, the manufacturer's protocol was followed. For jetPEI transfections, the appropriate volume of NaCl (see table 3.7) was added to two separate Eppis. Vector DNA was added to the NaCl in one Eppi, while jetPEI was added to the NaCl in the other Eppi. After brief vortexing and centrifugation, the NaCl containing jetPEI was added to the Eppi containing NaCl and DNA and vortexed again. After 20 min incubation at RT, the solution was added to the cells dropwise under constant, slow rotation of the culture dish. DNA vectors were always transfected 24 h after initial cell seeding. When jetPEI was used, the cell culture medium was replaced with fresh medium at 6 h post DNA transfection to prevent cell death. Cells were incubated at 37°C with 5% atmospheric CO₂ until irradiation and fixation 24 or 48 h after DNA transfections.

Table 3.7 jetPEI transfection solutions

Cell culture dish	150 mM NaCl	DNA	jetPEI
24 well (1 ml medium)	48 μ l	4 μ l	2 μ g
35 mm (2.2 ml medium)	100 μ l	4 μ l	1 μ g

Inhibitor treatments

The inhibitors listed in table 3.2 were added to the cell culture medium 1 h prior to irradiation. Cells were treated with an equal amount of DMSO as a control. Inhibitors and DMSO were maintained in the medium during the entire repair incubation time.

3.2.4 DNA damage induction

Cells were irradiated with either α -particles or X-rays for DSB induction. 30 min prior to irradiation, EdU (1 μ l/ml) was added to the cell culture medium. This thymidine analogue is incorporated into the DNA of replicating cells, thus marking all cells that are in S-phase at the time of irradiation or that enter S-phase during the repair incubation time. Furthermore, nocodazole (100 ng/ μ l) was added to the cell culture medium 30 min before IR. Nocodazole interferes with microtubule polymerization, causing a cell cycle arrest in prometaphase. Hence, nocodazole was used to prevent progression of cells from G2 to G1 phase to avoid contamination of the G1 population with cells that were irradiated in G2.

α -Particle irradiation

For α -particle-irradiation, cells were seeded in 24-well plates with a Mylar foil bottom (see section 3.2.2) at least 24 h prior to irradiation with 2 Gy. The radiation source was a ²⁴¹Americium plate with an activity of 48 MBq. ²⁴¹Americium is the most common radioactive isotope of Americium. The radiation source is encased in 2 μ m thick gold palladium alloy plating and has a half-life of 432.2 years. It emits α -particles with an average energy of 5.48 MeV as well as a negligible amount of γ -rays. During irradiation, the cells on the Mylar foil were approximately 3 mm away from the radiation source, thus the average energy on target was 3.66 MeV. The average LET of the emitted particles is 144.7 keV/ μ m at a fluence rate of $7.88 \cdot 10^4$ particles \cdot cm⁻²s⁻¹. The resulting dose rate for this source is 0.87 Gy/min (Fricke 2008).

X-Ray irradiation

For irradiation with X-rays, cells were seeded on sterile glass cover slips in cell culture dishes (see section 3.2.2) at least 24 h prior to irradiation. Cells were irradiated using a Philips X-ray tube equipped with a tungsten anode and a thin beryllium window. The setting for irradiation was 19 mA and 90 kV and a 1 mm aluminum plate was used for filtering of soft (low energy) X-rays and for holding of samples. Irradiation was performed under consideration of the dose doubling effect of glass slides (Kegel et al. 2007).

3.2.5 Immunofluorescence staining

Fixation and permeabilization

After repair incubation, cells were washed with PBS and fixed with 2.5% formaldehyde for 15 min at RT. After fixation, the cells were washed 3 times for 10 min with PBS and then incubated for 10 min at 4°C with 0.2% TritonX-100 for permeabilization. After washing with PBS/1%FCS (3 times for 10 min), BSA blocking solution was added for a minimum of 30 min at RT.

Staining

Cells were incubated with primary antibodies diluted in BSA blocking solution at 4°C overnight. Primary antibodies and corresponding dilutions are listed in table 3.3. The next day, cells were washed 3 times for 10 min with PBS/1%FCS/0.1%Tween and incubated for 30 min at RT with EdU-Click solution (Cy5). EdU-Click stains all cells that have incorporated EdU into the DNA, thus marking all S-phase cells. Manufacturer's instructions were followed. After 30 min, cells were washed 3 times for 10 min with PBS/1%FCS/0.1%Tween and then incubated for 60 min at RT with the appropriate secondary antibodies diluted in BSA blocking solution (see table 3.4). Cells were subsequently washed 3 times for 5 min with PBS/1%FCS/0.1%Tween and incubated with DAPI solution for 5 min to stain cell nuclei. Finally, cells were washed for 5 min with PBS. For X-ray irradiated cells, the glass coverslip was transferred to a microscope slide with 2 μ l of mounting medium and sealed with clear nail polish. For α -particle-irradiated cells, the PBS was removed from the wells and 7 μ l of mounting medium was added to each well. A glass coverslip was placed on top of the mounting medium.

3.2.5.1 BrdU foci staining

For visualization of BrdU resection foci, the thymidine analogue BrdU was added to the cell culture medium at a concentration of 15 $\mu\text{l/ml}$ 24 h prior to irradiation to allow sufficient time for BrdU incorporation into the genome. Cells were treated with EdU and nocodazole before irradiation with α -particles as described in section 3.2.4. After repair incubation, the cells were briefly washed with PBS; subsequently 0.5% TritonX-100 was added to the unfixed cells for 10 min at RT. This pre-extraction step was necessary to wash out the soluble, unincorporated BrdU in the cell. Due to the pre-extraction, cells did not adhere to the Mylar foil very strongly, thus extreme caution had to be taken when adding solutions and all incubations were done without shaking. Subsequently, cells were carefully washed with PBS and fixed by addition of 2% formaldehyde for 20 min at RT. The cells were washed 3 times for 5 min with PBS/1%FCS and then incubated with BSA blocking solution for a minimum of 20 min. The primary antibodies (BrdU and γH2AX , see table 3.3) were diluted in BSA blocking solution and added to the cells overnight. The staining was completed as described in section 3.2.5.

3.2.5.2 Ku80 foci staining

For Ku80 foci staining, cells were pre-extracted with CSK buffer and stained as previously described (Chanut et al. 2016). Additionally, cells were fixed with 2% PFA for 10 minutes after the secondary antibody staining.

3.2.5.3 Analysis

Microscopic Analysis

IF stainings were analyzed with the help of a semi-automated microscopy approach. Using Metafer software, cells were scanned for DAPI content and EdU signal intensity, resulting in a histogram depicting the different cell cycle phases (see figure 3.7, left panel). G1 or G2 phase cells were selected and relocated. For each experiment and condition a minimum of 40 cells were analyzed. For pRPA stainings in G1, only pRPA positive cells (cells with ≥ 1 pRPA focus) were evaluated.

For BrdU foci analysis, cells were also scanned using Metafer and the G1 population was selected. Images were taken and analyzed using ImageJ to ensure that only BrdU foci that co-localize with γ H2AX are evaluated.

Complementation experiments required simultaneous scanning of DAPI, EdU and GFP signals (or other protein tags, such as cMyc, HA, or FLAG). The G1 and GFP-positive cell populations were gated for analysis of GFP-positive G1 phase cells (see figure 3.7).

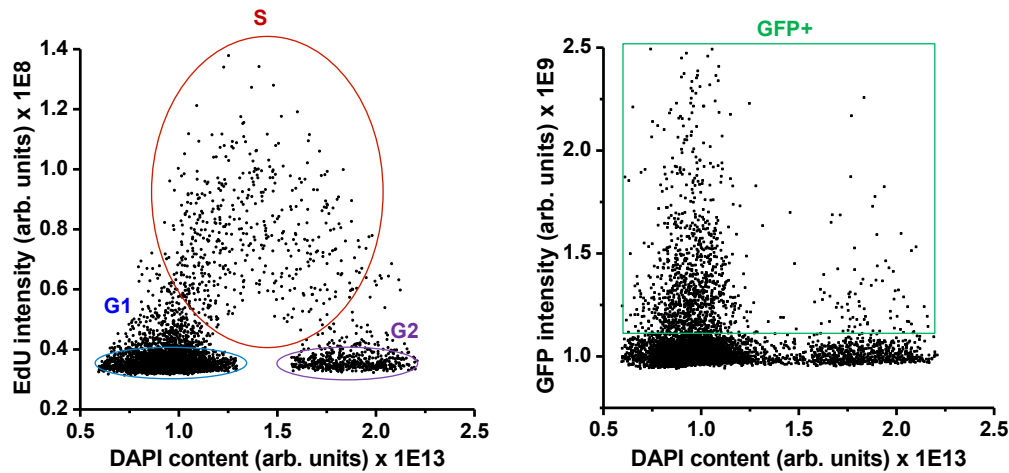


Figure 3.7. Identification of cell cycle phases using a semi-automated scanning system. Left panel: Cells were scanned for EdU and DAPI content. G1-, G2- and S-phase cells can be distinguished in the resulting histogram. Right panel: Cells were additionally scanned for GFP signal in complementation studies (Biehs et al. 2017).

Statistical analysis

To obtain independent, technical replicates, cells were seeded and treated on 3 different days for $n=3$. Each time, cells with different passage numbers were used and all solutions that were used were prepared fresh. For all data points with $n \geq 3$, the SEM was calculated between means of the independent experiments. All P values were calculated using a two-sample Student's t-test, which compared the mean values of the independent experiments (**= $p < 0.01$, ***= $p < 0.001$).

3.2.6 Amplification of DNA vectors

Transformation

To amplify DNA vectors, competent *E.coli* DH5 α cells were transformed. 10 ng of DNA were mixed with 100 μ l *E.coli* cells, incubated for 30 min on ice, 90 sec at 42°C and finally 90 sec on ice. 900 μ l LB media was added and cells were incubated for 1 h at 37°C with light shaking. Subsequently, cells were centrifuged at 2000 rpm for 2 min, 800 μ l of the supernatant was removed, and the pellet was resuspended in the remaining liquid and plated on an LB agar plate containing 1 μ l/ml ampicillin (or another antibiotic, depending on the resistance of the vector). The petri dish was incubated at 37°C overnight. The next day, a single colony was picked from the petri dish and added to 200 ml of LB medium containing 1 μ l/ml Ampicillin and incubated for approximately 24 h at 37°C. The resulting bacterial culture was used for a maxi preparation.

Maxi preparation

To isolate the DNA vectors from the bacterial cells, a maxi preparation was performed using a maxi prep kit (peqlab) and following the manufacturer's guidelines.

3.2.7 SDS-Page and Western Blot

Western Blot was used to check depletion efficiencies of siRNA treatments and transfection efficiencies of plasmids. Cells were seeded in 35 mm or 60 mm dishes for Western Blot analysis and transfected with siRNAs as described in section 3.2.3.

Cell Harvest

Cells were washed with ice-cold PBS and then harvested using a scraper and 2 ml ice-cold PBS. Cells were transferred to a 15 ml falcon. For efficient removal of all remaining cells, the cell culture dish was washed with 2 ml ice-cold PBS and cells were centrifuged for 3 min at 1500 rpm to form a cell pellet. The supernatant was removed.

Cell lysis

Depending on the size of the cell pellet, cells were resuspended in 50 - 200 μ l lysis buffer (RIPA buffer + protease inhibitor and Phosphostop). For complete cell lysis, the cell lysate was placed in an ultrasound bath for 3 times 1 min. In between, cells were vortexed and briefly placed on ice. Cells were incubated on ice for 30 min and subsequently centrifuged at 4°C and 13000 rpm for 30 min. The supernatant was transferred to a new micro tube.

Bradford protein assay

Protein concentration in samples was determined by Bradford protein assay. For each sample, 1 μl protein was added to 800 μl MilliQ. 200 μl Bradford reagent was added to each sample, briefly vortexed, and incubated for 5 min. Absorption was measured immediately at 590 nm using a Nanophotometer.

SDS PAGE and Western Blot

Samples were mixed with 5x loading buffer (Laemmli) and boiled for 5 min at 95°C to denature the proteins. Samples were loaded in gel pockets and electrophoresis buffer was added to the chamber. The gel was run for 10 min at 95 V for optimal accumulation of the proteins in the stacking gel. The voltage was increased to 130 V when the proteins entered the running gel. The total running time varied depending on the size of the protein of interest. After SDS PAGE, the proteins were transferred (blotted) to a PVDF membrane. The PVDF membrane was first activated by incubation in methanol for at least 1 min. The gel and the membrane were sandwiched tightly between multiple layers of filter paper and sponges; air bubbles were removed to ensure optimal transfer. The assembled gel holder cassette was placed inside the transfer chamber with the membrane facing the anode. Blotting buffer and an ice block were added to the chamber and a current of 310 mA was applied for approximately 3 h, depending on the size of the proteins of interest. After completion of protein transfer, the membrane was blocked with 5% nonfat milk in TBS-T for at least 1 h. The primary antibody (see table 3.3) was incubated with the membrane at 4°C overnight. The next day, the membranes were washed 3 times for 10 min in TBS-T before incubation with an HRP-conjugated secondary antibody (diluted in 1% nonfat milk, see table 3.4) for 1 h at RT. Finally, the membrane was washed 3 times for 10 min in TBS-T before signal detection. An HRP substrate was added to the membrane, resulting in a chemical reaction that releases luminol, which emits a chemiluminescent signal that was detected using ChemiSmart5000 or Fusion FX image acquisition systems.

4 Results

The purpose of this project was the characterization of the slow repair component in G1 phase of the cell cycle. Previous studies found biphasic DSB repair kinetics in G1 as well as in G2. The majority of breaks (approximately 80%) are repaired with fast kinetics via the c-NHEJ pathway in G1 and G2. The slow component in both cell cycles phases requires ATM signaling and Artemis (Riballo et al. 2004; Beucher et al. 2009). Complex DSBs or heterochromatic DSBs are repaired with slow kinetics. In G2, these breaks undergo DSB end resection and are subsequently repaired by HR (Yajima et al. 2013). The underlying repair mechanism in G1, however, remained unclear and was the focus of this thesis.

4.1 Artemis and CtIP

Artemis, a nuclease originally described for its role during V(D)J recombination, has DNA-PKcs-dependent endonuclease and intrinsic exonuclease activity (Moshous et al. 2001; Li et al. 2014). Previous studies showed that Artemis also functions during DSB repair, where it is specifically required for the repair of approximately 20% of X-ray-induced DSBs in G1 and G2 (Riballo et al. 2004; Beucher et al. 2009). The subset of DSBs that requires ATM and Artemis function is repaired with slow kinetics because those damages are located in the heterochromatin (Goodarzi et al. 2008). Therefore, a repair defect is observed in ATM- or Artemis-deficient cells at late time points (≥ 6 h) post IR (Beucher et al. 2009).

The endonuclease CtIP facilitates DSB end resection in S/G2 (Sartori et al. 2007). It was previously shown that depletion of CtIP in G2 can rescue the repair defect caused by the absence of the downstream HR factor Brca2 (Kakarougkas et al. 2013). Depletion of CtIP abrogates resection, therefore repair in CtIP-depleted cells presumably switches from resection-dependent HR to resection-independent c-NHEJ and the requirement for Brca2 is overcome.

While previous reports indicate that CtIP also has a role in G1 (Yun & Hiom 2009; Helmink et al. 2011; Quennet et al. 2011), CtIP was found to be dispensable for the repair of X-ray-induced DSBs in wt G1 cells, as CtIP depletion did not cause a repair defect (Barton et al. 2014).

To monitor DSB induction and repair, the highly sensitive γ H2AX assay was used. With this assay, γ H2AX foci, a posttranslational histone modification in response to DSB induction, can be visualized on a single cell level where one γ H2AX focus represents one DSB (Löbrich et al.

2010). In all experiments, nocodazole (prevents cells from progressing from G2 into G1) and EdU (marks cells upon entering S-phase) were added to the cell culture medium before IR and were maintained throughout the entire repair incubation time. This combined treatment ensured that only cells that were irradiated in G1 and remained in this cell cycle phase were analyzed.

To examine if CtIP is involved in the slow repair component in G1, wt 82-6 hTert and Artemis-deficient CJ179 hTert fibroblasts were treated with siCtIP before X-IR with 2 Gy. CJ179 hTert cells were additionally complemented with GFP or siRNA resistant GFP-CtIP-wt constructs. Transfection with an "empty" GFP vector served as a control and γ H2AX foci were analyzed in GFP-positive G1 cells at 8 h post IR.

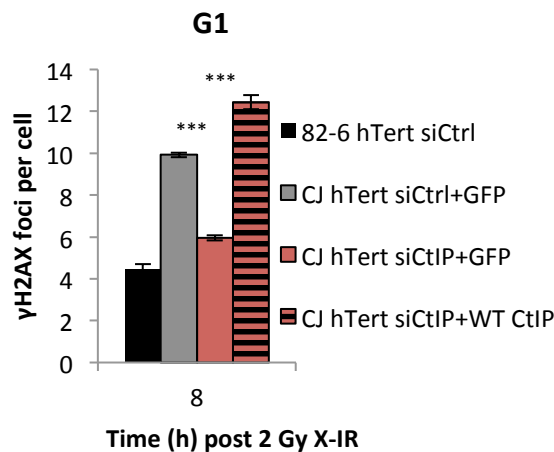


Figure 4.1 CtIP depletion rescues the Artemis repair defect in G1 after X-IR. Wt 82-6 hTert and Artemis-deficient CJ179 hTert fibroblasts were treated with siCtIP. 24 h later, cells were transfected with GFP or siRNA resistant GFP-CtIP-wt vectors. EdU and nocodazole were added before irradiation with 2 Gy X-IR. Cells were fixed 8 h post IR and stained with anti- γ H2AX and anti-GFP antibodies and DAPI. Samples were scanned using Metafer and only GFP+ G1 cells were analyzed. $n \geq 3$, background foci were subtracted, error bars represent SEM, statistical significance tested by Student's t-test (***) ($p < 0.001$), (knockdown efficiencies and vector expression were confirmed by Western Blot, see Biehs et al. 2017)

Consistent with previous reports, Artemis-deficient CJ179 hTert fibroblasts displayed impaired DSB repair during the slow repair component, resulting in substantially more residual γ H2AX foci at 8 h post 2 Gy in CJ179 hTert compared to wt 82-6 hTert cells (figure 4.1). Surprisingly, the number of γ H2AX foci was significantly reduced in CtIP-depleted CJ179 hTert cells compared to siControl (siCtrl)-treated CJ179 hTert cells (figure 4.1). Therefore, CtIP-depletion rescued the Artemis repair defect in G1 after X-IR. This observation is

reminiscent of the situation in G2 where CtIP depletion rescues the Brca2 repair defect. It indicates that CtIP plays a role in the slow repair component in G1 and that its function lies upstream of Artemis. Since CtIP is an established factor for end resection in S/G2, this result further suggests that in G1 (similar to G2), two pathways exist: a resection-independent and a resection-dependent pathway and repair can switch to another pathway when resection is inhibited.

To confirm that the siRNA treatment did not have any off-target effects that might account for the observed effect, siCtIP-treated CJ179 hTert cells were complemented with an siRNA-resistant GFP-CtIP-wt vector. After complementation with the GFP-CtIP-wt vector, the number of γ H2AX foci in CtIP-depleted CJ179 hTert cells was restored to the level observed in siCtrl-treated CJ179 hTert cells (Figure 4.1). Hence, the Artemis repair defect was restored after complementation with GFP-CtIP-wt, confirming the specificity of the CtIP siRNA.

After obtaining preliminary evidence that DSB repair in G1 involves CtIP, another tool to specifically study the slow repair component was established. To this end, the special qualities of α -IR were exploited. α -particles are a type of high-LET particle radiation; therefore the lesions induced by α -IR are highly complex and are expected to be repaired with slow kinetics (Okayasu 2012). To verify this, wt 82-6 hTert and Artemis-deficient CJ179 hTert fibroblasts were treated with siCtIP and the repair kinetics after 2 Gy α -IR were analyzed.

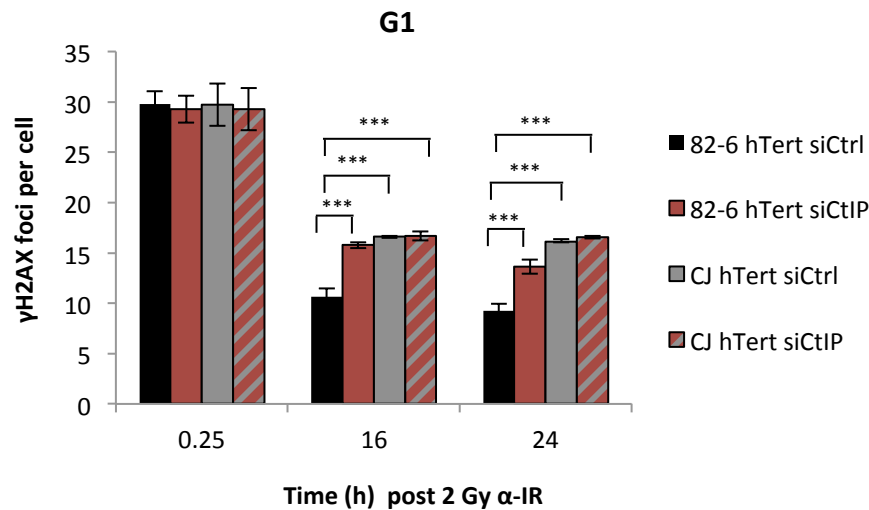


Figure 4.2 Artemis and CtIP are required for repair of complex DSBs. 82-6 hTert wt and Artemis-deficient CJ179 hTert fibroblasts were treated with siCtIP. EdU and nocodazole were added and cells were irradiated with 2 Gy α -IR. Cells were fixed at various times post IR and stained with an anti- γ H2AX antibody and DAPI. Cells were scanned using Metafer and only the G1 population was analyzed. $n \geq 3$, background foci were subtracted, error bars represent SEM, statistical significance tested by Student's t-test (***) ($p < 0.001$), (knockdown efficiencies were confirmed by Western Blot, see Biehs et al. 2017)

While the induction of DSBs was similar for both cell lines and conditions, the results displayed in figure 4.2 show that complex α -IR-induced DSBs are repaired with slow kinetics: approximately 33% of breaks remained unrepaired after 24 h in wt 82-6 hTert fibroblasts. Similar to results obtained after X-IR, Artemis-deficient CJ179 hTert fibroblasts displayed a repair defect compared to wt 82-6 hTert cells at 16 and 24 h post α -IR (figure 4.2). In contrast to X-IR, however, CtIP depletion in wt 82-6 hTert cells caused a repair defect at 16 and 24 h post 2 Gy α -IR that was similar to the Artemis repair defect (figure 4.2). This indicates that, due to increased complexity, complex DSBs require end processing steps before repair. Furthermore, γ H2AX foci numbers in siCtIP- and siCtrl-treated CJ179 hTert cells were similar at 16 and 24 h post IR. Therefore, CtIP depletion did not rescue the Artemis repair defect after α -IR, presumably due to the requirement for end processing of α -IR-induced breaks (figure 4.2). Despite the apparent differences in the repair kinetics between X-IR and α -IR, the results confirm that Artemis and CtIP are required for slowly repairing DSBs in G1. Moreover, siCtIP treatment in Artemis-deficient CJ179 hTert cells did not cause an additional

repair defect, indicating that Artemis and CtIP function in the same repair pathway (figure 4.2).

Repair of complex DSBs evidently requires CtIP in G1, an endonuclease known to facilitate end resection in S/G2. It was therefore hypothesized that complex DSBs undergo resection in G1 as well. IF staining of the ssDNA binding protein RPA phosphorylated at Thr21 (pRPA pT21) can be used as a marker for resection (Barton et al. 2014). After 2 Gy X-IR, pRPA foci are clearly visible in S/G2 where they indicate resection and repair by HR. Under these conditions, pRPA foci cannot be detected in G1 because X-IR-induced lesions are repaired with minimal end processing. α -particles, however, induce DNA lesions that are much more complex than X-IR-induced damages and previous studies found that complex damages have a greater propensity to undergo resection in G2 (Yajima et al. 2013; Shibata et al. 2011). Thus, exploiting the qualities of α -IR, a method was developed to visualize and quantify resection in G1.

To this end, α -irradiated HeLa cells were stained with anti-pRPA (pT21) and anti- γ H2AX antibodies. Indeed, pRPA foci, which co-localized with γ H2AX, were readily visible in G1 phase cells after α -IR (figure 4.3A). Due to the combined nocodazole and EdU treatment, only cells that were irradiated in G1 and stayed in this cell cycle phase were analyzed. Therefore, pRPA foci in G1 indicate DSBs that were resected in G1. This novel assay made it possible to directly visualize and quantify resection in G1.

After irradiation with 2 Gy α -particles, the formation of pRPA foci in G1 peaked around 2 h post IR in control cells. As time progressed, the number of pRPA foci steadily decreased, corresponding to ongoing DSB repair (figure 4.3B). In cells depleted of CtIP or Artemis, the number of pRPA foci was substantially lower than in siCtrl-treated cells up to 15 h post IR (figure 4.3B), indicating impaired resection. Furthermore, similar numbers of γ H2AX foci were induced for all conditions. Consistent with previous results (figure 4.2), DSBs were repaired slowly in siCtrl-treated cells. Following treatment with siCtIP or siArtemis, a repair defect was observed at ≥ 6 h post IR. After 24 h, approximately 33% of DSBs remained unrepaired in control cells, compared to approximately 50% of unrepaired DSBs in CtIP- or Artemis-deficient cells (figure 4.3B). Therefore, the results displayed in figure 4.3B suggest that CtIP and Artemis are required for resection and subsequent repair of complex DSBs in G1.

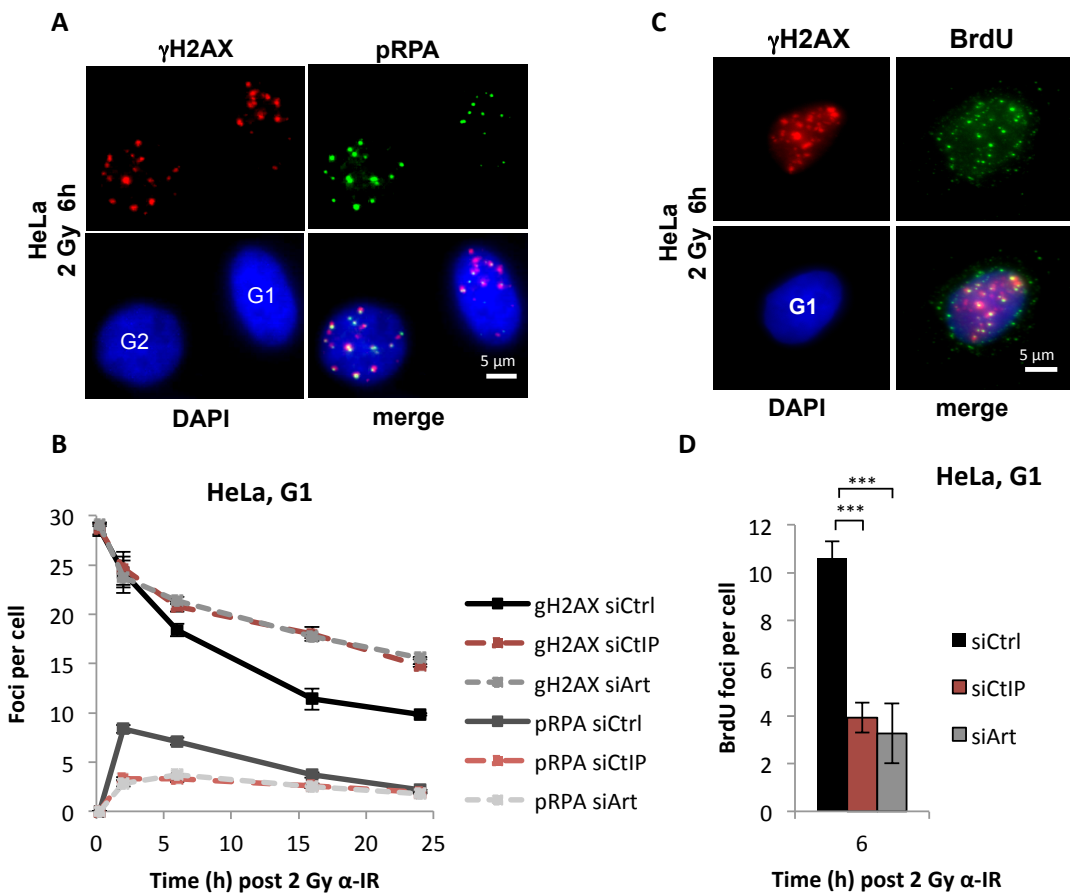


Figure 4.3 Resection and repair of complex DSBs in G1 requires Artemis and CtIP. All cells were treated with nocodazole and EdU prior to irradiation with 2 Gy α -IR. (A) HeLa cells were fixed 6 h post α -IR and stained with anti- γ H2AX and anti-pRPA (pT21) antibodies and DAPI. Images were acquired using Metafer. (Barton et al. 2014) (B) HeLa cells were treated with siCtIP or siArtemis and fixed at various times post α -IR. Cells were stained with anti- γ H2AX, anti-pRPA (pT21) and DAPI and scanned using Metafer. Only G1 cells were analyzed. $n \geq 2$ (C) HeLa cells were incubated with BrdU for 24 h before α -IR. Cells were pre-extracted to remove soluble BrdU, fixed 6 h post IR and stained with anti-BrdU and anti- γ H2AX antibodies and DAPI. Using Metafer, cells were scanned and images were acquired to show co-localization of BrdU and γ H2AX (Barton et al. 2014) (D) BrdU foci were quantified in G1 HeLa cells treated with siCtIP or siArtemis. Samples were scanned with Metafer, images were analyzed with ImageJ and only BrdU foci co-localizing with γ H2AX were quantified. $n \geq 3$, background foci were subtracted, error bars represent SEM, statistical significance tested by Student's t-test ($***=p<0.001$), (knockdown efficiencies were confirmed by Western Blot, see Biehs et al. 2017)

RPA is a protein that binds to ssDNA, hence pRPA foci are an indirect measurement for ssDNA and resection. Therefore, a defect in pRPA foci formation could be indicative of impaired recruitment of RPA to the DNA itself instead of impaired resection. To exclude this possibility, the results displayed in figure 4.3B were consolidated with BrdU resection foci. To this end, cells were incubated with the thymidine analogue BrdU for 24 h before α -IR to allow BrdU

incorporation into the genome. After pre-extraction to remove soluble BrdU, IF staining under non-denaturing conditions using an anti-BrdU antibody was carried out. Consequently, only resected ssDNA stretches were visible as BrdU foci (figure 4.3C). Samples were co-stained with an anti- γ H2AX antibody and images were acquired for analysis. Only BrdU foci that co-localize with γ H2AX were evaluated (figure 4.3C). The results presented in figure 4.3D show significantly reduced BrdU foci numbers in cells treated with siCtIP or siArtemis compared to control cells. This confirms the results obtained with the pRPA foci assay (figure 4.3B) and indicates that CtIP- and Artemis-dependent resection is occurring in G1.

Previous studies showed that the Artemis endonuclease function is important for DSB repair during the slow component in G1 and G2 (Riballo et al. 2004; Beucher et al. 2009). Having established that Artemis is required for resection in G1, the importance of its endonuclease function for resection in G1 was analyzed next. HeLa cells were treated with siArtemis to deplete endogenous Artemis proteins and subsequently transfected with GFP or siRNA-resistant cMyc-tagged Artemis constructs. To ascertain the role of the Artemis endonuclease function, an Artemis construct with a mutation in the nuclease domain (aspartic acid at position 37 mutated to asparagine, cMyc-Artemis-D37N) was used for complementation. After 2 Gy α -IR, pRPA foci were analyzed at 2 and 6 h in GFP- or cMyc-positive G1 cells.

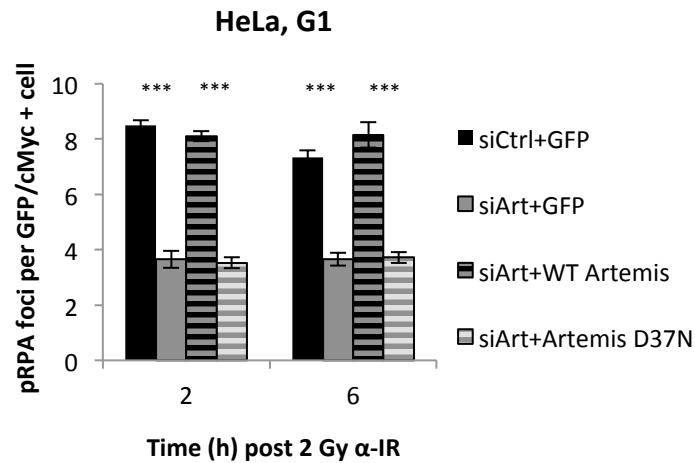


Figure 4.4 Resection in G1 requires the Artemis endonuclease function. HeLa cells were treated with siArtemis and transfected with GFP, siRNA resistant cMyc-Artemis-wt or endonuclease-deficient cMyc-Artemis-D37N vectors 24 h later. EdU and nocodazole were added before irradiation with 2 Gy α -IR. Cells were fixed at 2 and 6 h post IR and stained with anti-pRPA (pT21) and anti-GFP or anti-cMyc antibodies plus DAPI. Samples were scanned using Metafer. Only GFP/cMyc+ G1 cells were analyzed, $n \geq 3$, background foci were subtracted, error bars represent SEM, statistical significance tested by Student's t-test (***)= $p < 0.001$, (knockdown efficiencies and vector expression were confirmed by Western Blot, see Biehs et al. 2017)

Consistent with previous results (figure 4.3), pRPA foci numbers were significantly decreased after Artemis-depletion compared to cells treated with siCtrl (figure 4.4). The number of pRPA foci was restored to control levels after complementation with cMyc-Artemis-wt, but not after complementation with endonuclease-deficient cMyc-Artemis-D37N (figure 4.4). This indicates that the endonuclease function of Artemis is required for efficient resection in G1.

To facilitate resection and promote HR, CtIP is constitutively phosphorylated on amino acids Ser327 and Thr847 by CDK2 in S/G2. To test if these phosphorylation sites are also important for the resection process in G1, endogenous CtIP in HeLa cells was depleted with siRNA and cells were transfected with GFP, siRNA-resistant GFP-CtIP-wt or mutated GFP-CtIP constructs. In these CtIP vectors either the serine at position 327 was mutated to an alanine (GFP-CtIP-S327A) or the threonine at position 847 was mutated to an alanine (GFP-CtIP-T847A). Substitution of a serine or threonine with an alanine prevents the phosphorylation at this amino acid. Cells were irradiated with 2 Gy α -IR and pRPA foci were analyzed after 2 and 6 h in GFP-positive G1 cells.

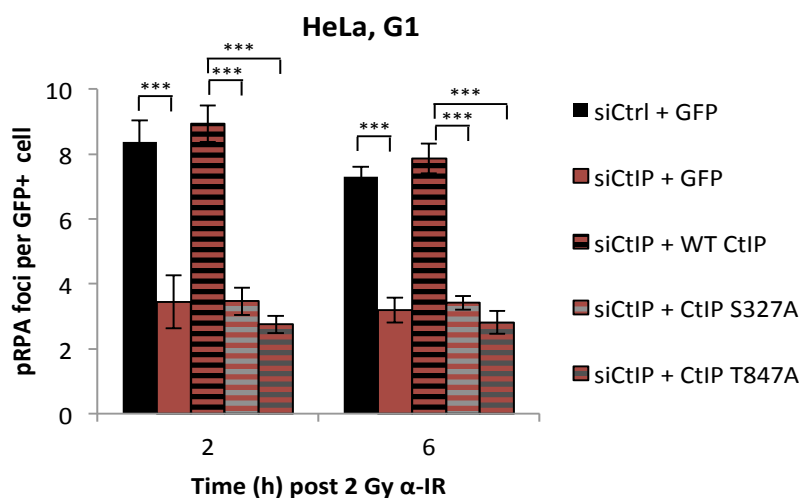


Figure 4.5 CtIP phosphorylation at Ser327 and Thr847 is required for G1 resection. HeLa cells were treated with siCtIP and transfected with GFP or various siRNA resistant GFP-CtIP vectors 24 h later. Nocodazole and EdU were added prior to irradiation with 2 Gy α -IR. Cells were fixed 2 and 6 h post IR and stained with anti-pRPA (pT21) and anti-GFP antibodies plus DAPI. Samples were scanned using Metafer and only GFP+ G1 cells were analyzed. $n \geq 3$, background foci were subtracted, error bars represent SEM, statistical significance tested by Student's t-test (**= $p < 0.01$), (***)= $p < 0.001$), (knockdown efficiencies and vector expression were confirmed by Western Blot, see Barton et al. 2014)

Consistent with previous results (figure 4.3), pRPA foci numbers were significantly reduced after depletion of endogenous CtIP compared to siCtrl-treated cells. Complementation with GFP-CtIP-wt restored pRPA foci numbers to control levels (figure 4.5). Complementation with GFP-CtIP-S327A or GFP-CtIP-T847A, on the other hand, did not restore the resection defect, as the pRPA foci numbers remained significantly lower in these samples compared to control cells (figure 4.5). This indicates that phosphorylation of CtIP at Ser327 and Thr847 is required for resection in G1.

The finding that the same CtIP phosphorylation sites, which are described for resection in S/G2, also play a role in G1 resection provoked the question which kinase mediates these phosphorylations. The phosphorylation of CtIP at Ser327 and Thr847 in S/G2 is mediated by CDK2 (Buis et al. 2012). To test if phosphorylation of CtIP by CDK2 also plays a role in G1, HeLa cells were treated with the CDK1/2 inhibitor roscovitine, irradiated with 2 Gy α -IR and pRPA foci were analyzed in G1 after 6 h.

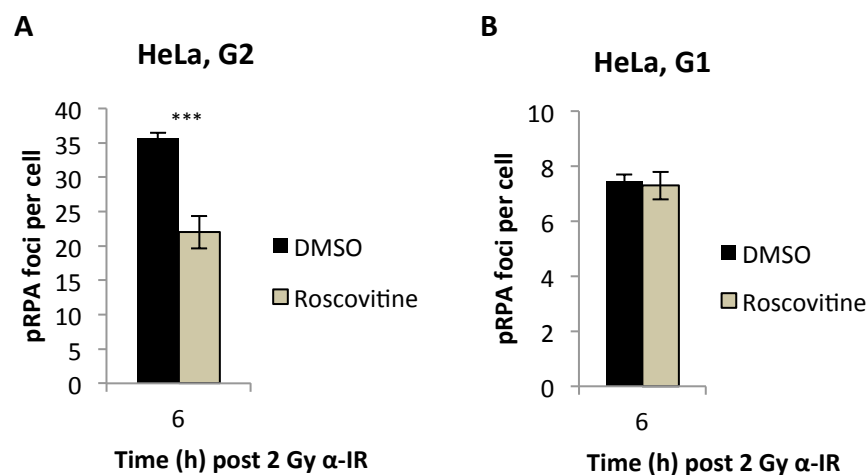


Figure 4.6 Resection in G1 is not dependent on CDK2. (A) and (B) HeLa cells were treated with DMSO or roscovitine; nocodazole and EdU were added prior to irradiation with 2 Gy α -IR. Cells were fixed 6 h later and stained with an anti-pRPA (pT21) antibody and DAPI. Samples were scanned using Metafer and either G1 or G2 phase cells were analyzed, $n \geq 3$, background foci were subtracted, error bars represent SEM, statistical significance tested by Student's t-test (***= $p < 0.001$), (Barton et al. 2014)

As expected, pRPA foci numbers in G2 were significantly reduced after roscovitine treatment compared to control cells. Since roscovitine inhibits CDK2, CtIP phosphorylation was impaired resulting in diminished pRPA numbers in G2 (figure 4.6A). In contrast, pRPA foci numbers in G1 were unaffected by roscovitine treatment compared to control cells, indicating that CtIP

phosphorylation in this cell cycle phase is not mediated by CDK2 (figure 4.6B). Hence, the results presented in figure 4.6 indicate that a different kinase phosphorylates CtIP in G1. In the following section the aim was to identify the kinase responsible for CtIP phosphorylation in G1.

4.2 Polo-like kinase 3

Polo-like kinases (Plks) belong to a family of serine/threonine kinases that can phosphorylate the same motifs (serine or threonine residue preceding a proline ([S/T]-P)) as CDKs (Elia et al. 2003). This family of kinases encompasses five family members (Plk1-5), that are important for the regulation of cell cycle progression and the DNA damage response (Bahassi 2011). To analyze a potential role for Plks during the repair of complex damages in G1, 82-6 hTert fibroblasts were treated with a Plk inhibitor (Plki) and γ H2AX foci were analyzed after 2 Gy α -IR. Of note, the Plk inhibitor that was used inhibits Plk1 as well as Plk3. Plk1 is the best characterized kinase in this family and is involved in regulation of mitosis and cytokinesis (De Cárcer et al. 2011). Plk3 has peak mRNA expression levels in G1 in thymidine-synchronized HeLa cells and is important for S-phase entry (Zimmerman & Erikson 2007).

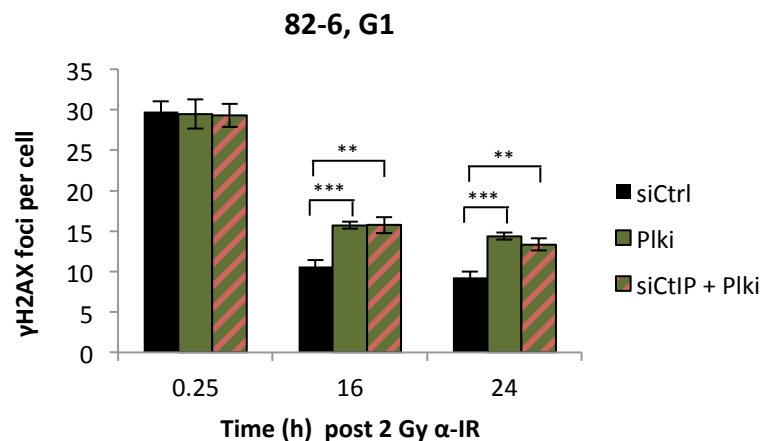


Figure 4.7 Repair of complex DSBs is dependent on Plk1/3. Wt 82-6 hTert fibroblasts were treated with Plki or siCtIP and Plki. EdU and nocodazole were added before 2 Gy α -IR and cells were fixed at various times. Cells were stained with an anti- γ H2AX antibody and DAPI. Samples were scanned using Metafer and only G1 cells were analyzed. $n \geq 3$, background foci were subtracted, error bars represent SEM, statistical significance tested by Student's t-test (***= $p < 0.001$, **= $p < 0.01$), (knockdown efficiencies were confirmed by Western Blot, see Barton et al. 2014)

The number of residual γ H2AX foci after Plki treatment was significantly increased at 16 and 24 h post IR compared to control cells (figure 4.7). This indicates that the repair of complex DSBs in G1 requires Plk1 and/or Plk3. The repair defect induced by Plki treatment was comparable to the effect observed after CtIP-depletion (figure 4.2). Further, combined treatment with siCtIP and Plki did not cause an additional repair defect compared to Plki treatment alone, suggesting that CtIP and Plk1/3 are operating in the same repair pathway (figure 4.7).

After obtaining the first indication that Plks also operate in the CtIP-dependent repair component in G1, the role of Plks during DNA end resection in G1 was evaluated using the pRPA assay. HeLa cells were treated with Plki and pRPA foci were quantified at 6 h post 2 Gy α -IR.

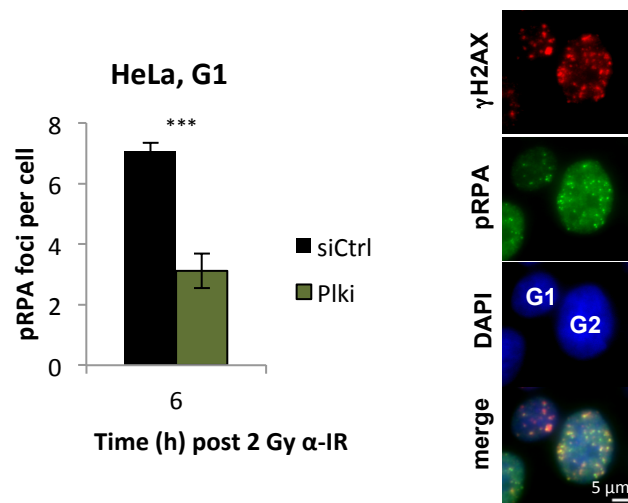


Figure 4.8 Resection in G1 is dependent on Plk1/3. HeLa cells were treated with Plki; EdU and nocodazole were added before irradiation with 2 Gy α -IR. Cells were fixed 6 h later and stained with an anti-pRPA (pT21) antibody and DAPI. Samples were scanned using Metafer and only G1 cells were analyzed. Images were acquired using Axiovision. $n \geq 3$, background foci were subtracted, error bars represent SEM, statistical significance tested by Student's t-test (***)= $p < 0.001$), (Barton et al. 2014)

The result presented in figure 4.8 show that pRPA foci levels in G1 were significantly reduced after Plki treatment compared to control cells, indicating that Plk1 and/or Plk3 are involved in the resection process in G1. To determine whether Plk1 or Plk3 promote resection in G1, siRNA depletion of each protein was established next. HeLa cells were treated with various Plk1 or Plk3 siRNAs and pRPA foci were quantified at 6 h post 2 Gy α -IR.

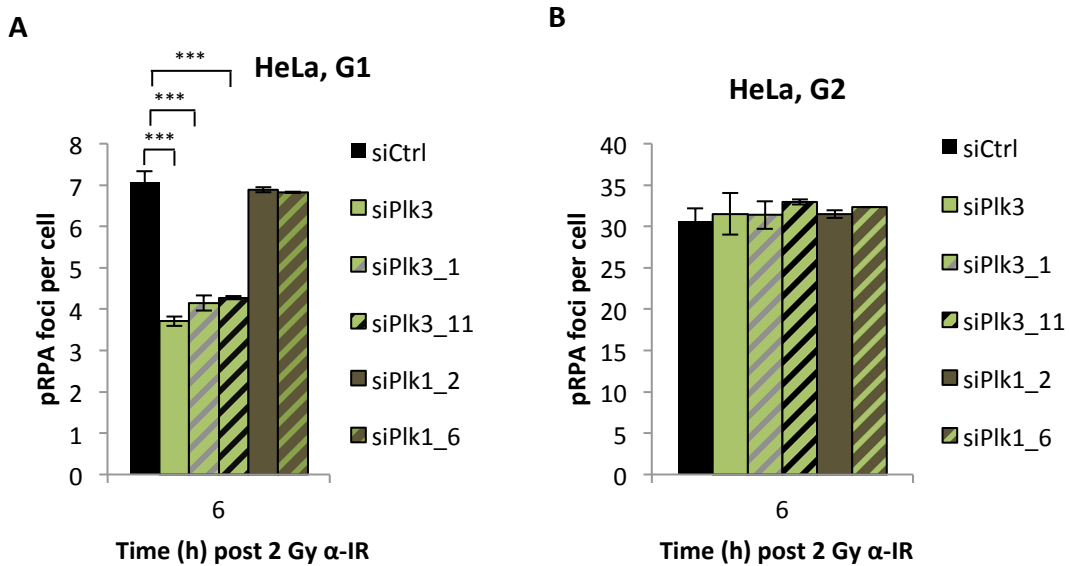


Figure 4.9 Plk3 promotes resection in G1. (A) and (B) HeLa cells were treated with various Plk1 and Plk3 siRNAs. EdU and nocodazole were added before irradiation with 2 Gy α -IR. Cells were fixed 6 h later and stained with an anti-pRPA (pT21) antibody and DAPI. Samples were scanned using Metafer and the G1 or G2 population was analyzed. $n \geq 3$, background foci were subtracted, error bars represent SEM, statistical significance tested by Student's t-test (***)= $p < 0.001$), (knockdown efficiencies were confirmed by Western Blot, see Barton et al. 2014)

The number of pRPA foci in G1 was significantly reduced after depletion of Plk3 compared to cells treated with siCtrl. Depletion of Plk1 in G1, on the other hand, did not have a significant impact on pRPA foci numbers compared to control cells (figure 4.9A). This indicates that Plk3 promotes resection in G1 while Plk1 is dispensable for the process. As a control, pRPA foci were also evaluated in G2 (figure 4.9B). As expected, none of the Plk siRNA treatments had an effect on pRPA numbers in G2, as in this cell cycle phase CtIP is phosphorylated by CDK2 (figure 4.6).

To consolidate this result, BrdU resection foci were analyzed in G1 after Plki treatment and siRNA depletion of Plk1 and Plk3. HeLa cells were incubated with BrdU for 24 hours prior to α -IR to allow BrdU incorporation into the genome. BrdU foci were analyzed at 6 h post IR.

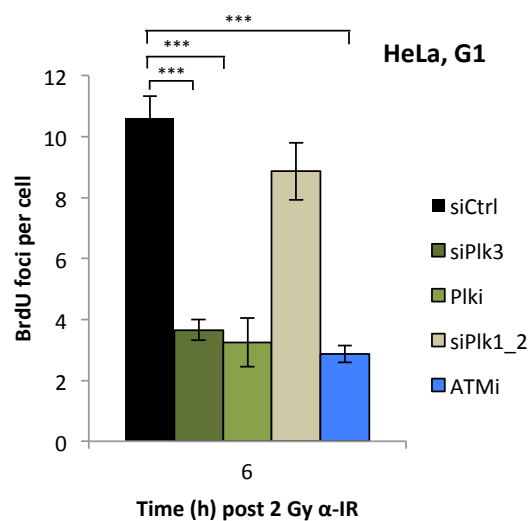


Figure 4.10 Plk3 and ATM promote resection in G1. Cells were treated with siPlk3 and siPlk1_2. BrdU was added to the culture medium 24 h before IR. Plki, ATMi, EdU, and nocodazole were added before irradiation with 2 Gy α -IR. 6 h later, cells were pre-extracted to remove soluble BrdU, fixed, and stained with anti-BrdU and anti- γ H2AX antibodies and DAPI. Cells were scanned with Metafer and pictures of G1 cells were acquired. Using ImageJ, pictures were analyzed and only BrdU foci that co-localize with γ H2AX were analyzed. $n \geq 3$, background foci were subtracted, error bars represent SEM, statistical significance tested by Student's t-test (***)= $p < 0.001$), (knockdown efficiencies were confirmed by Western Blot, see Barton et al. 2014)

BrdU foci numbers were significantly decreased in cells treated with siPlk3, Plki or ATMi compared to cells treated with siCtrl. Cells treated with siPlk1_2 did not have significantly different BrdU foci numbers compared to control cells (figure 4.10). Therefore, analysis of BrdU resection foci confirmed that resection in G1 is promoted by Plk3 but not Plk1. Additionally, the effect of ATM inhibition on G1 resection was analyzed in this experiment. Previous studies reported that ATM phosphorylates Plk3 in G1 after DNA damage (Bahassi et al. 2002). The results displayed in figure 4.10 show that BrdU foci numbers were significantly decreased after ATMi treatment compared to control cells. This suggests that resection was impaired because ATM inhibition presumably resulted in inefficient phosphorylation of Plk3 and accordingly inefficient phosphorylation of CtIP. It was not possible to evaluate the effect of ATMi in the pRPA foci assay, because the phosphorylation of RPA at T21 in response to IR is ATM-dependent (Block et al. 2004).

Figures 4.7 to 4.10 collectively indicate that the kinase Plk3 is required for the repair of complex DSBs and promotes the resection of complex breaks in G1. Further, the results presented thus far, indicate that CtIP phosphorylation at Ser327 and Thr847 is required for

resection in G1. Hence, the role of Plk3 in phosphorylating CtIP at the aforementioned amino acids was evaluated next. To this end, endogenous CtIP was depleted in HeLa cells and the cells were transfected with GFP, siRNA-resistant GFP-CtIP-wt, or phosphomimic GFP-CtIP constructs. In these vectors, a serine and/or threonine was replaced with glutamic acid (GFP-CtIP-S327E, GFP-CtIP-T847E or GFP-CtIP-S327E/T847E). Due to its negative charge, glutamic acid mimics the structure of a phosphorylated serine or threonine residue; therefore these vectors mimic a constitutive phosphorylation at the indicated amino acids. The cells were treated with 2 Gy α -IR and pRPA foci were quantified after 6 h in GFP-positive G1 cells.

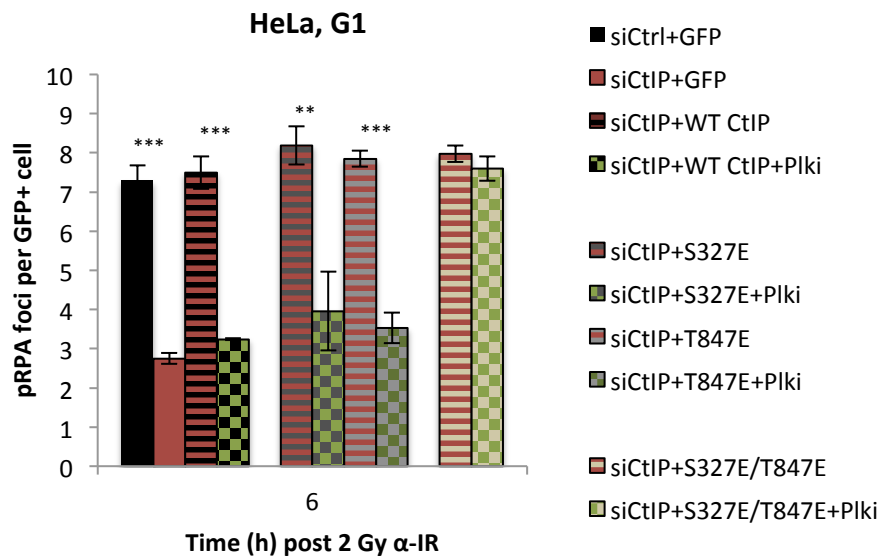


Figure 4.11 Plk3 phosphorylates CtIP at Ser327 and Thr847 in G1. HeLa cells were treated with siCtIP and transfected with GFP or various siRNA resistant GFP-CtIP vectors 24 h later. Nocodazole and EdU were added and cells were treated with Plki if indicated before irradiation with 2 Gy α -IR. Cells were fixed 6 h later and stained using anti-pRPA (pT21) and anti-GFP antibodies plus DAPI. Cells were scanned with Metafer and only GFP+ G1 cells were analyzed. $n \geq 3$, background foci were subtracted, error bars represent SEM, statistical significance tested by Student's t-test (**= $p < 0.01$, ***= $p < 0.001$) (knockdown efficiencies and vector expression were confirmed by Western Blot, see Barton et al. 2014)

Consistent with previous results (figure 4.3), depletion of endogenous CtIP resulted in significantly reduced pRPA foci numbers in G1 compared to siCtrl-treated cells. Complementation with GFP-CtIP-wt constructs restored the resection defect caused by CtIP depletion (figure 4.11, columns 1 to 3). When cells were complemented with GFP-CtIP-wt constructs and additionally treated with Plki, pRPA foci numbers in G1 were significantly

decreased compared to complementation with GFP-CtIP-wt alone (figure 4.11, columns 3 and 4). In the presence of Plki, the GFP-CtIP-wt construct could not be phosphorylated and therefore resection was impaired. Complementation with either one of the phosphomimic GFP-CtIP vectors (GFP-CtIP-S327E or GFP-CtIP-T847E) restored pRPA numbers to siCtrl levels. Additional treatment with Plki resulted in significantly impaired pRPA foci numbers compared to the complementation with either phosphomimic construct alone (figure 4.11, columns 5 to 8). In this case, even though one of the amino acids of the CtIP construct was constitutively phosphorylated (S327E or T847E), treatment with Plki inhibited the phosphorylation of the other amino acid. This result indicates that both amino acids, Ser327 and Thr847, have to be phosphorylated in a manner dependent on Plk3 to promote resection in G1 effectively.

Finally, complementation with GFP-CtIP-S327E/T847E vectors restored pRPA foci numbers to siCtrl levels. Strikingly, additional treatment with Plki did not cause a reduction in pRPA numbers (figure 4.11, columns 9 and 10). This indicates that the phosphomimic mutations at both amino acids overcame the requirement for Plk3 because even in the presence of Plki, the number of pRPA foci did not change compared to complementation with GFP-CtIP-S327E/T847E alone. Thus, when both Ser327 and Thr847 are constitutively phosphorylated, the kinase activity of Plk3 is not required to promote resection in G1. Collectively, these results provide evidence that Plk3 phosphorylates CtIP at Ser327 and Thr847 and that both phosphorylations have to occur for efficient resection to take place (figure 4.11).

All members of the Plk family possess a C-terminal polo-box domain (PBD) that binds to phosphorylated serine or threonine residues. The PBD regulates substrate binding, subcellular localization and catalytic activity of the kinase (Zitouni et al. 2014). To test if the Plk3 PBD is important for resection in G1, endogenous Plk3 was depleted with siRNA and HeLa cells were transfected with either GFP, siRNA-resistant FLAG-Plk3-wt or FLAG-Plk3- Δ PBD vectors. The Plk3 protein encoded by the FLAG-Plk3- Δ PBD vector contained a deleted PBD. Cells were treated with 2 Gy α -IR and pRPA foci were quantified after 2 and 6 h in GFP or FLAG-positive G1 cells.

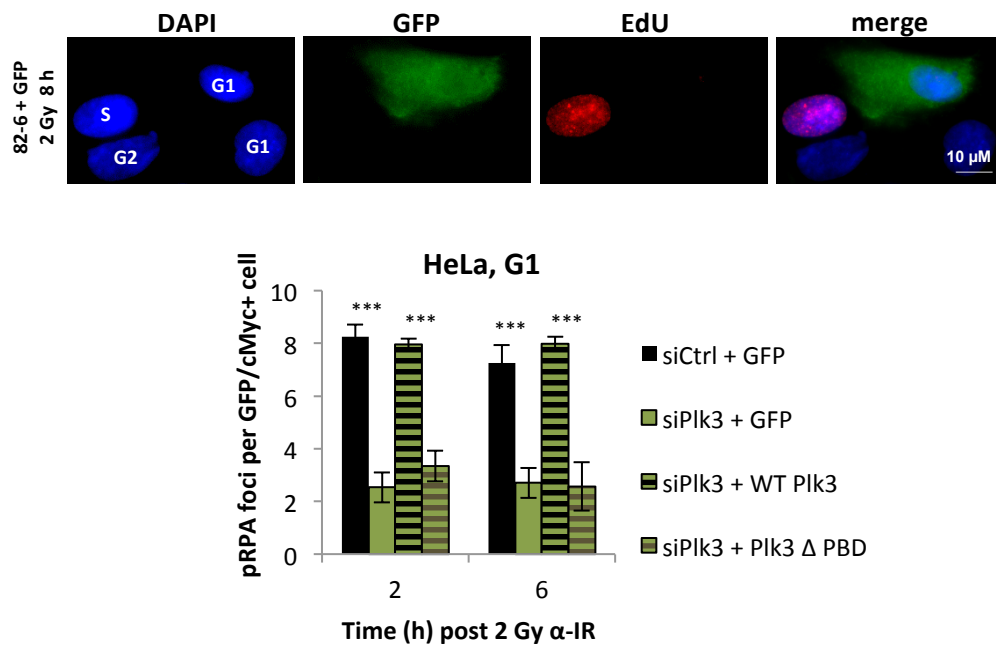


Figure 4.12 Resection in G1 requires the Plk3 PBD. HeLa cells were treated with siPlk3 and transfected with GFP or siRNA resistant FLAG-Plk3 vectors 24 h later. Nocodazole and EdU were added before irradiation with 2 Gy α -IR. Cells were fixed 2 and 6 h later and stained with anti-pRPA (pT21) and anti-GFP or anti-cMyc antibodies plus DAPI. Cells were scanned with Metafer and only GFP or cMyc+ G1 cells were analyzed. Images were acquired using Axiovision. $n \geq 3$, background foci were subtracted, error bars represent SEM, statistical significance tested by Student's t-test (***) ($p < 0.001$), (knockdown efficiencies and vector expression were confirmed by Western Blot, see Barton et al. 2014)

As previously observed (figure 4.9), depletion of Plk3 caused significantly decreased pRPA foci numbers in G1 compared to siCtrl-treated cells (figure 4.12). Complementation with the FLAG-Plk3-wt vector restored pRPA foci numbers to control levels. After complementation with the FLAG-Plk3- Δ PBD vector, significantly decreased pRPA foci numbers compared to complementation with the FLAG-Plk3-wt vector were observed in G1 (figure 4.12). These results suggest that Plk3 requires its PBD to promote resection in G1.

The results presented in this section provide compelling evidence that Plk3 is required for the repair of complex DSBs in G1 and promotes DSB end resection in this cell cycle phase. To test if Plk3, like CtIP, also functions upstream of Artemis in the slow repair component, the effect of Plk3-depletion on the Artemis repair defect after X-IR was analyzed next. To this end, wt 82-6 hTert and Artemis-deficient CJ179 hTert fibroblasts were treated with siPlk3 to deplete the endogenous Plk3 and transfected with GFP or siRNA-resistant FLAG-Plk3-wt constructs.

Cells were irradiated with 2 Gy X-IR and γ H2AX foci were analyzed 8 h later in GFP or FLAG-positive G1 cells.

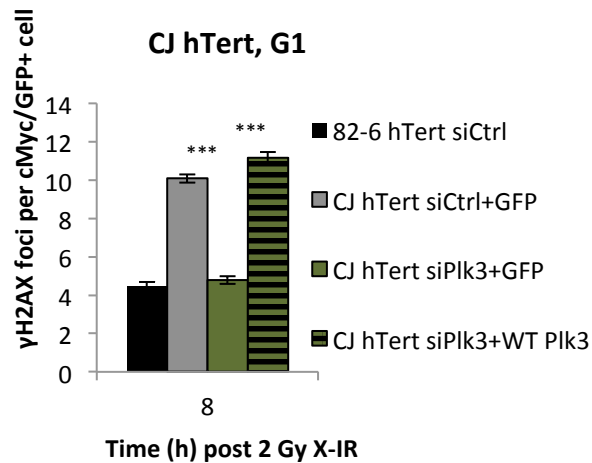


Figure 4.13 Plk3 depletion rescues the Artemis repair defect in G1 after X-IR. Wt 82-6 hTert or Artemis-deficient CJ179 hTert fibroblasts were treated with siPlk3 and transfected with GFP or siRNA resistant FLAG-Plk3-wt vectors after 24 h. Nocodazole and EdU were added before irradiation with 2 Gy X-IR. Cells were fixed 6 h later and stained with anti- γ H2AX and anti-GFP or anti-cMyc antibodies plus DAPI. Samples were scanned with Metafer and only GFP or FLAG+ G1 cells were analyzed. $n \geq 3$, background foci were subtracted, error bars represent SEM, statistical significance tested by Student's t-test (***) ($p < 0.001$), (knockdown efficiencies and vector expression were confirmed by Western Blot, see Biehs et al. 2017)

Consistent with previous results (figure 4.1), Artemis-deficient CJ179 hTert fibroblasts displayed a significant repair defect in G1 at 8 h post X-IR compared to wt 82-6 hTert cells (figure 4.13). Plk3 depletion significantly decreased the number of γ H2AX foci in Artemis-deficient cells to wt levels. Furthermore, complementation with a FLAG-Plk3-wt vector restored the Artemis repair defect, confirming that siPlk3 did not have any off-target effects (figure 4.13). Therefore, treatment with siPlk3, similar to treatment with siCtIP, rescued the Artemis repair defect. This provides further evidence that Plk3 function lies upstream of Artemis function during the slow repair component in G1. When CtIP-dependent resection is abolished by Plk3-depletion, the requirement for Artemis is lost and therefore the repair defect is no longer observed. This indicates that inhibition of resection by CtIP- or Plk3-depletion in G1 might cause a pathway switch from resection-dependent to resection-independent repair after X-IR.

4.3 Nucleases

The first part of this project established that CtIP-, Artemis- and Plk3-dependent DNA end resection occurs in G1. Resection in G2 is well characterized: it is initiated by Mre11 endonuclease, which makes an endonucleolytic, single-stranded incision approximately 300 nt away from the DSB end (Garcia et al. 2011). Subsequent resection occurs bi-directionally and requires the function of several nucleases and helicases. Mre11 exonuclease and EXD2 resect in 3' to 5' direction towards the DSB end, while Exo1 or BLM/DNA2 resect in 5' to 3' direction away from the DSB end (Shibata et al. 2014; Broderick et al. 2016). To further characterize the resection process in G1, the role of the aforementioned enzymes was analyzed next.

The involvement of Exo1, EXD2 and BLM/DNA2 can easily be tested by siRNA depletion. Mre11, however, is part of the MRN complex, which is important for the activation of ATM. Thus, using Mre11 siRNA will interfere with MRN complex formation and consequently ATM activation. Cells deficient in ATM display a repair defect at late time points post IR because ATM is important for Kap1 phosphorylation and subsequent chromatin relaxation (Riballo et al. 2004; Goodarzi et al. 2008; Beucher et al. 2009). Therefore, to avoid a confounding variable like insufficiently activated ATM, specific Mre11 endo- and exonuclease inhibitors (Mre11i endo and Mre11i exo) were obtained (Shibata et al. 2014). These inhibitors specifically target the endo- or exonuclease function of Mre11 without interfering with ATM activation. To confirm this, HeLa cells were treated with DMSO, Mre11i endo, or Mre11i exo before 2 Gy X-IR. Cells were stained with anti-pATM (S1981) and anti- γ H2AX antibodies at 30 min post IR. Formation of pATM foci in all irradiated samples and co-localization with γ H2AX confirmed that Mre11 inhibitors did not interfere with ATM activation (figure 4.14).

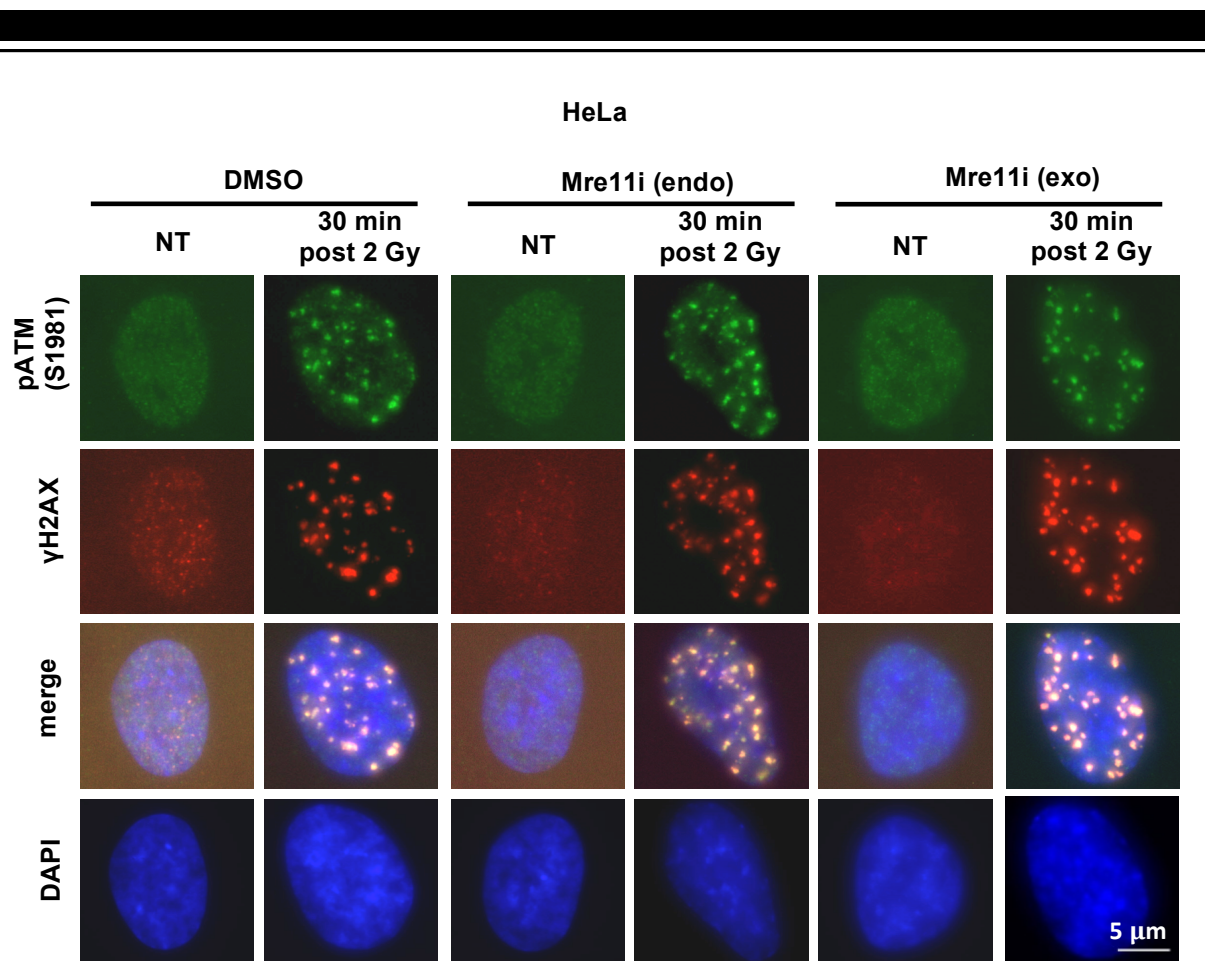


Figure 4.14 Formation of pATM foci after Mre11 inhibitor treatment. HeLa cells were treated with DMSO, Mre11i endo, or Mre11i exo. Nocodazole and EdU were added before irradiation with 2 Gy X-IR. Cells were fixed 30 min later and stained with anti-pATM (S1981) and anti- γ H2AX antibodies and DAPI. Images were acquired using Axiovision. NT=not treated (Bielski et al. 2017)

To further confirm the efficiency of the Mre11 nuclease inhibitors, γ H2AX data in G2 fibroblasts were compared with published results (Shibata et al. 2014). Brca2-deficient HSC62 hTert cells were treated with DMSO, Mre11i endo, Mre11i exo or different siRNAs. HSC62 hTert cells are defective in HR therefore they display a repair defect at late time points in G2. As previously discussed, after X-IR, a repair defect in G2 caused by lack of an HR factor can be rescued by depletion of an upstream factor that results in the inhibition of resection.

Figure 4.15A shows that significantly less residual γ H2AX foci were detected in Brca2-deficient G2 cells treated with Mre11i endo but not in cells treated with Mre11i exo compared to DMSO-treated cells. This result is in good agreement with previously published data (Shibata et al. 2014) and indicates that Mre11 endonuclease is involved in the initiation of resection and functions upstream of Mre11 exonuclease in G2. HSC62 hTert cells treated with

siExo1/BLM show the same number of γ H2AX foci as siCtrl-treated cells in G2. The Brca2 repair defect is not rescued in this case because in these cells resection is initiated by Mre11 endonuclease and resection can be extended towards the DSB end by Mre11 exo (3' to 5' direction), committing the repair of the breaks to HR. Strikingly, after depletion of siExo1/siBLM together with Mre11i exo inhibition, γ H2AX foci are considerably reduced compared to siCtrl-treated cells (figure 4.15A, last column). As previously reported by Shibata et al. (2014), the repair pathway can switch to resection-independent repair in G2, when resection is inhibited in both directions. (5' to 3' and 3' to 5') even after the ssDNA nick is made by Mre11 endonuclease, resulting in improved repair in a Brca2-deficient background.

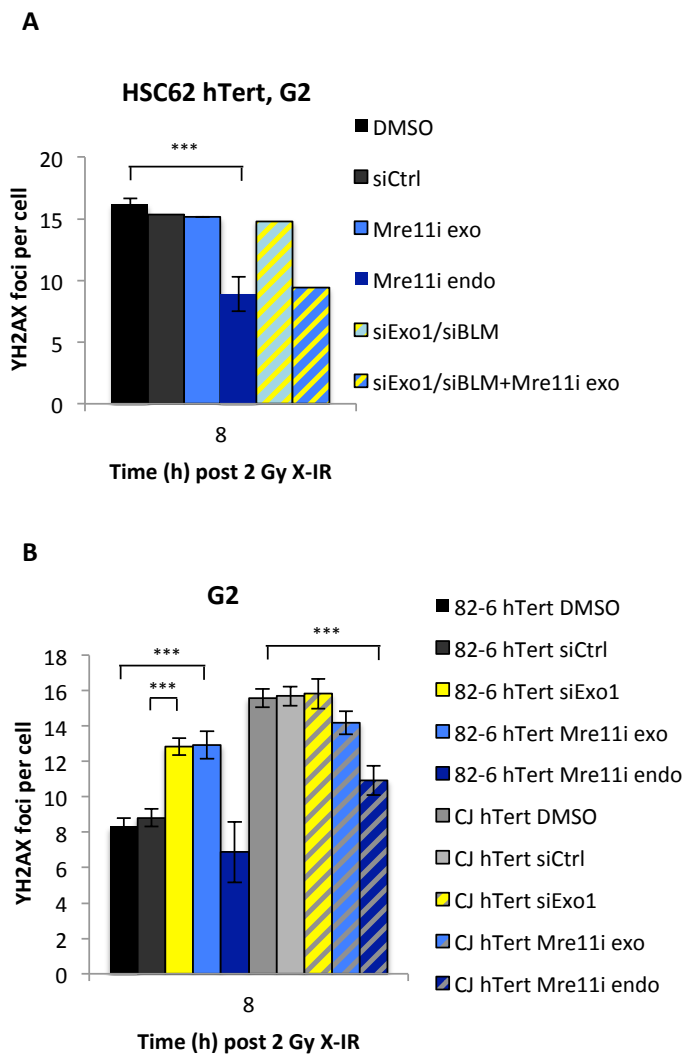


Figure 4.15 Control experiments with Mre11 endonuclease and exonuclease inhibitors. Fibroblast cells were treated with siRNA and/or Mre11 endo- or exonuclease inhibitors. Prior to X-IR with 2 Gy, nocodazole and EdU were added. (A) Brca2-deficient HSC62 hTert fibroblasts were fixed 8 h post IR and stained with an anti- γ H2AX antibody and DAPI. Samples were scanned using Metafer and only G2 cells were analyzed. $n \geq 1$ (B) Wt 82-6 hTert fibroblasts and Artemis-deficient CJ179 hTert fibroblasts were fixed 8 h post IR and stained with an anti- γ H2AX antibody and DAPI. Samples were scanned using Metafer and only G2 cells were analyzed. $n \geq 3$, background foci were subtracted, error bars represent SEM, statistical significance tested by Student's t-test (***)= $p < 0.001$), (knockdown efficiencies were confirmed by Western Blot, see Biehs et al. 2017)

Next, the effect of Mre11i and siExo1 in wt 82-6 hTert and Artemis-deficient CJ179 hTert fibroblasts after X-IR in G2 was analyzed. Shibata et al. (2014) previously reported that depletion of Exo1 or Mre11i exo treatment causes a repair defect in the slow component in G2 wt cells, because as soon as resection commences, repair is committed to HR but cannot be completed when Exo1 or Mre11 exonuclease are not available. Accordingly, Mre11i endo does not cause a repair defect in wt 82-6 hTert cells because resection is not initiated and breaks can be repaired by c-NHEJ. These results were confirmed in this study and are presented in figure 4.15B. Moreover, repair in Artemis-deficient CJ179 hTert cells was significantly improved in G2 after treatment with Mre11i endo (figure 4.15B), confirming that Mre11 endo functions upstream of Artemis in G2 to initiate resection.

After the Mre11 inhibitors were established and results in G2 phase were consolidated with published data, the involvement of nucleases during resection in G1 was analyzed using the pRPA assay. HeLa cells were treated with various siRNAs, Mre11i endo, or Mre11i exo, irradiated with 2 Gy α -IR, and pRPA foci were analyzed 2 h post IR.

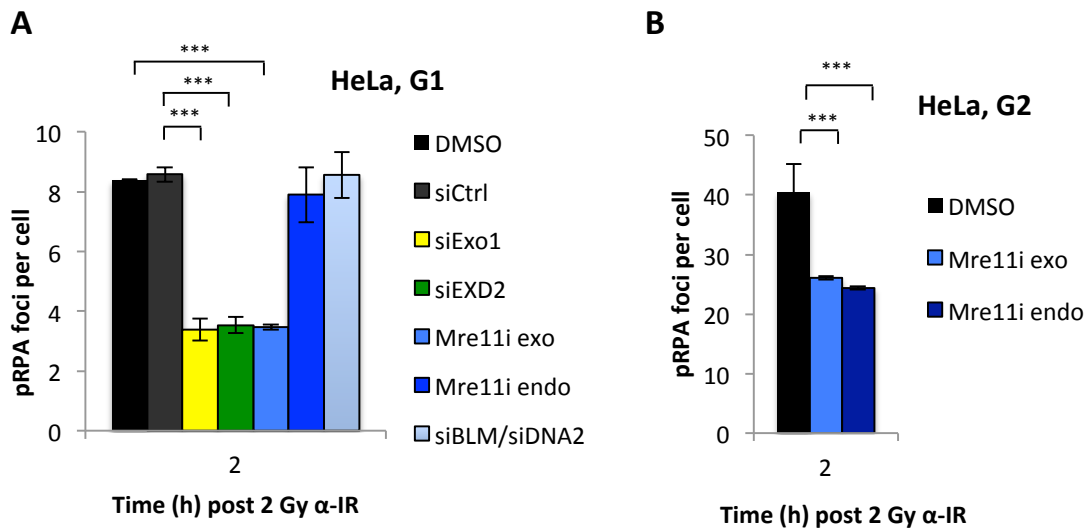


Figure 4.16 Resection in G1 requires specific nuclease activities. (A) and (B) HeLa cells were treated with various siRNAs, Mre11 exo- or Mre11 endonuclease inhibitors. EdU and nocodazole were added before irradiation with 2 Gy α -IR. Cells were fixed 2 h later and stained with an anti-pRPA (pT21) antibody and DAPI. Samples were scanned using Metafer and the G1 or G2 population was analyzed. $n \geq 3$, background foci were subtracted, error bars represent SEM, statistical significance tested by Student's t-test (***) ($p < 0.001$), (knockdown efficiencies were confirmed by Western Blot, see Biehs et al. 2017)

Figure 4.16A demonstrates that pRPA foci numbers were significantly decreased after treatment with siExo1, siEDX2, or Mre11i exo compared to DMSO- or siCtrl-treated cells.

Treatment with Mre11i endo or depletion of BLM/DNA2, on the other hand, did not affect the number of pRPA foci compared to control cells (figure 4.16A). This indicates that, similar to resection in G2, resection in G1 requires the activities of Exo1, EXD2, and Mre11 exonuclease. Contrary to G2, resection in G1 does not necessitate the activities of Mre11 endonuclease or BLM/DNA2. As a control, pRPA numbers were quantified in G2 cells after Mre11i endo or Mre11i exo. Both inhibitors caused significantly decreased pRPA foci numbers compared to DMSO-treated cells because both nuclease activities are required for resection in G2 (figure 4.16B).

The results obtained with the pRPA assay were then consolidated after X-IR in an Artemis rescue experiment. Wt 82-6 hTert and Artemis-deficient CJ179 hTert fibroblasts were treated with various siRNAs or Mre11 inhibitors and γ H2AX foci were enumerated at 8 h post 2 Gy X-IR. As expected, depletion of Exo1, EXD2, BLM/DNA2 or treatment with Mre11i did not have an effect on γ H2AX foci in wt G1 82-6 hTert fibroblasts. Loss of any one of these factors did not affect γ H2AX foci numbers in wt G1 cells, because after X-IR, the DSB repair pathway can switch to resection-independent repair (figure 4.17A). Consistent with previous results (figures 4.1 and 4.13), a repair defect was observed in Artemis-deficient CJ179 hTert G1 fibroblasts at 8h post X-IR. Strikingly, the number of γ H2AX foci was significantly decreased after depletion of Exo1, EXD2 or Mre11i exo treatment. Mre11i endo treatment or depletion of BLM/DNA2, on the other hand, did not affect the number of γ H2AX foci in Artemis-deficient cells (figure 4.17A). This confirms the result from the pRPA assay, indicating that Exo1, EXD2 and Mre11 exo are all involved in resection in G1, while Mre11 endo and BLM/DNA2 are dispensable for the process. Further, this result suggests that Exo1, EXD2 and Mre11 exonuclease all function upstream of Artemis in the initiation of resection, because the requirement for Artemis is overcome after depletion or inhibition of one of the factors.

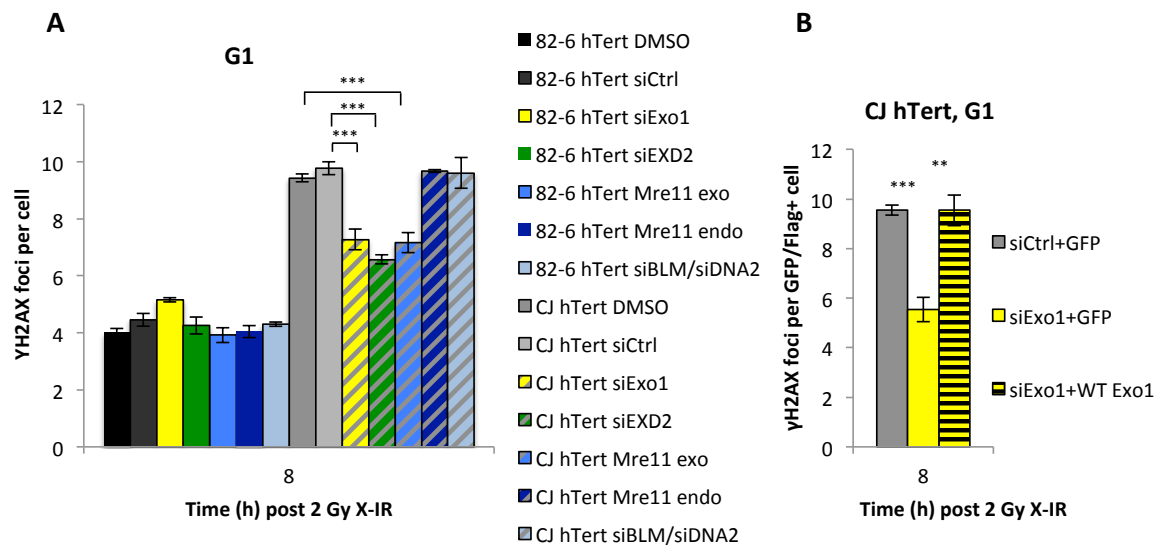


Figure 4.17 Depletion of Exo1, EXD2, or Mre11i exo treatment rescue the Artemis repair defect in G1 after X-IR. (A) Wt 82-6 hTert and Artemis-deficient CJ179 hTert fibroblasts were treated with various siRNAs or Mre11 endo- or exonuclease inhibitors. Nocodazole and EdU were added before irradiation with 2 Gy X-IR. Cells were fixed 8 h later and stained with an anti- γ H2AX antibody and DAPI. Samples were scanned using Metafer and only G1 cells were analyzed. **(B)** CJ179 hTert fibroblasts were treated with siExo1 and transfected with GFP or siRNA resistant FLAG-Exo1-wt vectors 24 h later. EdU and nocodazole were added before irradiation with 2 Gy X-IR. Cells were fixed 8 h later and stained with anti- γ H2AX and anti-GFP or anti-FLAG antibodies plus DAPI. Samples were scanned using Metafer and only GFP- or FLAG-positive G1 cells were analyzed. $n \geq 3$, background foci were subtracted, error bars represent SEM, statistical significance tested by Student's t-test, (**= $p < 0.01$, ***= $p < 0.001$), (knockdown efficiencies and vector expression were confirmed by Western Blot, see Biehs et al. 2017)

To exclude potential off-target effects from the siRNA treatment, CJ179 hTert cells were treated with siExo1 to deplete the endogenous protein, and transfected with GFP or siRNA-resistant FLAG-Exo1-wt constructs. γ H2AX foci were scored 8 h post 2 Gy X-IR in GFP- or FLAG-positive G1 cells. Consistent with the results shown in figure 4.17A, γ H2AX foci were significantly reduced after siExo1 treatment compared to siCtrl-treated cells (figure 4.17B). After complementation with a FLAG-Exo1-wt construct, γ H2AX foci levels increased significantly compared to siExo1-treated cells, i.e. the Artemis repair defect was restored (figure 4.17B). Complementation with an Exo1-wt construct restored the Artemis repair defect in Exo1-depleted Artemis-deficient CJ179 hTert cells, because resection could be initiated after complementation with a functional Exo1 protein, resulting in the requirement for Artemis. The results presented in figure 4.17B confirm that siExo1 did not have any off-target effects.

4.4 53BP1 and Brca1

The previous sections established that the slow repair component in G1 involves Artemis- and CtIP-dependent DSB end resection that is regulated by Plk3. Further, the nucleases Exo1, EXD2, and Mre11 exonuclease, which were all previously described for their role during resection in S/G2, were identified as novel players during resection in G1.

However, it remained unclear how resection in G1 is regulated. Recently, a regulatory network was identified that is involved in DSB repair pathway choice through the control of DSB end resection. This regulatory circuit comprises the antagonistic actions of p53 binding protein (53BP1) and Brca1. 53BP1 is a mediator protein that is recruited to the chromatin surrounding DSBs through a complex signaling pathway that ultimately results in the ubiquitination of histones H2A and H2AX by the E3 ubiquitin ligases ring finger protein 8 (RNF8) and ring finger protein 168 (RNF168). For stable 53BP1 binding to chromatin, two histone modifications are required: the constitutive H4K20me2 chromatin mark as well as the DNA damage-induced ubiquitylated H2A or H2AX (Noon & Goodarzi 2011; Zimmermann & De Lange 2014).

In G1, 53BP1 and its effector proteins RAP1 interacting factor 1 (Rif1) and Pax transactivation domain-interacting protein (PTIP) are recruited to the chromatin surrounding a DSB where they stimulate NHEJ and block the accumulation of Brca1. In S/G2, phosphorylated CtIP forms a complex with Brca1 and antagonizes Rif1 accumulation at DSBs (Escribano-Díaz et al. 2013; Escribano-Diaz & Durocher 2013).

According to the literature, 53BP1 protects DSB ends from resection in G1. Therefore, it was hypothesized that depletion of 53BP1 via siRNA will result in excessive resection and an increase in pRPA foci levels. To test this, HeLa cells were treated with si53BP1, irradiated with 2 Gy α -IR and analyzed at 6 h post IR.

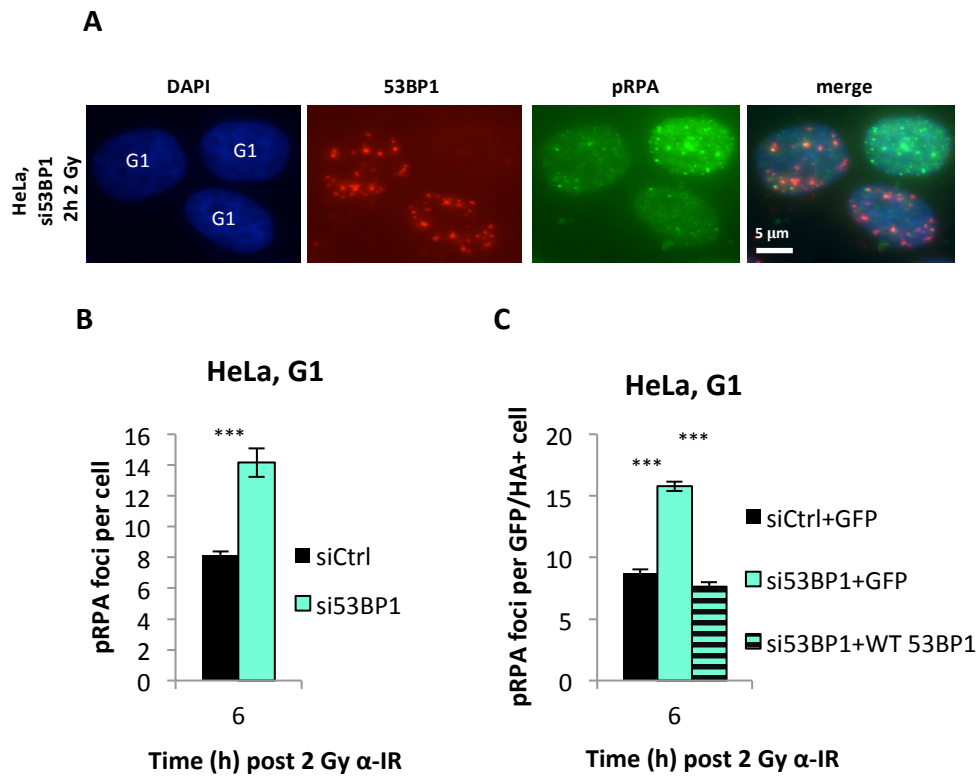


Figure 4.18 Depletion of 53BP1 causes hyper-resection in G1. HeLa cells were treated with si53BP1, EdU and nocodazole were added before irradiation with 2 Gy α -IR. Cells were fixed 2 h or 6 h later and stained with anti-53BP1 and anti-pRPA (pT21) antibodies and DAPI. (A) Images were acquired using Metafer. (B) Quantification of pRPA foci in G1 cells treated with si53BP1. (C) Endogenous 53BP1 was depleted by siRNA and cells were transfected with GFP or siRNA resistant HA-53BP1-wt vectors 24 h later. Cells were additionally stained with an anti-HA antibody and scanned with Metafer and only GFP or HA+ G1 cells were quantified. $n \geq 3$, background foci were subtracted, error bars represent SEM, statistical significance tested by Student's t-test (***= $p < 0.001$), (knockdown efficiencies and vector expression were confirmed by Western Blot, see Biehs et al. 2017)

The transfection efficiency for si53BP1 can be easily monitored by IF staining with an anti-53BP1 antibody. Cells that were efficiently depleted of 53BP1 showed intensified pRPA staining and visibly elevated pRPA foci numbers (figure 4.18A), indicating hyper-resection. The quantification shown in figure 4.18B confirmed this observation. Depletion of 53BP1 caused a significant increase in pRPA foci compared to cells treated with siCtrl (figure 4.18B), indicating that more DSB end resection was occurring after 53BP1 depletion. To exclude potential off-target effects of the siRNA, HeLa cells were depleted of endogenous 53BP1 and transfected with GFP or siRNA-resistant HA-53BP1-wt constructs. Consistent with the results presented in figure 4.18B, significantly increased pRPA foci levels were observed after depletion of 53BP1 compared to siCtrl-treated cells (figure 4.18C). Complementation with

HA-53BP1-wt restored the pRPA foci level to siCtrl levels, confirming that the siRNA was specific for 53BP1 (figure 4.18C).

The tumor suppressor Brca1 plays a pivotal role in maintaining genome stability and has two important functional domains (Christou & Kyriacou 2013). The N-terminal RING domain is responsible for the E3 ubiquitin ligase activity of Brca1 and also mediates the interaction with Bard1. The tandem C-terminal BRCT domains recognize and bind to proteins that are phosphorylated by ATM and ATR after DNA damage (Clark et al. 2012). In asynchronously cycling HeLa cells, the Brca1 expression level in G1 is similar to S/G2 phase. The accumulation of Brca1 at sites of DNA damage in G1, however, is inhibited by 53BP1 and its effectors RIF1 and PTIP (Escribano-Díaz et al. 2013; Feng et al. 2015).

Here, a pathway is described that involves resection in G1. This provokes the question how resection-dependent repair in G1 is possible if the DSB ends are protected by 53BP1 and Brca1 accumulation is inhibited. Thus, the first step was to compare Brca1 foci formation after X-IR and α -IR. To this end, HeLa cells were irradiated with 2 Gy X-IR or α -IR, fixed 2 h later, and stained with anti-Brca1 and anti- γ H2AX antibodies. As expected, and in agreement with the literature, Brca1 did not show robust accumulation at DSBs in G1 after X-IR, as opposed to G2 where Brca1 formed clear foci that co-localized with γ H2AX (figure 4.19A). Strikingly, after α -IR, robust Brca1 accumulation at DSBs was observed in G1 as well as in G2 (figure 4.19B).

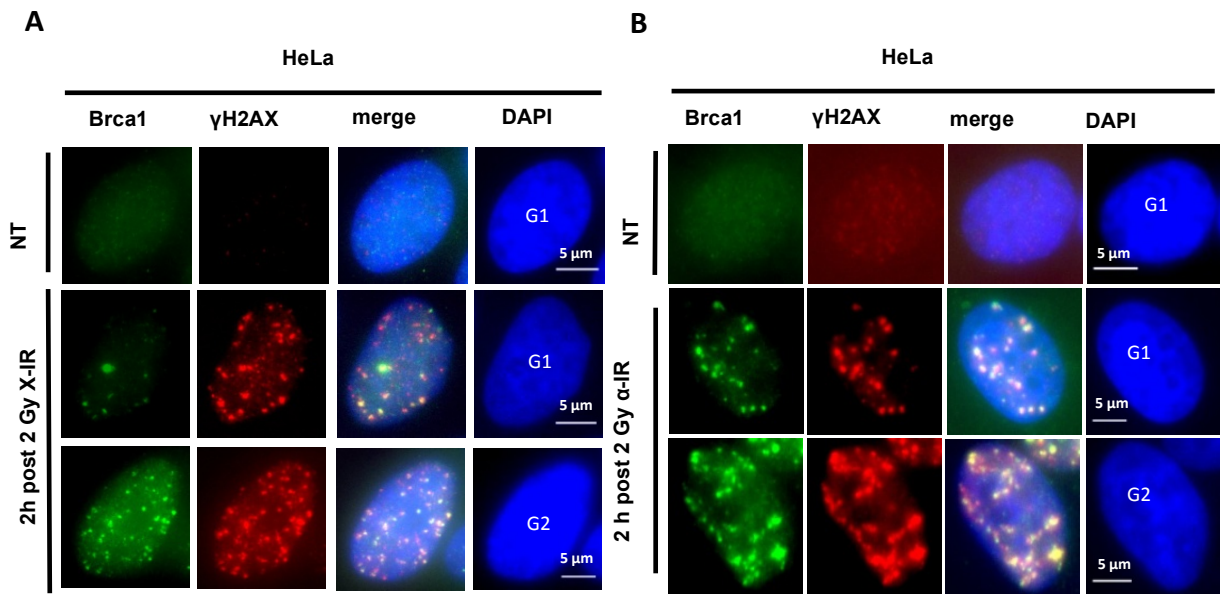


Figure 4.19 Brca1 accumulation at DSBs after X-IR and α -IR. HeLa cells were treated with EdU and nocodazole before irradiation with (A) 2 Gy X-IR or (B) 2 Gy α -IR. Cells were fixed 2 h post IR and stained with anti-Brca1 (D9) and anti- γ H2AX antibodies plus DAPI. Images were acquired using Metafer. NT=not treated (Biehs et al. 2017)

The images presented in figure 4.19B suggest that after α -IR, Brca1 accumulation at DSBs is not inhibited in G1. The complex damages induced by α -IR are resected to an extent in G1 that allows RPA binding to the ssDNA regions. For stable binding of RPA, the ssDNA stretch must be at least 30 nt long (Bochkareva et al. 2002), which would be difficult to achieve if resection was completely blocked by 53BP1 bound to chromatin around the DSB. Based on the observed Brca1 accumulation at DSB sites after α -IR (figure 4.19B), it was hypothesized that Brca1 might be involved in the displacement of 53BP1 in G1 to allow limited resection. To elucidate this assumption, HeLa cells were treated with siBrca1, irradiated with 2 Gy α -IR and fixed 6 h later. Significantly less pRPA foci were detected in siBrca1-treated cells compared with the siCtrl-treated samples, indicating that Brca1 promotes resection in G1 (figure 4.20). Cells that were double depleted of 53BP1 and Brca1, however, displayed the same phenotype as 53BP1 depletion alone (figure 4.18): pRPA foci were significantly elevated compared to control cells (figure 4.20). This result indicates that the function of Brca1 in G1 is the displacement of 53BP1 to allow resection. Therefore, once 53BP1 is depleted, Brca1 is also not required anymore.

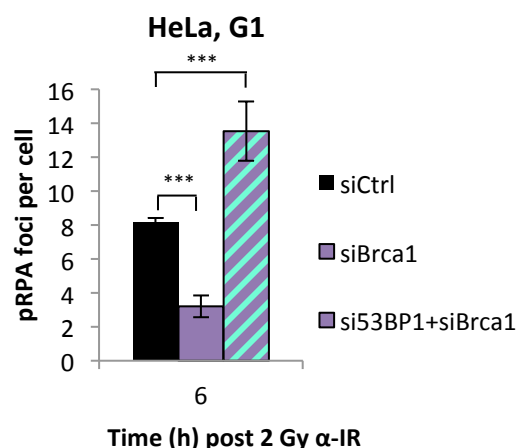


Figure 4.20 Brca1 promotes resection and is required for displacement of 53BP1 in G1. HeLa cells were treated with siBrca1 or siBrca1/si53BP1. Nocodazole and EdU were added before irradiation with 2 Gy α -IR, cells were fixed 6 h later and stained with an anti-pRPA (pT21) antibody and DAPI. Samples were scanned using Metafer and only G1 cells were analyzed. $n \geq 3$, background foci were subtracted, error bars represent SEM, statistical significance tested by Student's t-test (***) ($p < 0.001$), (knockdown efficiencies were confirmed by Western Blot, see Biehs et al. 2017)

As previously described, Brca1 has two important functional domains. To determine if one or both of these domains are important for resection in G1, stable MEF cell lines expressing either a Brca1 wt gene, a mutation in the Brca1 RING domain (I26A) or a mutation in the Brca1 BRCT domain (S1655F) were used next. The cells were irradiated with 2 Gy α -IR, fixed 2 and 6 h later and pRPA foci were quantified in G1.

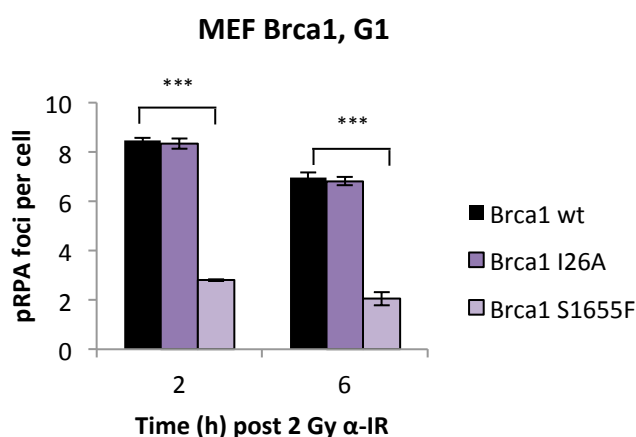


Figure 4.21 The Brca1 BRCT domain is required for resection in G1. Stable MEF cells expressing either the wt Brca1 protein, Brca1 with a mutated RING domain (I26A) or Brca1 with a mutated BRCT domain (S1655F) were treated with EdU and nocodazole and irradiated with 2 Gy α -IR. Cells were fixed at 2 and 6 h post IR and stained with an anti-pRPA (pT21)

antibody and DAPI. Samples were scanned using Metafer and only G1 cells were analyzed. $n \geq 3$, background foci were subtracted, error bars represent SEM, statistical significance tested by Student's t-test ($***=p<0.001$), (Biehs et al. 2017)

The analysis of pRPA foci in G1 after α -IR revealed that pRPA foci numbers were significantly reduced in MEF cells expressing a mutated Brca1 BRCT domain (S1655F) compared to MEF cells with a wt Brca1 protein (figure 4.21). A mutation in the RING domain (I26A), on the other hand, did not affect pRPA foci numbers compared to Brca1 wt cells (figure 4.21). This indicates that the BRCT domain, but not the RING domain, is required for resection in G1. In S/G2, the Brca1 BRCT domain mediates the interaction between CtIP phosphorylated at Ser327 and Brca1 (Escribano-Díaz et al. 2013). Since CtIP is involved in the repair of complex breaks in G1 and it is also phosphorylated at the same amino acid (Ser327) that is important for the interaction with Brca1 in S/G2, it is likely that CtIP and Brca1 also interact in G1.

Lastly, the effect of Brca1-depletion on the Artemis repair defect was analyzed. Wt 82-6 hTert and Artemis-deficient CJ179 hTert fibroblasts were treated with siBrca1 and γ H2AX foci were enumerated at 8 h after 2 Gy X-IR.

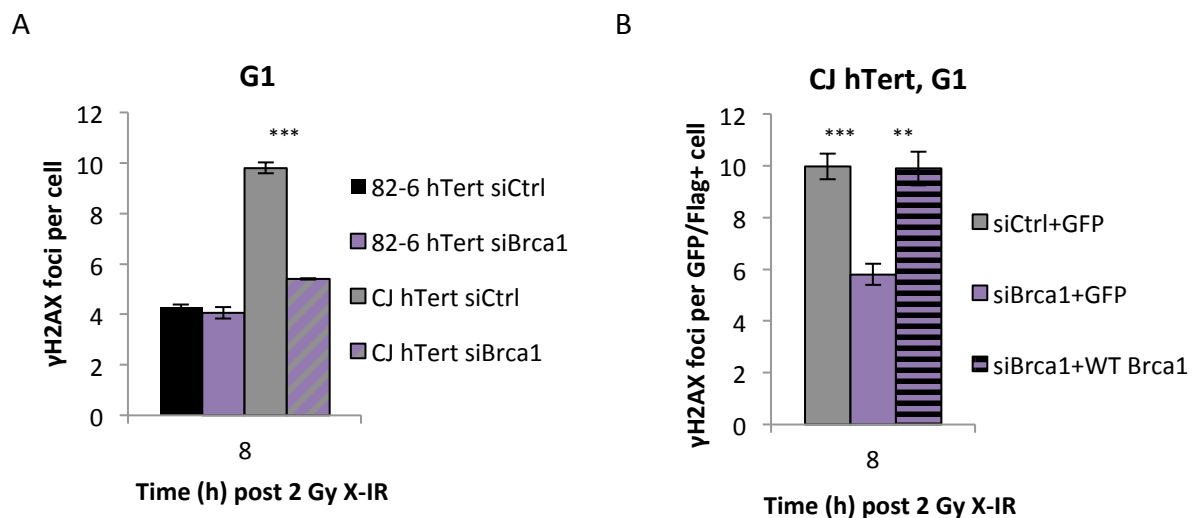


Figure 4.22 Brca1 depletion rescues the Artemis repair defect in G1 after X-IR. All fibroblast cells were treated with EdU and nocodazole prior to irradiation with 2 Gy X-IR and were fixed 8 h later. **(A)** Wt 82-6 hTert fibroblasts and Artemis-deficient CJ179 hTert fibroblasts were treated with siBrca1 and stained with an anti- γ H2AX antibody and DAPI. Samples were scanned using Metafer and only G1 cells were analyzed. **(B)** Artemis-deficient CJ179 hTert fibroblasts were treated with siBrca1 and transfected with GFP or FLAG-Brca1-wt vectors 24 h later. Cells were stained with anti- γ H2AX, anti-GFP or anti-FLAG antibodies and DAPI. Samples were scanned using Metafer and only GFP or FLAG+ G1 cells were analyzed. $n \geq 3$, background foci were subtracted, error bars represent SEM, statistical significance tested by Student's t-test, ($***=p<0.001$, $**=p<0.01$) (knockdown efficiencies and vector expression were confirmed by Western Blot, see Biehs et al. 2017)

Brca1 depletion did not have any effect on γ H2AX foci numbers in G1 wt 82-6 hTert cells compared to siCtrl-treated cells (figure 4.22A). Consistent with previous observations (figures 4.1, 4.13 and 4.17), Artemis-deficient CJ179 hTert cells showed elevated γ H2AX foci numbers at 8 h post X-IR in G1 compared to wt 82-6 hTert cells (figure 4.22A). Brca1 depletion caused a significant reduction in γ H2AX foci in Artemis-deficient cells compared to siCtrl-treated cells (figure 4.22A). Hence, Brca1 depletion rescued the Artemis repair defect in G1. This result provides further evidence that Brca1 is involved in the slow repair component in G1 where it functions upstream of Artemis in the initiation of resection.

To exclude potential off-target effects of the Brca1 siRNA treatment, CJ179 hTert fibroblasts were treated with siBrca1 to deplete the endogenous protein and transfected with GFP or siRNA-resistant FLAG-Brca1-wt constructs. Consistent with the results presented in figure 4.22A, the number of γ H2AX foci was significantly reduced after siBrca1 depletion compared to siCtrl-treated cells (figure 4.22B). After complementation with FLAG-Brca1-wt, γ H2AX foci numbers were significantly elevated compared to siBrca1-treated cells (figure 4.22B). Thus, the Artemis repair defect was restored, indicating that the siRNA treatment did not have any off-target effects.

4.5 Resection in G1 after high X-ray doses

In this project two methods were mainly used to study resection in G1: the pRPA assay after α -IR and the Artemis rescue experiment after X-IR. Quantification of pRPA foci in G1 provided a tool to directly measure resection in G1, while the Artemis rescue experiments provided indirect evidence that factors are involved in the slow repair component. The X-ray dose used for all these experiments was too low (2 Gy) to detect pRPA foci in G1 because the majority of breaks are quickly rejoined by fast, resection-independent c-NHEJ. The subset of DSBs which are Artemis-dependent after low doses of X-IR, presumably get resected because repair in the heterochromatic regions is delayed, therefore allowing more time for resection to occur (Goodarzi et al. 2008). However, this resection is not extensive enough for RPA binding and pRPA foci detection, and consequently α -IR was used for pRPA foci measurements in G1. To exclude the possibility that pRPA foci formation is an artifact of α -IR, HeLa cells were irradiated with a very high dose of X-IR (20 Gy) to induce a plethora of DNA damages in the cell. Presumably, the repair of such high numbers of DSBs will be slowed down, resulting in a

higher probability that some break ends undergo resection that is extensive enough for RPA binding.

To this end, HeLa cells were treated with siCtIP, siArtemis, siExo1, siBrca1, Mre11i (endo) or Mre11i (exo), irradiated with 20 Gy X-IR and pRPA foci were analyzed after 4 h. Indeed, after irradiation with 20 Gy X-IR, robust pRPA foci formation was observed in G1 HeLa cells (figure 4.23A). Of note, depletion of the aforementioned proteins (except Mre11 endonuclease) resulted in significantly reduced pRPA foci numbers compared to control cells (figure 4.23B). This indicates that the resection observed in G1 cells after high doses of X-IR is dependent on the same key proteins as resection of α -IR-induced DSBs.

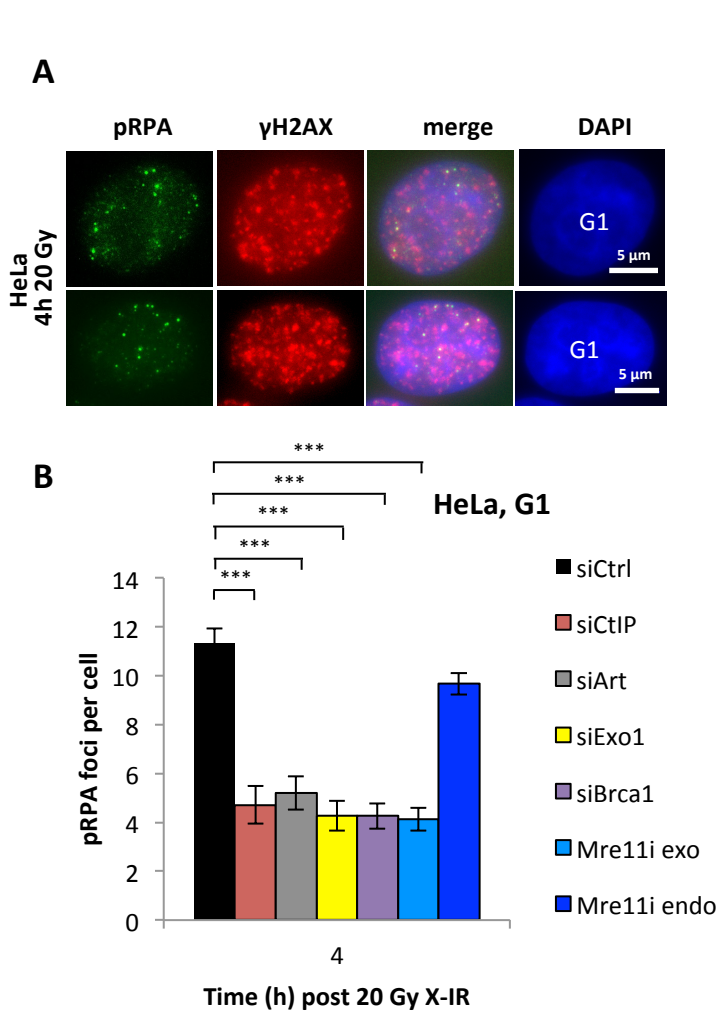


Figure 4.23 pRPA foci form in G1 after high doses of X-IR. HeLa cells were treated with nocodazole and EdU before irradiation with 20 Gy X-IR. Cells were fixed 4 h later and stained with anti-pRPA (pT21) or anti- γ H2AX antibodies and DAPI. (A) Images were acquired using Metafer. (B) Cells were treated with various siRNAs before irradiation. Samples were scanned using Metafer and only G1 cells were analyzed. $n \geq 3$, background foci were subtracted, error bars represent SEM, statistical significance tested by Student's t-test (** $p < 0.001$), (knockdown efficiencies were confirmed by Western Blot, see Biehs et al. 2017)

4.6 C-NHEJ or alt-NHEJ?

The results presented thus far indicate that resection-dependent DSB repair occurs in G1. CtIP-dependent resection is a crucial step in alt-NHEJ, a backup repair pathway that operates in the absence of the core c-NHEJ protein Ku70/80 (Mansour et al. 2013). Hence, the final section of this project was dedicated to the analysis whether the pathway described here represents c-NHEJ or alt-NHEJ. One of the key players required for alt-NHEJ is PARP1. Similar to Ku, PARP1 is a highly abundant nuclear protein with affinity to bind DSB ends (Grundy et al. 2014). Hence, to test if the resection-dependent pathway described here represents repair by alt-NHEJ, fibroblast cells were treated with the PARP inhibitor PJ34 (PARPi), to block PARP1 activity, and DSB repair was monitored after α -IR or X-IR.

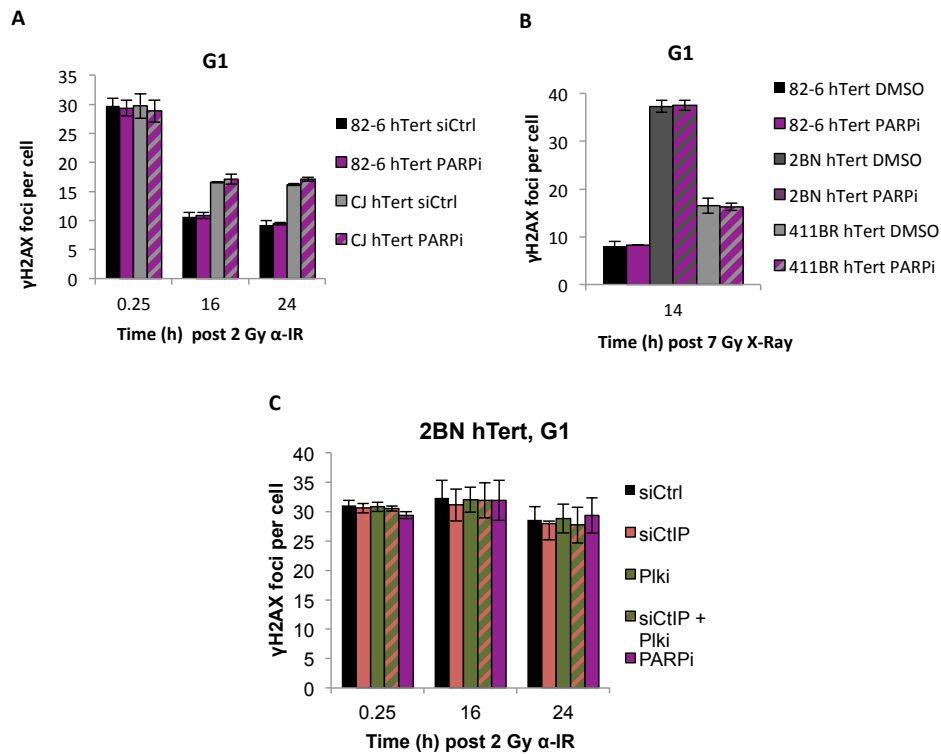


Figure 4.24 PARPi treatment does not affect DSB repair in G1. All cells were treated with nocodazole and EdU prior to IR. **(A)** Wt 82-6 hTert and Artemis-deficient CJ179 hTert fibroblasts were treated with PARPi and irradiated with 2 Gy α -IR. Cells were fixed at various times post IR and stained with an anti- γ H2AX antibody and DAPI. Samples were scanned using Metafer and only G1 cells were analyzed (Biehs et al. 2017). **(B)** Wt 82-6 hTert, XLF-deficient 2BN hTert and hypomorphic Lig4-deficient 411BR hTert fibroblasts were treated with PARPi and irradiated with 7 Gy X-IR and fixed 14 h later. Cells were stained with an anti- γ H2AX antibody and DAPI and scanned using Metafer. Only G1 cells were analyzed (Biehs et al. 2017). **(C)** XLF-deficient 2BN hTert fibroblasts were treated with siCtIP, Plki, and PARPi and irradiated with 2 Gy α -IR. Cells were fixed at various times post IR and stained with an anti- γ H2AX antibody and DAPI. Samples were scanned using Metafer and only G1 cells were analyzed. $n \geq 3$, background foci were subtracted, error bars represent SEM

Treatment with PARPi did not have an effect on the repair of DSBs in G1 wt 82-6 hTert or Artemis-deficient CJ179 hTert fibroblasts after α -IR (figure 2.24A), indicating that DSBs are not repaired by alt-NHEJ. This indication was substantiated with two different c-NHEJ-mutant cell lines. XLF-deficient 2BN hTert and hypomorphic Lig4-deficient 411BR hTert fibroblasts were treated with PARPi and γ H2AX foci were enumerated at 14 h post 7 Gy X-IR in G1. XLF-deficient cells displayed a substantial repair defect compared to wt cells due to lack of the core c-NHEJ factor XLF. Treatment with PARPi did not have an effect on γ H2AX foci numbers in XLF-deficient cells (figure 4.24B). Hypomorphic Lig4-deficient cells also displayed a repair defect compared to wt cells. Due to the residual Lig4 activity in these cells, the repair defect was milder than in XLF-deficient cells and PARPi treatment did not affect DSB repair in these cells (figure 4.24B). After 2 Gy α -IR, almost no repair was observed in XLF-deficient 2BN hTert fibroblasts up to 24h after DNA damage induction. PARPi treatment or depletion of CtIP and Plki did not affect γ H2AX foci numbers at any time point (figure 4.24C). Collectively, the results presented in figure 2.24 suggest that repair of complex DSBs and repair of X-IR-induced DSBs in the slow repair component is not dependent on alt-NHEJ.

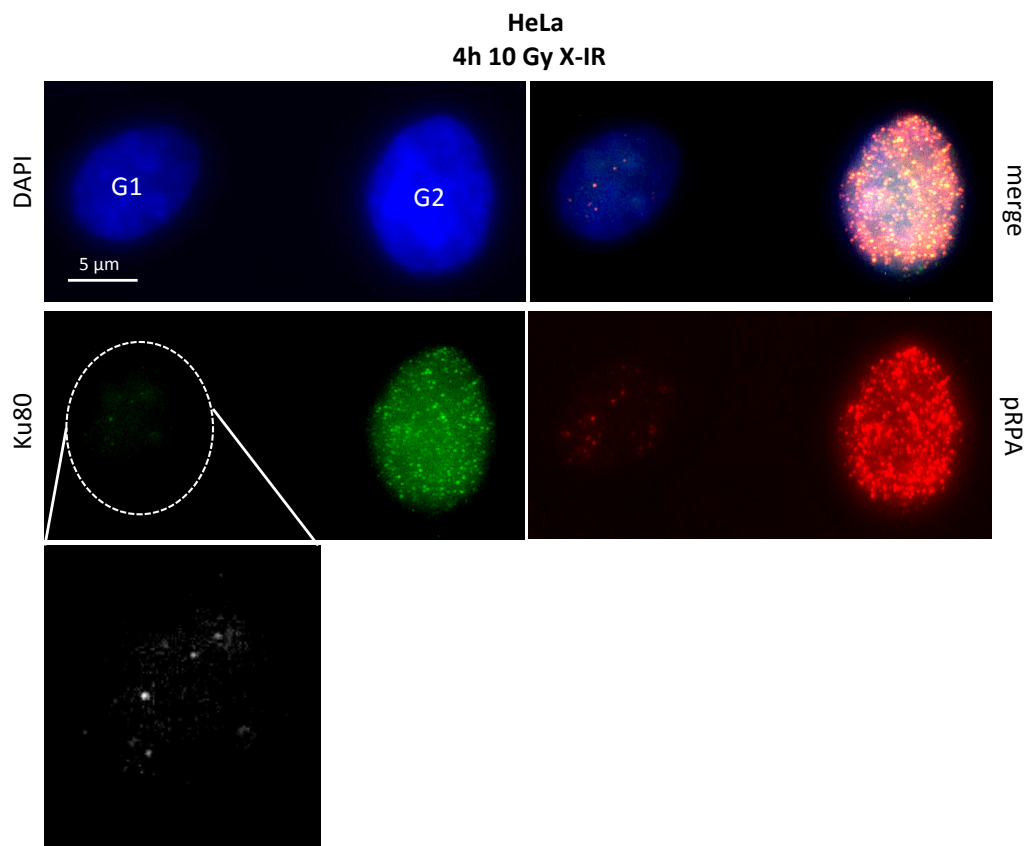


Figure 4.25 Ku80 foci co-localize with pRPA foci in G1. HeLa cells were irradiated with 10 Gy X-rays and pre-extracted with CSK buffer at 4 h post IR. After fixation, cells were stained with anti-pRPA (pT21) and anti-Ku80 antibodies plus DAPI. Images were acquired using Axiovision.

If the repair of resected DSBs in G1 is completed by c-NHEJ, then Ku should be bound to the DSB ends. However, IF staining of Ku molecules is technically challenging due to the fact that only one Ku molecule is bound to the DSB end. IF staining of γ H2AX, for instance, is simple because several megabase chromatin domains around the DSB are phosphorylated resulting in a high local density of the protein, which can be easily detected by antibody staining. Based on recently published staining protocols that involve RNase digestion and pre-extraction steps (to wash out unbound Ku proteins), IF staining of Ku foci was successfully established (Britton et al. 2013; Chanut et al. 2016). HeLa cells were irradiated with 10 Gy X-IR, pre-extracted and stained with anti-Ku80 and anti-pRPA antibodies at 4 h post IR. The images displayed in figure 4.25 show clear Ku80 foci in G1 that co-localize with pRPA, indicating that DSB ends are resected while Ku remains bound to the DSB end (figure 4.25). Thus, this finding further substantiates the claim that the slow repair component in G1 represents resection-dependent c-NHEJ.

5 Discussion

DSBs are repaired with biphasic kinetics in G1 and G2 phase. Simple DSBs are quickly rejoined in the first couple of hours after damage induction. Heterochromatic DSBs or complex DSBs harboring additional lesions at the break site, on the other hand, are repaired with slow kinetics (Riballo et al. 2004; Beucher et al. 2009). The fast repair component in both cell cycle phases represents c-NHEJ. Slowly repairing DSBs in G2 undergo extensive resection and are subsequently repaired by HR (Zafar et al. 2010). Slowly repairing DSBs in G1 are repaired via a sub-pathway of NHEJ that requires ATM signaling and Artemis. Therefore, cells deficient in either one of these factors display a repair defect at late time points (4 to 8 h) post IR in G1 and G2 (Riballo et al. 2004; Beucher et al. 2009). Recent evidence suggests that CtIP plays a role during repair in G1 (Yun & Hiom 2009; Quennet et al. 2011), suggesting that limited end resection may be occurring. This work helped to shed light on the mechanism underlying the slow repair component in G1.

Stretches of ssDNA can be visualized and quantified by IF staining against RPA, which binds to ssDNA immediately after DSB ends are resected to protect against degradation, thus providing an indirect measure of resected ssDNA. RPA becomes hyper-phosphorylated in response to DNA damage. After irradiation with low doses of LET X-rays (2 Gy), pRPA foci, indicating breaks that are undergoing resection and subsequent repair by HR, can be observed in S and G2 cells. Under these conditions, however, pRPA foci are not visible in G1 phase because the majority of simple DSBs are quickly repaired by c-NHEJ with minimal end processing. For stable binding of the heterotrimeric RPA protein to ssDNA, a minimum of 30 nt have to be resected (Bochkareva et al. 2002). Thus, X-ray-induced breaks are usually not resected extensively enough in G1 for pRPA binding and subsequent detection by IF. Only after very high doses of X-rays (10-20 Gy), pRPA foci are visible in G1 (figure 2.25). While an increase in the X-ray dose does not necessarily increase the chemical complexity of the individual breaks, the high number of damages increases the potential for individual DSBs to occur in close proximity. Therefore, the damages may be more clustered than after low doses of X-IR. This presumably slows down the repair machinery, allowing more time for resection to occur and thus increasing the probability that some breaks are resected to the extent that is necessary for RPA binding.

To avoid irradiation with unphysiologically high X-ray doses, the high LET qualities of alpha particles were exploited to specifically induce complex lesions that are known to undergo

resection to a greater extent in G2 (Shibata et al. 2011) and that are repaired with slow kinetics. It was hypothesized that such lesions would require a greater extent of end processing in G1 as well. Indeed, after α -IR, robust pRPA foci formation was observed in G1 HeLa cells (figure 4.3A). To verify that pRPA foci really represent stretches of ssDNA, BrdU foci were quantified under non-denaturing conditions as previously described (Beucher et al. 2009). BrdU foci analysis confirmed that DSB ends are resected in G1 (figures 4.3C and D, and 4.10). These results are in line with other recently published studies that observed limited DSB end resection in G1 phase cells after heavy ion irradiation (Yajima et al. 2013; Averbeck et al. 2014).

5.1 CtIP and Plk3

CtIP is a well-described factor that promotes DSB end resection in S/G2 and recent evidence suggests that it also has functions in G1 (Quennet et al. 2011; Zhou et al. 2014). The stress response protein Plk3 is required for S-phase entry and is phosphorylated in G1 after DNA damage (Bahassi et al. 2002).

Due to the higher complexity and the increased necessity for end processing, the repair of complex DSBs is dependent on Plk3 and CtIP even in wt cells; therefore, a repair defect was observed in G1 after siCtIP or Plk3 treatment after α -IR (figures 4.2 and 4.7). The formation of pRPA foci was diminished after Plk3 or CtIP depletion, indicating that these factors promote resection in G1 (figures 4.3B and 4.9).

In S/G2, CtIP is phosphorylated by CDK2 at the amino acids Ser327 and Thr847. Phosphorylations of the same amino acids are also required for resection in G1 (figure 4.5), however, in this cell cycle phase CtIP is not phosphorylated by CDKs (figure 4.6). The serine/threonine kinase Plk3 was identified as the kinase that phosphorylates CtIP in G1 at Ser327 and Thr847 (Barton et al. 2014 and figure 4.11).

Co-immunoprecipitation (co-IP) studies with phosphospecific CtIP antibodies further revealed that the phosphorylations at Ser327 and Thr847 in G1 follow a defined time course. While the phosphorylation at Ser327 can be detected 30 min after IR, the phosphorylation at Thr847 occurs 120 min after IR (Barton et al. 2014). Moreover, as opposed to S/G2, where CtIP is phosphorylated constitutively by CDK2, the phosphorylation of CtIP by Plk3 in G1 is DNA damage dependent (Barton et al. 2014).

Plk3 is a member of the polo-like kinase family. All kinases in this family possess a C-terminal polo-box domain (PBD), which is involved in the targeting of the kinase activity to subcellular structures. The PBD physically binds to substrates; therefore, it acts as a molecular mediator to bring the kinase domain into spatial proximity with its substrate. The PBD of Plk3 is subdivided into two polo-box motifs: PB1 and PB2 that form the phosphopeptide binding molecule together (Park et al. 2010). The importance of the Plk3 PBD for resection in G1 was analyzed in this project and the results suggest that a functional PBD is required for resection in G1 (figure 4.12), indicating that Plk3 might physically interact with CtIP in G1.

Indeed, co-IP experiments showed that Plk3 physically binds to CtIP phosphorylated at Ser327 via its PBD (Barton et al. 2014). The initial binding of the Plk3 PBD fully activates Plk3, which then phosphorylates other CtIP proteins at Ser327. Given the defined time course of CtIP phosphorylations observed in co-IP studies, it was proposed that initial binding of the Plk3 PBD to CtIP at Ser327 triggers the robust phosphorylation of other CtIP proteins at Ser327 and subsequently the phosphorylation at Thr847 (Barton et al. 2014 and figure 5.1). It is not yet clear, which kinase mediates the initial phosphorylation of CtIP at Ser327. Two different models have been proposed for Plk1, the most studied of all the Plks, and could theoretically apply to Plk3. The "self-priming" model proposes that Plk3 itself phosphorylates CtIP at Ser327, producing the optimal target for its own PBD to bind to CtIP. The "non-self priming" mechanism suggests that the initial phosphorylation is carried out by another, yet unknown, priming kinase. This initial priming of CtIP could, for instance, be carried out by CDK4/6 in G1 (Park et al. 2010; Barton et al. 2014).

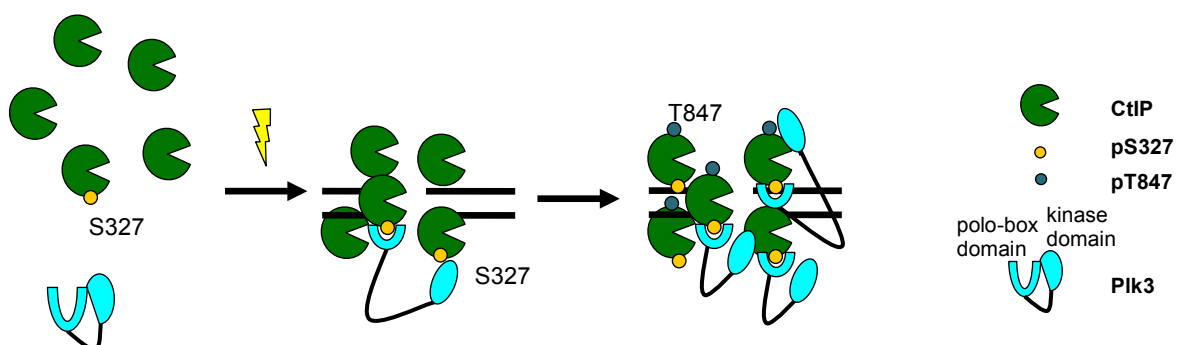


Figure 5.1 Plk3 binds to CtIP via its PBD. After IR, Plk3 binds to CtIP phosphorylated at Ser327. This initial priming could be carried out by Plk3 itself ("self-priming") or by another unknown kinase ("non-self-priming"). Once Plk3 binds to CtIP pSer327, its kinase domain first phosphorylates other CtIP molecules at Ser327 and later on Thr847 (Barton et al. 2014).

5.2 Artemis

Artemis physically binds to DNA-PKcs and gains endonuclease function after DNA-PKcs autophosphorylation (Chang & Lieber 2016). Previous studies showed that Artemis is specifically needed for the slow repair component and approximately 20% of DSBs are dependent on Artemis for repair in G1 and G2 (Riballo et al. 2004; Beucher et al. 2009).

In G2, it was previously reported that depletion of CtIP rescues the repair defect of a downstream HR factor like Brca2 (Kakarougkas et al. 2013), because after inhibition of resection in G2, DSB repair can switch to resection-independent c-NHEJ. In G1, CtIP or Plk3 depletion did not have an impact on DSB repair in X-irradiated wt cells (Barton et al. 2014), but a repair defect was observed in Artemis-deficient cells in the slow repair component. Depletion of either CtIP or Plk3 rescued the Artemis repair defect after X-IR in G1. This indicates that both factors are required for the slow repair component in G1 where they function upstream of Artemis (figures 4.1 and 4.13). This result further suggests, similar to the situation in G2, the presence of a resection-dependent and a resection-independent repair pathway in G1. If resection is inhibited in G1, the repair of X-IR-induced damages can switch to resection-independent NHEJ, thus the requirement for Artemis is bypassed and the repair defect of Artemis-deficient cells is lost.

The data obtained here suggest that Artemis promotes resection in G1, as pRPA foci levels are decreased after Artemis depletion (figure 4.3B). Further, resection in the endonuclease-deficient Artemis D37N mutant was significantly impaired (figure 4.4). This indicates that the endonuclease activity of Artemis, which was previously found to be important for DSB repair in the slow repair component in G1 and G2, is also important for resection in G1.

A previous study proposed a model in which Artemis cleaves the ssDNA-dsDNA junction, generating blunt DSB ends suitable for ligation (Goodarzi et al. 2006). However, such a model is not compatible with the observation that pRPA foci numbers decrease when Artemis is depleted. If this model were true, pRPA numbers would increase in the absence of Artemis, since RPA-covered ssDNA overhangs would persist. The results obtained here indicate that in the absence of Artemis, pRPA foci formation is impaired (figure 4.3B), therefore binding of RPA to ssDNA must occur downstream of Artemis function. Hence, a different model was proposed. Structural studies have identified a small channel in the DNA-PKcs molecule, which can bind ssDNA but not dsDNA (Williams et al. 2008; Williams et al. 2014). Therefore, the resected ssDNA strand could be threaded into the ssDNA channel on DNA-PKcs, forming a

hairpin-like structure that precludes RPA binding. Being the only nuclease in vertebrates that can open hairpins (Chang & Lieber 2016), Artemis subsequently cleaves the resulting structure, forming ssDNA stretches that are long enough for RPA binding. Even if the ssDNA strand is not threaded into the DNA-PKcs channel, it was previously shown that Artemis has the ability to distort a number of common physiological DNA structures, like 3' or 5' overhangs, into hairpin-like conformations that are ideal cleavage substrates (Chang & Lieber 2016). Thus, a model in which Artemis cleaves hairpin-like structures in different positions, resulting in ssDNA stretches that may be long enough for RPA binding can be proposed (figure 5.2).

5.3 Distinct nuclease requirements for resection in G1

To date, DSB end resection was mainly studied in the context of HR in S/G2 phase, where it necessitates the activity of various different nucleases and helicases, namely Exo1, EXD2, Mre11 endo- and exonuclease function and BLM/DNA2. Since the pathway described here also involves resection, the roles of these nucleases in G1 were analyzed. Monitoring pRPA foci after α -IR revealed that similar to G2, resection in G1 requires Exo1, Mre11 exonuclease and EXD2. Contrary to G2, Mre11 endonuclease function and BLM/DNA2 are dispensable for resection in G1 (figure 4.16A). This result was supported by the finding that Exo1 or EXD2 depletion or Mre11 exonuclease inhibition rescued the Artemis repair defect after X-IR, while Mre11 endonuclease inhibition and BLM/DNA2 depletion did not have this effect (figure 4.17A).

Based on the finding that Mre11 endonuclease activity is dispensable for G1 resection and taking into account that resection in G1 ought to be much more limited than in G2, it was postulated that, as opposed to bidirectional resection in G2, resection in G1 starts from the DSB end. Previous studies showed that upon DNA-PKcs binding, the Ku heterodimer can translocate inward on the DNA strand by roughly one helical turn (Yoo & Dynan 1999; Turchi et al. 2000). Such an inward translocation of Ku could expose DSB ends for resection by either Mre11 exonuclease and EXD2 or Exo1. Owing to the opposing polarities of these nucleases, either one of the DNA strands could be digested (Biehs et al. 2017, figure 5.2). As previously discussed, the resulting ssDNA strand could then be threaded into a small channel in the DNA-PKcs protein, which is perfectly sized to fit single-stranded DNA (Williams et al. 2008; Williams et al. 2014; Jette & Lees-Miller 2015).

Artemis rescue experiments indicated that Artemis function lies downstream of CtIP, Plk3, Mre11 exonuclease function, Exo1 and EXD2 (figures 4.1, 4.13 and 4.17A). Furthermore, while Artemis depletion caused a repair defect in G1, depletion or inhibition of the aforementioned factors did not impair DSB repair in wt cells. Collectively, this suggests that repair in wt G1 cells after X-IR can switch to a resection-independent pathway when any one of these factors is missing. Artemis depletion, on the other hand, causes a repair defect in wt cells and seems to function at a very late stage of NHEJ. Therefore, a model was postulated where the nuclease activities of Mre11 exonuclease, Exo1 or EXD2 initiate resection from the DSB end. After formation of a hairpin-like resection intermediate, Artemis is necessary to resolve this structure. This cleavage can occur at various positions, resulting in ssDNA stretches of varying length, some suitable for RPA binding (figure 5.2).

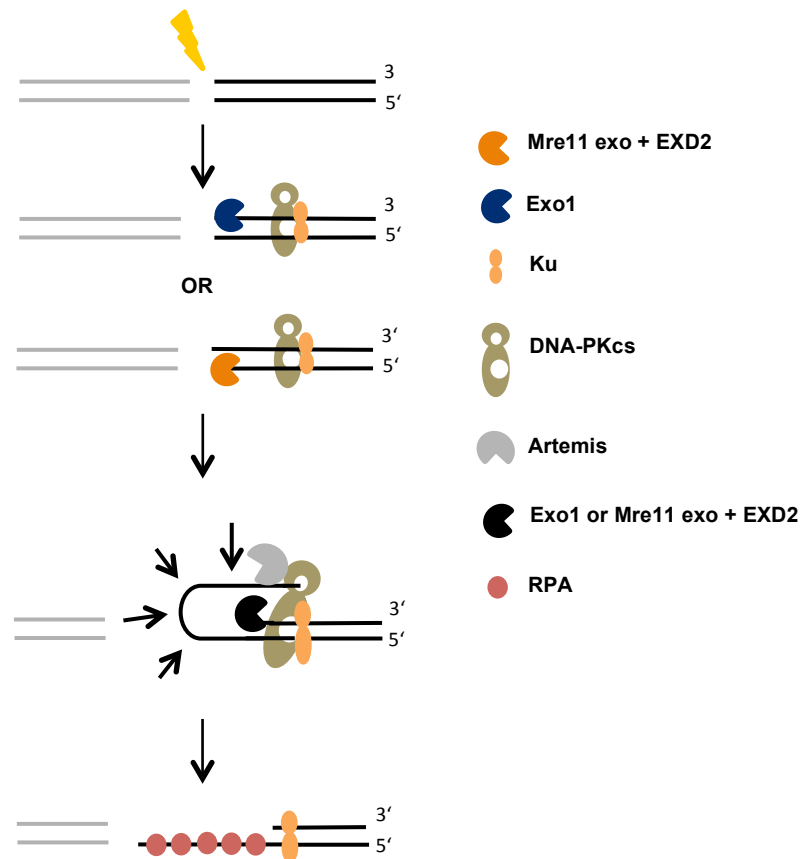


Figure 5.2 Speculative model for resection in G1. After DSB induction in G1, Ku rapidly binds to the DSB ends and translocates away from the break end upon DNA-PKcs binding to expose the ends for nucleolytic degradation. End resection then starts from the break end by the nuclease activities of either Mre11 exonuclease and EXD2 or Exo1. Ku remains bound to the DNA while the resulting ssDNA stretch might be threaded into the ssDNA-binding channel in DNA-PKcs. The endonuclease activity of Artemis then resolves the resection intermediates by cleaving the hairpin at varying locations (indicated by black arrows). This results in the formation of a ssDNA structure suitable for RPA binding (modified from Biehs et al. 2017).

5.4 53BP1 and the Brca1-CtIP interaction in G1

DSB end resection is controlled in a cell cycle-specific manner by the antagonistic activities of 53BP1 and Brca1 (Escribano-Díaz et al. 2013). The level of Brca1 expression in asynchronously cycling G1 HeLa cells is similar to S/G2, but its recruitment to DSBs in G1 is blocked by 53BP1 and its effector proteins (Escribano-Díaz et al. 2013). Rif1 is one of two effector proteins of 53BP1 and its recruitment to DSBs in G1 depends on ATM-phosphorylated 53BP1. Thus, in G1, 53BP1 and RIF1 protect DSB ends from resection, thereby promoting resection-independent c-NHEJ (Escribano-Díaz et al. 2013). PTIP is the second effector protein of 53BP1. It interacts directly with 53BP1 and is also involved in the suppression of end resection, but Rif1 and PTIP seem to be involved in blocking end resection at different stages of the resection process, or they may be involved in blocking specific nucleases (Callen et al. 2013). In S/G2, Brca1 inhibits the ATM-dependent phosphorylation of 53BP1, therefore blocking the accumulation of Rif1 and PTIP at DSBs (Feng et al. 2015).

The repair pathway proposed here involves end resection in G1 phase where DSB ends are usually protected from resection by 53BP1. After 53BP1 depletion a significant increase in resection was observed, consistent with the idea that 53BP1 is protecting the ends from resection (figure 4.18). Preliminary data with Rif1-deficient MEF cells also showed a similar phenotype (data not shown). Several studies have analyzed Brca1's role during NHEJ. Brca1 interacts with and stabilizes Ku80 bound to DSBs (Wei et al. 2008; Jiang et al. 2013), suggesting a potential role for Brca1 in NHEJ. To allow limited end resection in G1, Brca1 presumably needs to displace the factors, which are protecting DSB ends. Indeed, after α -IR, robust Brca1 foci formation was observed at DSBs in G1, indicating Brca1 recruitment to damage sites (figure 4. 19B). Depletion of Brca1 by siRNA treatment resulted in impaired resection. Double-depletion of Brca1 and 53BP1 resulted in a phenotype similar to depletion of 53BP1 alone, indicating that the function of Brca1 in G1 is the displacement of 53BP1, similar to its function in G2 (figure 4.20).

Experiments with stable MEF cell lines carrying either a wt Brca1 protein or a mutated form of the protein revealed that the phospho-recognition BRCT domain of Brca1 is required for efficient resection in G1 (figure 4.21). The results further indicated that the Brca1 RING domain, which mediates the E3 ligase activity, is not required for resection in G1 (figure 4.21). However, it has been suggested that the Brca1 I26A mutation may be hypomorphic and therefore some residual E3 ligase activity may be present (Feng et al. 2015). Thus, further

experiments with a different Brca1 RING domain mutant are necessary to confirm that the E3 ligase activity is not required for resection in G1.

In S/G2, Brca1 interacts with CtIP phosphorylated at Ser327 to promote resection and HR (Christou & Kyriacou 2013). Here, it was discovered that CtIP phosphorylation at Ser327 is also important for resection in G1, thus it was hypothesized that CtIP and Brca1 also interact in G1. Using co-IP, a Plk3-dependent interaction between Brca1 and CtIP pSer327 was detected 60 minutes after damage induction in G1 (Biehs et al. 2017). Collectively, the data suggest that the phosphorylation of CtIP at Ser327 in G1 after DNA damage results in an interaction with the Brca1 BRCT domain to promote DSB end resection.

A recent study proposed that the interaction between CtIP and Brca1 is dispensable for the initiation of resection during HR but is involved in the regulation of resection speed and efficiency (Cruz-Garcia et al. 2014). According to the data obtained here, the interaction between CtIP pSer327 and Brca1 seems to be indispensable for resection in G1 because pRPA foci formation is significantly impaired in MEF cells with a mutated Brca1 BRCT domain. However, the assay used here is not suitable to determine resection speed and length. Since the formation of pRPA foci is dependent on the resection of a minimum amount of DNA (approximately 30 nt for stable RPA binding, (Bochkareva et al. 2002)), there are only two possible scenarios: either a pRPA focus is formed or not. The length of the resected DNA cannot be measured with this technique; hence it is not possible to measure how the interaction of CtIP and Brca1 affects the speed of resection in G1 with this assay. To further elucidate this issue, single-molecule analysis of resection tracks (SMART) could be applied to gain more insight into resection speed in G1 (Cruz-Garcia et al. 2014). Alternatively, pRPA foci could be monitored at later time points to determine if a delayed peak in pRPA foci formation can be observed in the BRCT mutant cells. Since resection in G1 is much more limited than in G2, it is possible that slow resection occurs in BRCT mutant cells but it cannot be detected because the threshold for pRPA formation is not reached. Thus, it is not clear if the Brca1-CtIP interaction in G1 only determines the speed of resection, as it does in G2, or if it is indispensable for resection.

In figure 4.18 it was demonstrated that resection proceeds in an uncontrolled manner after 53BP1 depletion. A recent study has shed light on what happens when resection in G1 can proceed unhindered. In a 53BP1-deficient background, DSB repair in G1 switches to PARP1-

dependent alt-NHEJ (Bakr et al. 2016). Whether the pathway characterized here represents c-NHEJ or alt-NHEJ was therefore analyzed next.

5.5 Error-prone repair is completed by c-NHEJ in G1

In G1, only NHEJ is available for the repair of DSBs. In addition to the canonical pathway (c-NHEJ), a backup pathway called alt-NHEJ exists that repairs DSBs when ends are not protected by the core c-NHEJ protein Ku70/80 (Mansour et al. 2013). As alt-NHEJ also involves CtIP-dependent resection, several experiments with a PARP inhibitor (PARPi) were performed to elucidate whether the pathway described here represents c-NHEJ or alt-NHEJ. Treatment of wt fibroblast cells with PARPi did not have an effect on DSB repair after X-IR or α -IR (figures 4.24A and B). PARPi treatment also did not affect the repair of DSBs in hypomorphic Lig4-deficient cells or in XLF-deficient cells (figures 4.24A and B). Additionally, treatment with Plki and/or siCtIP did not have any effect on DSB repair in XLF-deficient cells (figure 4.24C). Collectively, these results suggest that repair during the slow repair component represents c-NHEJ, not alt-NHEJ.

Furthermore, the IF staining displayed in figure 4.25 shows Ku80 and pRPA foci in G1 that co-localize at 4 h post 10 Gy X-IR. The co-localization between Ku80 and pRPA foci in G1 was confirmed using confocal microscopy and line-blot analysis. As a control, Rad51 foci were stained in G2 and almost no co-localization was observed (Biehs et al 2017). This result is in good agreement with a recent study that shows that in S-phase Ku- and RPA-binding occurs on resected one-ended DSBs concomitantly until Rad51 is loaded onto the ssDNA (Chanut et al. 2016). Moreover, this result confirms the presence of the structure illustrated in the very last step of figure 5.2 (RPA binding in the presence of Ku) and further supports the notion that resection-dependent repair in G1 is completed by c-NHEJ and not alt-NHEJ.

The analysis of Ku80 foci shown in figure 4.25 was done after X-IR. Previous studies have reported that, due to the occurrence of CDS, heavy ion IR generates a larger number of short DNA fragments, compared to low LET IR. Since Ku binding to the DSB end and DNA-PK kinase activity require a minimum length of DNA, DNA-PK activity and Ku-dependent repair are inhibited by the short DNA fragments generated by high LET heavy ion IR (Wang et al. 2008; Pang et al. 2011). The results presented here indicate that α -IR-induced DSBs are repaired using c-NHEJ in G1, suggesting that the DNA fragments generated by α -IR are long

enough to promote Ku-dependent repair. Nonetheless, the co-localization of Ku80 and pRPA foci needs to also be examined after α -IR to confirm efficient Ku80 binding to these DSB ends.

The results presented here further indicate that the interplay between 53BP1 and Brca1 is important for c-NHEJ to ensue. A recent paper by Bakr et al. (2016) reported that in a 53BP1-deficient background, DSBs are resected in a CtIP- and Mre11-dependent manner in G1 and are ultimately repaired by PARP1-dependent alt-NHEJ. Repair in wt cells, on the other hand, is completed by c-NHEJ (figures 4.24 and 4.25). Hence, a pathway switch occurs from c-NHEJ to alt-NHEJ when 53BP1 is lost and resection can proceed unhindered. Rejoining of DSBs by resection-dependent c-NHEJ is therefore promoted by the interplay between Brca1 and 53BP1 and its limiting effects on end resection (Biehs et al. 2017).

Based on these findings, three potential scenarios for NHEJ repair in G1 can be proposed. In normal wt cells, the ends are protected by 53BP1. Repair of all DSBs is initially attempted by resection-independent c-NHEJ: simple DSBs are quickly rejoined with minimal end processing. If quick rejoining fails, due to heterochromatic localization or increased break complexity, end resection is initiated. Plk3 phosphorylates CtIP at Ser327 and Thr847, triggering CtIP interaction with Brca1, and resulting in regulated displacement of 53BP1 from the break end to allow limited end resection and subsequent repair by resection-dependent c-NHEJ. Relocalization of 53BP1 to the periphery of the focus, as described for G2, could be a potential mechanism for this displacement in G1 (Kakarougkas et al. 2013). The interplay between Brca1 and 53BP1 is important, because in a 53BP1-deficient situation resection can proceed uninhibited and repair switches to alt-NHEJ, presumably because the resected DNA stretches are too long for c-NHEJ to operate.

Furthermore, analysis of chromosomal translocations revealed that the resection-dependent pathway described here is highly error prone. A considerable amount of translocations are formed in the slow repair component in a manner dependent on CtIP and Artemis (Barton et al. 2014, Biehs et al. 2017). Moreover, a G1-specific NHEJ-reporter assay was used to study resection-dependent repair in G1. This assay monitors the rejoining of two distant I-SceI-induced restriction sites with loss of the intervening fragment. Sequencing of the restriction sites revealed additional deletions, with sizes ranging up to 40 nt, providing additional evidence that this pathway has the potential to be highly mutagenic (Biehs et al. 2017).

5.6 Outlook

5.6.1 Significance of resection-dependent c-NHEJ

Here, a resection-dependent pathway is characterized that functions during the slow repair component in G1. This error-prone pathway contributes to the formation of translocations and, due to end resection, can result in deletions at the break site. Complex α -IR-induced lesions require extensive end processing steps before ligation and are therefore repaired by resection-dependent c-NHEJ in G1. After X-IR, repair of heterochromatic DSBs is delayed and channeled into resection-dependent c-NHEJ. Strikingly, if resection in G1 is inhibited, for instance by depletion of CtIP, the repair of X-IR-induced damages can switch to resection-independent c-NHEJ. This provokes the question why such an error-prone pathway evolved in the first place if a switch to resection-independent repair is possible? Some potential explanations are discussed in the following paragraphs.

The switch to a resection-independent pathway in G1 is only possible after low LET irradiation. Breaks induced by high LET α -particles, however, must be resected before repair. Taking into consideration that the majority of cells in the human body are post-mitotic and therefore HR is not available for repair, resection-dependent c-NHEJ may have evolved specifically for the repair of complex lesions, as a substantial amount of natural background radiation consists of the α -particle emitter radon.

Another possible scenario is that slowly repairing DSBs in G1 are resected in order to induce a cell-cycle checkpoint through ATR signaling. Cell-cycle checkpoints are initiated after DNA damage to extend the time window the cell has to repair the lesions. Resected ssDNA in the cell is rapidly coated by RPA to protect it from nucleolytic degradation. RPA bound to ssDNA acts as a platform for the recruitment of the ATR interacting protein (ATRIP) complex. ATR subsequently phosphorylates the checkpoint kinase 1 (Chk1), which results in the initiation of a cell-cycle checkpoint in S and G2 (Zou & Elledge 2003; Sorensen & Syljuasen 2012).

ATR-dependent checkpoint activation was thought to be restricted to S/G2 phase. In this thesis, however, it was shown that DSB end resection also occurs in G1. Moreover, it was demonstrated that after complex damage, the extent of resection is sufficient for pRPA foci formation. Hence, ATR activation and Chk1 phosphorylation may occur in G1 phase after α -particle radiation. Presumably, Chk1 phosphorylation in G1 will not be CDK-dependent, as it is in S/G2, but dependent on Plk3, the kinase that regulates CtIP in G1. In line with these predictions, a recent study by Gamper et al. (2013) revealed that the ATR kinase is functional in G1 and has a role in the DDR. They also observed RPA foci formation in synchronized G1 cells after γ -irradiation, indicating the generation of short ssDNA stretches in G1 that are efficient in activating ATR signaling, but the authors could only speculate about the origin of ssDNA stretches in G1 (Gamper et al. 2013). Another study found that Exo1- and BLM-dependent resection is required for the activation of a G1/S checkpoint in budding yeast (Balogun et al. 2013). The results presented here confirm the presence of RPA-coated ssDNA in G1 and elucidate the mechanism by which it is generated. Thus, resection-dependent c-NHEJ could play a role in the initiation and maintenance of an ATR-dependent cell-cycle checkpoint response in G1 and the activation of a G1/S checkpoint may be of particular importance for slowly repairing DSBs in G1.

Another potential explanation for the use of resection-dependent repair in G1 is based on a number of recent publications regarding the role of RNA-DNA hybrids in DSB repair. One study found that HR in yeast cells requires the formation of transient RNA-DNA hybrids. This study proposes that in response to a DSB, RNA polymerase II is recruited to the 3' ssDNA overhangs that form during resection where it begins to transcribe the ssDNA. The newly synthesized RNA has high affinity to bind to the ssDNA overhang generated during resection, effectively competing with RPA binding to the ssDNA. RNase H is then required for the degradation of the RNA-DNA hybrid structures to allow full RPA loading on the ssDNA and subsequent completion of repair (Ohle et al. 2016). If these RNA-DNA hybrid structures have to be resolved before HR can be completed, the obvious question is why the cell even initiates transcription to form RNA in the first place. One possibility suggested in this study is that the transcription machinery also recruits chromatin remodelers and histone chaperones to the DSB that are required for the opening of chromatin to allow resection (Ohle et al. 2016). Another paper published in 2014 provides evidence for RNA-templated HR in yeast. This study found that DSBs that occur in actively transcribed regions can be repaired via HR that uses the transcribed RNA as a template. The annealing between RNA and DNA was promoted

by yeast as well as human Rad52 proteins *in vitro*, suggesting that human cells could also be taking advantage of RNA-templated DSB repair (Keskin et al. 2014). Recently, evidence for error-free RNA-templated c-NHEJ in actively transcribed genes in human cells has been reported. This study proposes that nascent RNA transcripts can serve as a template to restore original genomic sequences using a c-NHEJ-mediated pathway (Chakraborty et al. 2016). Based on these studies, a highly appealing model for resection-dependent c-NHEJ can be proposed. The reporter assay data provided evidence that nucleotides are lost during the resection process (Biehs et al. 2017), but no data about how many nucleotides are lost during the repair of α -IR-induced DSBs is available. Complex DSBs could potentially be resected to an even greater extent in G1 and so far, no mechanism is known which could preserve the genetic information. A role for RNA templates and polymerases to restore missing nucleotide sequences in the pathway proposed here could implicate that this repair pathway is less error-prone than previously thought. While RNA-templated repair has so far only been studied in actively transcribed regions, the study by Ohle et al. (2016) suggests that end resection in G1 could trigger the transcription of RNA that could potentially be used as a template at a later stage during c-NHEJ. The pRPA-covered ssDNA strands that are formed after Artemis cleavage of resection intermediates would not undergo endonucleolytic cleavage to form blunt ends but instead the ends might be anchored together by an RNA molecule that also acts as a template for DNA synthesis by polymerases. Such a model is highly speculative, as RNA-templated c-NHEJ repair has yet to be demonstrated for IR-induced DSBs in non-transcribed regions, and will need to be investigated in the future.

5.6.2 Factors limiting end resection in G1

In G2, end resection needs to be extensive (up to 3500 bp, (Zhou et al. 2014)) to generate 3' ssDNA overhangs for Rad51 nucleoprotein filament formation, strand invasion, and homology search. Resection in G1, on the other hand, where a homologous template is not available for repair, needs to be limited to prevent the deletion of large DNA segments. Thus, a number of different factors presumably limit the extent of end resection in G1 to prevent large deletions and consequential genomic instability. As shown in figure 2.25, Ku remains bound to the DNA ends and the extent to which Ku translocates inwards is likely one of the factors that limit resection in G1.

As previously discussed, resection is inhibited by 53BP1 bound to the chromatin around DSB ends. A recent study found that in G2, the size of 53BP1 foci doubles after 8 hours post IR, creating a core that is devoid of 53BP1 and ubiquitin chains (Kakarougkas et al. 2013). They propose that Brca1 promotes the relocalization of 53BP1 to the periphery of radiation-induced foci. This process is initiated by the Brca1-dependent priming of 53BP1 which removes the inhibitory impact that 53BP1 has on the deubiquitylating enzyme POH1. As a result, POH1 removes Rap80 and ubiquitin chains from the core, promoting the loss of 53BP1. Resection can subsequently occur in the core that has been vacated by 53BP1 and Rap80 (Kakarougkas et al. 2013). Rap80 therefore restricts resection in G2 and might play a role in G1 as well. Preliminary data indicate that Rap80 also plays a role in regulating resection in G1. In an Artemis-deficient background, depletion of Rap80 causes an Artemis repair defect at early times (personal communication with A. Shibata). An Artemis repair defect is usually only observed at late time points post IR, as Artemis is specifically required for the slow repair component. However, it appears that cells deficient in Rap80, undergo fast excessive resection, and therefore have a dependence on Artemis even at early time points. Whether the mechanism in G1 is the same as in G2 and involves the activity of POH1 and Rap80 will be investigated in more detail in the future. Kakarougkas et al. did not observe an enlargement of 53BP1 foci in G1, however they did not use high LET radiation for damage induction. It would be interesting to see if a similar repositioning of 53BP1 can be observed in G1 cells that undergo resection after α -IR.

A recent study reported that the phosphorylation-specific prolyl isomerase Pin1 plays an essential role in the control of CtIP-dependent end resection in S/G2 (Steger et al. 2013). Using its peptidylprolyl isomerase domain, Pin1 can isomerize proteins phosphorylated at S/T-P motifs. This causes a conformational change from cis to trans in the phosphorylated protein, which can act as a molecular switch. They found that depletion of Pin1 results in increased resection in G2 and thus decreased NHEJ frequency. They proposed a model in which CtIP is phosphorylated by CDK2 (in S/G2) on residue Thr315, which triggers Pin1 binding to CtIP. Subsequent CtIP phosphorylation at Ser276 by an unknown kinase results in Pin1-mediated isomerization of CtIP. This leads to CtIP ubiquitylation and subsequent degradation by the proteasome (Steger et al. 2013). Thus, Pin1 plays a role in limiting the extent of end resection. Moreover, it was found that Pin1 interacts with 53BP1, Brca1 and CtIP (Steger et al. 2013; Sartori & Steger 2013). Steger et al. reported low levels of CtIP-pThr315 in G1, consistent with low CDK2 activity in this cell cycle phase. However, this study

did not investigate CtIP phosphorylation after IR and the potential for other kinases to phosphorylate S/T-P motifs on CtIP in G1. Moreover, mass spectrometry data from a more recent study suggest that the major Pin1 binding site, the CtIP Thr315 residue, is indeed phosphorylated in G1 (Barton et al. 2014). Thus, a potential role for Pin1 in G1 should be investigated in future studies.

A recent study by Orthwein et al. found that Brca1 plays a dual role in promoting HR (Orthwein et al. 2015). Besides its well-described role in the regulated displacement of 53BP1 to promote end resection, Brca1 also forms a complex with Palb2-Brca2. This complex formation is restricted to S/G2 phase. Thus, in G1, HR is suppressed not only by suppression of end resection but also by inhibition of Brca1-Palb2-Brca2 complex formation and therefore restriction of Brca2 recruitment. Strikingly, this study reports that the suppression of HR is reversible. Once the inhibitory signaling by Crl3-Kaep1 is removed, Brca1-Palb2-Brca2 complex formation is possible resulting in activation of HR in G1. In addition to Brca1-Palb2-Brca2 complex formation, resection has to be activated to observe Rad51 foci formation in G1 (Orthwein et al. 2015). Orthwein et al. achieved this by depletion of 53BP1 (to allow Brca1 recruitment) and transfection with a constitutively active CtIP plasmid. In the pathway described here, CtIP is active and Brca1 is recruited to the damage site, so presumably the only factor preventing HR during the slow repair component in G1 is the lack of Brca2 recruitment. This ought to be investigated in more detail in future studies.

Besides shedding light on the repair mechanism underlying the slow component in G1, the results presented in this thesis also have clinical relevance. In-depth knowledge of the mechanism underlying the resection process in G1 will help in the development of therapeutic gene targeting approaches in post-mitotic tissues as proposed by Orthwein et al. (2015). Moreover, this study has helped to characterize a Plk3-regulated repair mechanism in G1 that involves DSB end resection. Abnormal expression of Plk3 has been found in different types of tumors and Plk3-targeted treatment options are currently being examined (Helmke et al. 2016).

6 References

- Asaithamby, A. & Chen, D.J., 2011. Mechanism of cluster DNA damage repair in response to high-atomic number and energy particles radiation. *Mutation Research - Fundamental and Molecular Mechanisms of Mutagenesis*, 711(1–2), pp.87–99.
- Asaithamby, A., Hu, B. & Chen, D.J., 2011. Unrepaired clustered DNA lesions induce chromosome breakage in human cells. *Proceedings of the National Academy of Sciences of the United States of America*, 108(20), pp.8293–8.
- Averbeck, N.B. et al., 2014. DNA end resection is needed for the repair of complex lesions in G1-phase human cells. *Cell Cycle*, 13(16), pp.2509–2516.
- Bahassi, E.M. et al., 2002. Mammalian Polo-like kinase 3 (Plk3) is a multifunctional protein involved in stress response pathways. *Oncogene*, 21(43), pp.6633–40.
- Bahassi, E.M., 2011. Polo-like kinases and DNA damage checkpoint: beyond the traditional mitotic functions. *Experimental biology and medicine*, 236(6), pp.648–657.
- Bakr, A. et al., 2016. Impaired 53BP1/RIF1 DSB mediated end-protection stimulates CtIP-dependent end resection and switches the repair to PARP1-dependent end joining in G1. *Oncotarget*, 7(36).
- Balogun, F.O., Truman, A.W. & Kron, S.J., 2013. DNA resection proteins Sgs1 and Exo1 are required for G1 checkpoint activation in budding yeast. *DNA Repair*, 12(9), pp.751–760.
- Barton, O. et al., 2014. Polo-like kinase 3 regulates CtIP during DNA double-strand break repair in G1. *The Journal of Cell Biology*, 206(7), pp.877–894.
- Beucher, A. et al., 2009. ATM and Artemis promote homologous recombination of radiation-induced DNA double-strand breaks in G2. *The EMBO journal*, 28(21), pp.3413–27.
- Biehs, R. et al., 2017. DNA double-strand break resection occurs during non-homologous end-joining in G1 but is distinct from resection during homologous recombination. *Molecular Cell*, 65, pp.671–684.
- Binz, S.K., Sheehan, A.M. & Wold, M.S., 2004. Replication Protein A phosphorylation and the cellular response to DNA damage. *DNA Repair*, 3(8–9), pp.1015–1024.
- Block, W.D., Yu, Y. & Lees-Miller, S.P., 2004. Phosphatidylinositol 3-kinase-like serine/threonine protein kinases (PIKKs) are required for DNA damage-induced phosphorylation of the 32 kDa subunit of replication protein A at threonine 21. *Nucleic Acids Research*, 32(3), pp.997–1005.
- Bochkareva, E. et al., 2002. Structure of the RPA trimerization core and its role in the multistep DNA-binding mechanism of RPA. *The EMBO Journal*, 21(7), pp.1855–1863.
- Britton, S., Coates, J. & Jackson, S.P., 2013. A new method for high-resolution imaging of Ku foci to decipher mechanisms of DNA double-strand break repair. *Journal of Cell Biology*, 202(3), pp.579–595.
- Broderick, R. et al., 2016. EXD2 promotes homologous recombination by facilitating DNA end resection. *Nature cell biology*, 18(3), pp.271–280.
- Buis, J. et al., 2012. Mre11 regulates CtIP-dependent double-strand break repair by interaction with CDK2. *Nature structural & molecular biology*, 19(2), pp.246–52.
- Callen, E. et al., 2013. 53BP1 mediates productive and mutagenic DNA repair through distinct phosphoprotein interactions. *Cell*, 153(6), pp.1266–1280.
- Cannavo, E. & Cejka, P., 2014. Sae2 promotes dsDNA endonuclease activity within Mre11-Rad50-Xrs2 to resect DNA breaks. *Nature*, 514(7520), pp.122–125.
- De Cárcer, G., Manning, G. & Malumbres, M., 2011. From Plk1 to Plk5: Functional evolution of Polo-like kinases. *Cell Cycle*, 10(14), pp.2255–2262.
- Chakraborty, A. et al., 2016. Classical non-homologous end-joining pathway utilizes nascent RNA for error-free double-strand break repair of transcribed genes. *Nature Communications*, 7(May), p.13049.
- Chan, D. et al., 2002. Autophosphorylation of the DNA-dependent protein kinase

- catalytic subunit is required for rejoining of DNA double-strand breaks. *Genes & Development*, 16, pp.2333–2338.
- Chang, H.H.Y. & Lieber, M.R., 2016. Structure-Specific nuclease activities of Artemis and the Artemis: DNA-PKcs complex. *Nucleic Acids Research*, 44(11), pp.4991–4997.
- Chanut, P. et al., 2016. Coordinated nuclease activities counteract Ku at single-ended DNA double-strand breaks. *Nature Communications*, 7, p.12889.
- Christou, C.M. & Kyriacou, K., 2013. BRCA1 and Its Network of Interacting Partners. *Biology*, 2(1), pp.40–63.
- Ciccica, A. & Elledge, S.J., 2010. The DNA Damage Response: Making It Safe to Play with Knives. *Molecular Cell*, 40(2), pp.179–204.
- Clark, S.L. et al., 2012. Structure-Function of the Tumor Suppressor Brca1. *Computational and Structural Biotechnology Journal*, 1(1), pp.1–8.
- Cruz-Garcia, A., Lopez-Saavedra, A. & Huertas, P., 2014. BRCA1 accelerates CtIP-mediated DNA-end resection. *Cell Reports*, 9(2), pp.451–459.
- Dai, Y. et al., 2003. Nonhomologous end joining and V(D)J recombination require an additional factor. *Proceedings of the National Academy of Sciences of the United States of America*, 100(5), pp.2462–2467.
- Davis, A. & Chen, D., 2013. DNA double strand break repair via non-homologous end-joining. *Translational Cancer Research*, 2(3), pp.130–43.
- Elia, A.E.H. et al., 2003. The molecular basis for phosphodependent substrate targeting and regulation of Plks by the Polo-box domain. *Cell*, 115(1), pp.83–95.
- Escribano-Díaz, C. et al., 2013. A Cell Cycle-Dependent Regulatory Circuit Composed of 53BP1-RIF1 and BRCA1-CtIP Controls DNA Repair Pathway Choice. *Molecular Cell*, 49(5), pp.872–883.
- Escribano-Díaz, C. & Durocher, D., 2013. DNA repair pathway choice - a PTIP of the hat to 53BP1. *EMBO reports*, 14(8), pp.665–6.
- Feng, L. et al., 2015. Cell cycle-dependent inhibition of 53BP1 signaling by BRCA1. *Cell Discovery*, 1, p.15019.
- Fricke, A., 2008. *Untersuchungen zur Chromatinstruktur und DNA-Doppelstrangbruch-Reparatur in menschlichen Zellen mittels ionisierender Strahlung*.
- Gamper, A.M. et al., 2013. ATR kinase activation in G1 phase facilitates the repair of ionizing radiation-induced DNA damage. *Nucleic Acids Research*, 41(22), pp.10334–10344.
- Garcia, V. et al., 2011. Bidirectional resection of DNA double-strand breaks by Mre11 and Exo1. *Nature*, 479(7372), pp.241–4.
- Goodarzi, A.A. et al., 2008. ATM Signaling Facilitates Repair of DNA Double-Strand Breaks Associated with Heterochromatin. *Molecular Cell*, 31(2), pp.167–177.
- Goodarzi, A.A. et al., 2006. DNA-PK autophosphorylation facilitates Artemis endonuclease activity. *The EMBO journal*, 25(16), pp.3880–9.
- Goodarzi, A.A. & Jeggo, P.A., 2013. *The Repair and Signaling Responses to DNA Double-Strand Breaks* 1st ed., Elsevier Inc.
- Grundy, G.J. et al., 2014. One ring to bring them all-The role of Ku in mammalian non-homologous end joining. *DNA Repair*, 17, pp.30–38.
- Hada, M. & Georgakilas, A.G., 2008. Formation of clustered DNA damage after high-LET irradiation: a review. *Journal of radiation research*, 49(3), pp.203–210.
- Helmke, C., Becker, S. & Strebhardt, K., 2016. The role of Plk3 in oncogenesis. *Oncogene*, 35(2), pp.135–47.
- Hiom, K., 2010. Coping with DNA double strand breaks. *DNA Repair*, 9(12), pp.1256–1263.
- Huertas, P. & Jackson, S.P., 2009. Human CtIP mediates cell cycle control of DNA end resection and double strand break repair. *The Journal of biological chemistry*, 284(14), pp.9558–9565.
- Iliakis, G., Murmann, T. & Soni, A., 2015. Alternative end-joining repair pathways are the ultimate backup for abrogated classical non-homologous end-joining and homologous recombination repair: Implications for the formation of chromosome translocations. *Mutation Research - Genetic Toxicology and Environmental*

- Mutagenesis*, 793, pp.166–175.
- Iwabuchi, K. et al., 2003. Potential role for 53BP1 in DNA end-joining repair through direct interaction with DNA. *Journal of Biological Chemistry*, 278(38), pp.36487–36495.
- Jette, N. & Lees-Miller, S.P., 2015. The DNA-dependent protein kinase: a multifunctional protein kinase with roles in DNA double strand break repair and mitosis. *Prog Biophys Mol Biol*, 2(2), pp.194–205.
- Jiang, G. et al., 2013. BRCA1-Ku80 protein interaction enhances end-joining fidelity of chromosomal double-strand breaks in the G1 phase of the cell cycle. *Journal of Biological Chemistry*, 288(13), pp.8966–8976.
- Kakarougkas, A. et al., 2013. Co-operation of BRCA1 and POH1 relieves the barriers posed by 53BP1 and RAP80 to resection. *Nucleic Acids Research*, 41(22), pp.10298–10311.
- Kegel, P. et al., 2007. X-irradiation of cells on glass slides has a dose doubling impact. *DNA Repair*, 6(11), pp.1692–1697.
- Keskin, H. et al., 2014. Transcript-RNA-templated DNA recombination and repair. *Nature*, 515(7527), pp.436–9.
- Li, S. et al., 2014. Evidence that the DNA endonuclease ARTEMIS also has intrinsic 5'-exonuclease activity. *Journal of Biological Chemistry*, 289(11), pp.7825–7834.
- Lieber, M.R., 2010. The Mechanism of Double-Strand DNA Break Repair by the Nonhomologous DNA End Joining Pathway. *Annu Rev Biochem*, (79), pp.181–211.
- Löbrich, M. et al., 2010. gH2AX foci analysis for monitoring DNA double-strand break repair: Strengths, limitations and optimization. *Cell Cycle*, 9(4), pp.662–669.
- Ma, Y. et al., 2002. Hairpin opening and overhang processing by an Artemis/DNA-dependent protein kinase complex in nonhomologous end joining and V(D)J recombination. *Cell*, 108(6), pp.781–794.
- Mansour, W.Y. et al., 2013. The absence of Ku but not defects in classical non-homologous end-joining is required to trigger PARP1-dependent end-joining. *DNA Repair*, 12(12), pp.1134–1142.
- Mansour, W.Y., Rhein, T. & Dahm-Daphi, J., 2010. The alternative end-joining pathway for repair of DNA double-strand breaks requires PARP1 but is not dependent upon microhomologies. *Nucleic Acids Research*, 38(18), pp.6065–6077.
- Mazón, G., Mimitou, E.P. & Symington, L.S., 2010. SnapShot: Homologous recombination in DNA double-strand break repair. *Cell*, 142(4), pp.10–11.
- Mehta, A. & Haber, J.E., 2014. Sources of DNA double-strand breaks and models of recombinational DNA repair. *Cold Spring Harbor Perspectives in Biology*, 6(9).
- Moshous, D. et al., 2001. Artemis, a novel DNA double-strand break repair/V(D)J recombination protein, is mutated in human severe combined immune deficiency. *Cell*, 105(2), pp.177–186.
- Newhauser, W.D. & Durante, M., 2011. Assessing the risk of second malignancies after modern radiotherapy. *Nature Reviews Cancer*, 11(6), pp.438–448.
- Noon, A.T. & Goodarzi, A.A., 2011. 53BP1-mediated DNA double strand break repair: Insert bad pun here. *DNA Repair*, 10(10), pp.1071–1076.
- O'Driscoll, M. et al., 2001. DNA ligase IV mutations identified in patients exhibiting developmental delay and immunodeficiency. *Molecular Cell*, 8(6), pp.1175–1185.
- Ochi, T. et al., 2015. PAXX, a paralog of XRCC4 and XLF, interacts with Ku to promote DNA double-strand break repair. *Science*, 347(6218), pp.185–188. Available at: <http://www.ncbi.nlm.nih.gov/pubmed/25574025>.
- Ohle, C. et al., 2016. Transient RNA-DNA Hybrids are Required for Efficient Double-Strand Break Repair. *Cell*, pp.1001–1013.
- Okayasu, R., 2012. Repair of DNA damage induced by accelerated heavy ions-A mini review. *International Journal of Cancer*, 130(5), pp.991–1000.
- Orthwein, A. et al., 2015. A mechanism for the suppression of homologous recombination in G1 cells. *Nature*, 528(7582), pp.422–426.
- Pang, D. et al., 2011. Radiation-generated Short DNA Fragments May Perturb Non-homologous End-joining and Induce Genomic Instability. *Journal of Radiation*

-
- Research*, 52(3), pp.309–319.
- Park, J.E. et al., 2010. Polo-box domain: a versatile mediator of polo-like kinase function. *Cellular and molecular life sciences : CMLS*, 67(12), pp.1957–1970.
- Pines, A. et al., 2013. Touching base with PARPs: Moonlighting in the repair of UV lesions and double-strand breaks. *Trends in Biochemical Sciences*, 38(6), pp.321–330.
- Quennet, V. et al., 2011. CtIP and MRN promote non-homologous end-joining of etoposide-induced DNA double-strand breaks in G1. *Nucleic Acids Research*, 39(6), pp.2144–2152.
- Riballo, E. et al., 2004. A pathway of double-strand break rejoining dependent upon ATM, Artemis, and proteins locating to γH2AX foci. *Molecular Cell*, 16(5), pp.715–724.
- Rogakou, E.P. et al., 1998. DNA Double-stranded Breaks Induce Histone H2AX Phosphorylation on Serine 139. *The Journal of Biological Chemistry*, 273(10), pp.5858–5868.
- Rogakou, E.P. et al., 1999. Megabase chromatin domains involved in DNA double-strand breaks in vivo. *The Journal of cell biology*, 146(5), pp.905–16.
- Sage, E. & Harrison, L., 2011. Clustered DNA lesion repair in eukaryotes: Relevance to mutagenesis and cell survival. *Mutation Research - Fundamental and Molecular Mechanisms of Mutagenesis*, 711(1–2), pp.123–133.
- Sancar, A. et al., 2004. Molecular mechanisms of mammalian DNA repair and the DNA damage checkpoints. *Annual Review of Biochemistry*, 73(1), pp.39–85.
- Sartori, A.A. & Steger, M., 2013. Prolyl isomerization: A new PIN code for DSB repair. *Cell Cycle*, 12(17), pp.2717–2718.
- Sartori, A. a et al., 2007. Human CtIP promotes DNA end resection. *Nature*, 450(7169), pp.509–514.
- Savage, K.I. & Harkin, D.P., 2015. BRCA1, a “complex” protein involved in the maintenance of genomic stability. *FEBS Journal*, 282(4), pp.630–646.
- Schipler, A. & Iliakis, G., 2013. DNA double-strand-break complexity levels and their possible contributions to the probability for error-prone processing and repair pathway choice. *Nucleic Acids Research*, 41(16), pp.7589–7605.
- Shakya, R. et al., 2011. BRCA1 tumor suppression depends on BRCT phosphoprotein binding, but not its E3 ligase activity. *Science (New York, N.Y.)*, 334(6055), pp.525–8.
- Shibata, A. et al., 2014. DNA Double-Strand Break Repair Pathway Choice Is Directed by Distinct MRE11 Nuclease Activities. *Molecular Cell*, 53(1), pp.7–18.
- Shibata, A. et al., 2011. Factors determining DNA double-strand break repair pathway choice in G2 phase. *The EMBO journal*, 30(6), pp.1079–1092.
- Sorensen, C.S. & Syljuasen, R.G., 2012. Safeguarding genome integrity: The checkpoint kinases ATR, CHK1 and WEE1 restrain CDK activity during normal DNA replication. *Nucleic Acids Research*, 40(2), pp.477–486.
- Stap, J. et al., 2008. Induction of linear tracks of DNA double-strand breaks by alpha-particle irradiation of cells. *Nature methods*, 5(3), pp.261–266.
- Steger, M. et al., 2013. Prolyl isomerase PIN1 regulates DNA double-strand break repair by counteracting DNA end resection. *Molecular Cell*, 50(3), pp.333–343.
- Strahlenschutzkommission, 2013. *Determining radiation exposure Recommendation by the German Commission on Radiological Protection*,
- Thompson, L.H., 2012. Recognition, signaling, and repair of DNA double-strand breaks produced by ionizing radiation in mammalian cells: The molecular choreography. *Mutation Research - Reviews in Mutation Research*, 751(2), pp.158–246.
- Turchi, J.J., Henkels, K.M. & Zhou, Y., 2000. Cisplatin-DNA adducts inhibit translocation of the Ku subunits of DNA-PK. *Nucleic acids research*, 28(23), pp.4634–41.
- Wang, H. et al., 2008. The Ku-dependent non-homologous end-joining but not other repair pathway is inhibited by high linear energy transfer ionizing radiation. *DNA Repair*, 7(5), pp.725–733.

-
- Wang, M. et al., 2006. PARP-1 and Ku compete for repair of DNA double strand breaks by distinct NHEJ pathways. *Nucleic Acids Research*, 34(21), pp.6170–6182.
- Wei, L. et al., 2008. Rapid recruitment of BRCA1 to DNA double-strand breaks is dependent on its association with Ku80. *Molecular and cellular biology*, 28(24), pp.7380–93.
- Williams, D.R. et al., 2008. Cryoelectron Microscopy Structure of the DNA-dependent Protein Kinase Catalytic Subunit (DNA-PKcs) at Subnanometer Resolution Reveals α -Helices and Insight into DNA Binding. *Structure*, 16(3), pp.468–477.
- Williams, G.J. et al., 2014. Structural insights into NHEJ: building up an integrated picture of the dynamic DSB repair super complex, one component and interaction at a time. *DNA Repair*, 17, pp.110–120.
- Yajima, H. et al., 2013. The complexity of DNA double strand breaks is a critical factor enhancing end-resection. *DNA Repair*, 12(11), pp.936–946.
- Yoo, S. & Dynan, W.S., 1999. Geometry of a complex formed by double strand break repair proteins at a single DNA end: recruitment of DNA-PKcs induces inward translocation of Ku protein. *Nucleic acids research*, 27(24), pp.4679–4686.
- Yu, X. & Chen, J., 2004. DNA Damage-Induced Cell Cycle Checkpoint Control Requires CtIP, a Phosphorylation-Dependent Binding Partner of BRCA1 C-Terminal Domains DNA Damage-Induced Cell Cycle Checkpoint Control Requires CtIP, a Phosphorylation-Dependent Binding Partner of BRCA1. *Molecular and Cellular Biology*, 24(21), pp.9478–9486.
- Yun, M.H. & Hiom, K., 2009. CtIP-BRCA1 modulates the choice of DNA double-strand-break repair pathway throughout the cell cycle. *Nature*, 459(7245), pp.460–463.
- Zafar, F. et al., 2010. Homologous recombination contributes to the repair of DNA double-strand breaks induced by high-energy iron ions. *Radiat Res*, 173(1), pp.27–39.
- Zhou, Y. et al., 2014. Quantitation of DNA double-strand break resection intermediates in human cells. *Nucleic Acids Research*, 42(3), pp.1–11.
- Zimmerman, W.C. & Erikson, R.L., 2007. Polo-like kinase 3 is required for entry into S phase. *Proceedings of the National Academy of Sciences of the United States of America*, 104(6), pp.1847–52.
- Zimmermann, M. & De Lange, T., 2014. 53BP1: Pro choice in DNA repair. *Trends in Cell Biology*, 24(2), pp.108–117.
- Zitouni, S. et al., 2014. Polo-like kinases: structural variations lead to multiple functions. *Nat Rev Mol Cell Biol*, 15(7), pp.433–452.
- Zou, L. & Elledge, S.J., 2003. Sensing DNA damage through ATRIP recognition of RPA-ssDNA complexes. *Science (New York, N.Y.)*, 300(June), pp.1542–1548.

7 Appendix

7.1 Curriculum Vitae

Name: Monika Steinlage
Date of Birth: July 23rd 1984
Place of Birth: Heidelberg, Germany

Doctoral Thesis

08/2012 - 12/2016 **Technical University Darmstadt**
Radiation Biology and DNA Repair
AG Prof. Dr. Markus Löbrich

Education

10/2009 – 06/2012 **Johannes Gutenberg University Mainz**
Master of Science *Biomedicine* 1,2

08/2006 – 08/2008 **Florida Atlantic University, Florida USA**
Bachelor of Science *Psychobiology* 1,0

05/2004 – 05/2006 **Broward College, Florida USA**
Associate in Arts *Biology* 1,0

08/1995 – 03/2003 **Gymnasium am Kurfürstlichen Schloss Mainz**
Abitur 1,9

7.2 Publications

- 2017 Biehs R*, **Steinlage M***, Barton O*, et al. "DNA double-strand break resection occurs during non-homologous end-joining in G1 but is distinct from resection during homologous recombination." *Mol. Cell* Vol.65 671-684
- 2014 Barton O, Künzel J, Naumann SC, Diemer-Biehs R, **Steinlage M**, et al. "Polo-like kinase 3 regulates CtIP during DNA double-strand break repair in G1." *J. Cell Biol.* Vol.206 No.7 877-894.
- 2014 **Steinlage M**, Mirsch J, Schäfer R, Fournier C and Löbrich M. "Biodosimetry of alpha particle-induced DNA double-strand breaks in murine bones and soft tissues." *GSI Scientific Report*.
- 2013 **Steinlage M**, Mirsch J, Conrad S, Fournier C, Taucher-Scholz G and Löbrich M. "Visualization of DNA double-strand breaks induced by high LET particles and X-rays in murine bones and soft tissues." *GSI Scientific Report*.
- 2012 **Steinlage M**, Conrad S, Scholz M, Fournier C, Taucher-Scholz G and Löbrich M. "Visualization of DNA double-strand breaks induced by heavy ions in murine tissues." *GSI Scientific Report*.

7.3 Poster Presentations

- 2015 **Steinlage M**, Barton O, Diemer-Biehs R, Löbrich M. *A canonical non-homologous end joining pathway involves CtIP- and Artemis-dependent resection in G1 phase cells*. Poster session presented at: IMB Conference: DNA Repair and Genome Stability in a Chromatin Environment. 2015 June 4-7; Mainz, Germany.
- 2014 **Steinlage M**, Barton O, Löbrich M. *Alpha particle-induced DNA double-strand breaks in G1 phase are repaired via a CtIP-dependent c-NHEJ pathway*. Poster session presented at: 13th Biennial Meeting of the German Society for Research on DNA Repair. 2014 Sep 8-12; Mainz, Germany.

7.4 Author Contributions

Table 7.1 Author contributions "Plk3 regulates CtIP in G1"

Barton,O., Naumann,S., Diemer-Biehs,R., Künzel,J., Steinlage,M., et al. (2014)

Polo-like kinase 3 regulates CtIP during DNA double-strand break repair in G1.

J. Cell. Biol. 206, 877-894

Figure	Person	
1	a	OI
	b	OI
	c	JKü
	d	JKü
	e	JKü
2	a	Stn
	b	Stn
	c	MS
	d	MS
3	a	MS (image+graph) OI (Western Blot)
	b	NM
	c	OI
	d	RB
4	a	MS (graph) OI (Western Blot, small) Stn (Western Blot, large)
	b	OL
	c	NM
	d	NM
5	a	OI
	b	OI
	c	MS
	d	MS (graph) OI (Western Blot)
6	a	OL
	b	JW
	c	OL
	d	OI
	e	MS (graph) OI (Western Blot)
7	a	OI
	b	JKü
	c	JKü
	d	RB
8	a	MS
	b	OI
	c	OI
	d	STN

Figure	Person	
S1	a	OI
	b	OI
	c	JKü
	d	JKü
	e	Stn
	f	Stn
	g	Stn
	h	MS
S2	a	MS (graph) OI (Western Blot+images)
	b	OI
	c	OI
	d	RB
	e	RB
S3	a	MS (graph) OI (Western Blots)
	b	MS
	c	OL
	d	OI (left panel) NM (right panel)
S4	a	OI
	b	OI
	c	OI
	d	OI
	e	MS (graph) OI (Western Blot+images)
S5	a	JW
	b	JKü
	c	RB
	d	OI
	e	OI
Table1	Experiment	LF
	Statistic	Harvard
	Analysis	RB

OI=Olivia Barton

RB=Ronja Biehs

MS=Monika Steinlage

JKü=Julia Künzel

StN=Steffen Naumann

LF=Lin Feng

NM=Nodar Makharashvili

JW=Jiadong Wang

Table 7.2 Author contributions "Resection occurs during NHEJ in G1"

Biehs,R.* , Steinlage,M.* , Barton,O*., Juhász,S., et al. (2017)

DNA DSB resection occurs during NHEJ in G1 but is distinct from resection during HR.

Mol. Cell 65, 671-684

Figure	Person	Figure	Person			
1	a	JKü	S1	a	CB	
	b	JKü		b	JKü	
	c	JKü		c	BB, RB, MS	
	d	JKü		d	BB, RB, MS	
	e	JKü		e	SJ	
	f	RB, RW		f	SJ, MS	
	g	MS		S2	a	JKü
	h	OI			b	JKü, CB
2	a	OI	c		JKü, CB	
	b	RB (Western Blot)	d		CB (flow cytometry)	
	c	MS	e		MS (images)	
	d	RB/MS (Western Blot)		RB (graph)		
	e	JKü		OI		
	f	MS	S3	a	OI	
3	a	RB		b	CB (flow cytometry)	
	b	RB		c	MS (Images+graph)	
	c	RB		d	MS	
	d	RB		e	MS	
	e	RB		f	RB (analysis), MS (experiment)	
	f	RB		RB (analysis), MS (experiment)		
4	a	MS	S4	a	MS	
	b	RB (Western Blot)		b	JKü	
	c	MS		c	RB	
	d	MS (left graph)		d	MS	
	e	MS		e	RB, MS	
5	a	MS	S5	a	MS (left graph)	
	b	MS			RB/MS (Western Blot)	
	c	RB (Western Blot)			RB (right graph)	
	d	RB		b	RB	
	e	MS (left graph)		c	MS (graph)	
	f	MS		d	RB/MS (Western Blot)	
6	a	OI	e	MS		
	b	MS (graph)	S6	a	OI	
	c	RB (Western Blot)		b	OI (left+middle graphs+Western Blot)	
	d	RB (right graph)		c	JKü (right graph)	
	e	RB/MS (Western Blot)		OI (graph+Western Blot+small images)		
	f	AS (graph)		MS (large images)		
7	a	JS (IP CtIP), AG (Input)	S7	a	RB	
	b	SJ (IP Brca1)		b	RB	
	c	SJ		c	RB	
	d	MS	Table1	RB		
	RB					

RB=Ronja Biehs MS=Monika Steinlage
 JKü=Julia Künzel AS=Atsushi Shibata
 JS=Julian Spies RW=Ratna Weimer
 OI=Olivia Barton CB=Christel Braun
 SJ= Szilvia Juhasz AG=Anne Groher
 BB=Bettina Basso

7.5 Danksagung

Mein besonderer Dank gilt Herrn Prof. Dr. Markus Löbrich für die Möglichkeit meine Dissertation in seiner Arbeitsgruppe anzufertigen und die Unterstützung in dieser Zeit.

Bei Herrn Prof. Dr. Alexander Löwer möchte ich mich ganz herzlich für die kurzfristige Übernahme des Zweitgutachtens bedanken.

Ich danke Frau Prof. Dr. Claudia Fournier und Herrn Prof. Dr. Franz Rödel für ihre Bereitschaft als Prüfer bei meiner Disputation dabei zu sein.

Ganz besonders möchte ich mich bei Ronja Biehs bedanken. Dafür, dass ich mit dir immer alles noch mal durchdiskutieren konnte. Dafür, dass du mir immer geduldig alle Fragen beantwortet hast. Dafür, dass du mir immer geholfen hast, egal worum es ging. Wir waren das perfekte Team.

Für die Hilfe bei der Korrektur dieser Arbeit möchte ich Anugrah Gawai, Ronja Biehs, Amira ElBakry und Dr. Michael Ensminger danken. Bei Szilvia Juhász möchte ich mich für ihre tatkräftige Unterstützung bedanken, ganz besonders in den letzten paar Monaten. Ein ganz besonderer Dank geht außerdem an Julia Künzel für ihren uneingeschränkten Rückhalt, besonders in den schweren Zeiten.

Meiner Arbeitsgruppe danke ich dafür, dass ihr mich immer wieder daran erinnert habt, dass man nicht aufgeben darf. Außerdem möchte ich mich ganz herzlich bei allen TAs bedanken. Während zwei Revisionen habe ich oft eure Hilfe und Zeit in Anspruch genommen und wusste euer Engagement immer zu schätzen.

Last but not least möchte ich mich bei meiner Familie für eure bedingungslose Unterstützung und Geduld bedanken.

